Electronic Theses and Dissertations

Theses, Dissertations, and Major Papers

2011

Development of a shear test to determine the cyclic behaviour of sheet materials

Md. Samsul Sarker
University of Windsor

Follow this and additional works at: https://scholar.uwindsor.ca/etd

DEVELOPMENT OF A SHEAR TEST TO DETERMINE THE CYCLIC BEHAVIOUR OF SHEET MATERIALS

by

Md. Samsul Alam Sarker

A Thesis
Submitted to the Faculty of Graduate Studies
Through the Department of Mechanical, Automotive and Materials Engineering in Partial
Fulfillment of the Requirements for the Degree of Master of Applied Science at the University of
Windsor

Windsor, Ontario, Canada
2011
© 2011 Md. Samsul Alam Sarker

DEVELOPMENT OF A SHEAR TEST TO DETERMINE THE CYCLIC BEHAVIOUR OF SHEET MATERIALS

by
Md. Samsul Alam Sarker

APPROVED BY:

_____

Dr. S. Das, Outside Program Reader
Department of Civil & Environmental Engineering

_____

Dr. J. Johrendt, Department Reader
Department of Mechanical, Automotive and Materials Engineering

_____

Dr. D. Pusca, Co-Advisor
Department of Mechanical, Automotive and Materials Engineering

_____

Dr. D. E. Green, Advisor
Department of Mechanical, Automotive and Materials Engineering

_____

Dr. Biao Zhou, Chair of Defence
Department of Mechanical, Automotive and Materials Engineering

September 20, 2011

AUTHOR'S DECLARATION OF ORIGINALITY

I hereby certify that I am the sole author of this thesis and no part of this thesis has been published or submitted for publication.

I certify that, to the best of my knowledge, my thesis does not infringe upon anyone's copyright nor violate any proprietary rights, and that any ideas, techniques, quotations, or any other material from the work of other people included in my thesis, published or otherwise, are fully acknowledged in accordance with the standard referencing practices. Furthermore, to the extent that I have included copyrighted material that surpasses the bounds of fair dealing within the meaning of the Canada Copyright Act. I certify that I have obtained a written permission from the copyright owner(s) to include such material(s) in my thesis.

I declare that this is a true copy of my thesis, including any final revisions, as approved by my thesis committee and the Graduate Studies office, and this thesis has not been submitted for a higher degree to any other University or Institution.

ABSTRACT

In many industrial stamping operations, the sheet material is subject to a series of loading and reverse loading cycles. In order to accurately predict the outcome of such forming processes, numerical simulation models rely on advanced constitutive models to rigorously reproduce the cyclic work hardening behaviour of the sheet material.

The objective of this research was to develop a testing facility that is capable of generating the experimental stress-strain data of sheet materials when they are subjected to cyclic shearing loads. A suitable specimen geometry and a corresponding loading fixture were designed and fabricated.

Cyclic shear tests were successfully carried out on four different grades of automotive sheet steel using this new testing fixture mounted in a universal testing machine. The experimental data thus generated can be used to determine the material parameters in advanced constitutive models, in order to virtually simulate metal forming operations and the subsequent springback.

DEDICATION

To my parents, my wife Ferdoush Jahan, my daughters Raika Alam and Aniba Alam, for their encouragement, endless support, love and inspiration to complete this research.

ACKNOWLEDGEMENTS

TABLE OF CONTENTS

LIST OF FIGURES

LIST OF TABLES

LIST OF ABBREVIATIONS

AHSS	Advanced High Strength Steels
AISI	American Iron and Steel Institute
AKDQ	Aluminum Killed Draw Quality
ANN-EA	Artificial Neural Network Evolutionary Algorithm
ASTM	American Society for Testing and Materials
BNC	Bayonet Neill–Concelman
BPNN	Back Propagation Neural Network
CAD	Computer Aided Design
DAP	Data Acquisition Processor
DAT	Data Acquisition Tool
DIC	Digital Image Correlation
DOE	Design of Experiments
DP	Duel Phase
DQSK	Draw Quality Semi-Killed
EA	Evolutionary Algorithm
EDM	Electrical Discharge Machine
FE	Finite Element
FEA	Finite Element Analysis
FEM	Finite Element Method
GA	Genetic Algorithm
GA-BP	Genetic Algorithm Back Propagation
GB	Gigabyte
HSLA	High Strength Low Alloy
HSS	High Strength Steel
Hz	Hertz
IH	Isotropic Hardening
KN	Kilo Newton
LS-OPT	LS-Dyna Optimization

MPa	Mega Pascal
NAFR	Non Associate Flow Rule
NKH	Non Linear Kinematic Hardening
PB	Pre-stretching and Bending
RAM	Random Access Memory
RD	Rolling Direction
RIK	Rotational Isotropic Kinematic
RS	Random Search
SB	Simultaneous Stretching and Bending
SD	Shearing Direction
SSC	Shear Tensile Stress Condition
TD	Transverse Direction
TRIP	Transformed Induced Plasticity
TSC	Tensile Stress Condition
UTS	Ultimate Tensile Strength
WS	Without Stretching
Yld	Yield

LIST OF SYMBOLS

Symbol	Description
f	Function
σ_e	Effective stress (or flow stress)
σ_{eng}	Engineering stress
σ, σ_{true}	True stress
σ_y	Yield stress
σ_{y0}	Initial Yield stress
ε_{eng}	Engineering strain
$\varepsilon, \varepsilon_{true}$	True strain
ε_p	Plastic strain
$\bar{\varepsilon}$	Effective strain
p	Accumulated effective plastic strain
(p)	Isotropic hardening function
τ, τ_S	Shear stress
γ	Shear strain
α-Fe	Ferrite
γ-Fe	Austenite
F_i	Instantaneous tensile load
A_0	Initial area
D^p	Rate of plastic deformation
L_0	Initial Length
L_i	Instantaneous Length
ln	Natural logarithm
K	Strength index of material
l	Length of sheared area
n	Strain hardening exponent
n_p	Unit vector direction of plastic strain rate

n_*	Unit vector direction of kinematic motion
r	Slot radius
w	Width of sheared area
t	Thickness of sheet metal
B	Initial size
F	Force
H	Height of calibrated volume
L	Length of calibrated volume
W	Width of calibrated volume
R	Bending radius
R_i	Isotropic hardening component
S	Cauchy stress deviator
Y	Radius of yield surface in the deviatoric space
c	Tool gap in bending
e	Punch displacement in bending
w	Die opening in bending
α	Springback angle
$α_b$	Back stress deviator/tensor
$α_*$	Relative kinematic motion of the yield surface
β	Center of the bounding surface
θ	Bending angle
∅	Diameter
N-m	Newton-meter
Δρ	Springback quantity of bending radius
Δβ	Springback quantity of bending angle
Δθ	Changes in springback angle
δθ	Time dependent springback angle
F_b	Back force

1. INTRODUCTION

Sheet metal forming processes are commonly used to produce a multitude of parts for the automotive, aerospace, appliance and farm equipment industries. The manufacture of sheet metal components often requires one or more stamping operations in which the sheet material is stretched, drawn and bent between two mating dies to give it the desired shape. Stamping has actually been one of the most cost-effective ways of mass producing parts, especially for automotive components.

In an age where fuel consumption and weight reduction have become significant preoccupations, the automotive industry is driven to manufacture the body and structure of passenger vehicles using either high strength steel, aluminum or magnesium sheets. In view of the higher cost of magnesium and aluminum, however, the trend has been to use increasing proportions of high strength steel so that body components can be produced with thinner gauges without compromising the structural integrity (i.e. the torsional and bending stiffness) and the crash resistance of the vehicle. In particular, advanced high strength steels (AHSS) such as dual phase (DP) and transformed induced plasticity (TRIP) steels have now become common automotive sheet materials, and the trend continues to be for automotive body panels and structures to be made from steel grades that have increasing tensile strength.

The main challenges of producing sheet metal parts are, first of all, to satisfy the design specifications in terms of the geometric dimensions and tolerances of the part, and secondly, to avoid any defects such as excessive thinning, splits, wrinkles, surface damage and inconsistent or uncontrolled springback. Indeed, after a part has been stamped and then removed from the dies, the removal of external constraints allows the stresses in the part to decrease until the residual

stresses reach a state of equilibrium. The recovery of elastic deformations is an inevitable characteristic of metallic materials that can lead to significant changes in the shape of a part. For instance, bent shapes will tend to unbend, drawn channels will tend to exhibit sidewall curl and open parts will tend to twist.

Springback is actually a complex phenomenon: the nature and amount of deviation from the intended part geometry depends on the mechanical properties of the sheet material, on the level of stresses and strains that are attained in the part at the end of the forming process, and on the constraints that come from the shape of the part itself. Therefore, as stamped automotive parts are made from increasingly higher strength sheet materials, the magnitude and complexity of springback also increases. It is not surprising therefore that the single most costly challenge for suppliers of automotive stamped parts is to control the springback.

Traditionally, springback has been minimized by stamping prototype parts and then reworking the dies, and successively repeating this process by trial and error until the parts fit properly in a checking fixture. However, this way of building dies can be very costly and time-consuming, even when it is carried out by experienced tool & die makers, and may not always lead to a well-controlled manufacturing process. Furthermore, building a production die that is designed with incorrect springback compensation can cause significant difficulties in downstream operations such as poor fit-up in a welded subassembly. In some cases, tooling revisions may be required which could delay the start of production. Therefore the prediction of springback, especially in parts made from AHSS, is of critical importance to suppliers of automotive stampings.

The competition in the automotive industry is such that stamping dies must be designed and built right the first time so that the parts produced have the exact shape and dimensions that are

specified by the product designer. This signifies that springback must be known and accounted for when the dies are designed. The most efficient way for this to be done is to use state-of-the-art numerical simulation to predict the outcome of a stamping operation. Indeed, commercial finite element analysis (FEA) software is routinely used to dynamically simulate the stamping process as well as predict the springback [1] after stamping for many complex automotive parts. Once springback has been predicted for a virtual model of the part, the shape of the die can be compensated to eliminate or minimized springback before the dies are built.

The finite element method is widely used in the industry to predict the springback of stamped parts [1], and consists of building a virtual model of the entire stamping process with all the tooling surfaces that interact with the sheet metal. The blank and the dies are discretized into a large number of elements, mechanical properties are assigned to each component and the kinematics and boundary conditions of the stamping process are virtually reproduced. During the numerical simulation the die surfaces gradually close into their mating position by a series of small incremental steps, and as a result of the constraints and forces applied to the blank it progressively deforms into the desired shape. During each increment, the equations of motion are solved at each integration point in each element of the blank and the strains and stresses are computed. After the forming process is simulated, springback is also predicted by virtually opening the dies and allowing the formed part to elastically unload to its equilibrium position.

The accuracy of the numerical analysis depends on a large number of factors, but in particular on the constitutive model that is selected to describe the behaviour of the sheet material. Much research has been devoted to developing constitutive models that are capable of reproducing the behaviour of sheet materials, and today, various advanced constitutive models are available in commercial FEA software to simulate the elasto-plastic deformation and

springback of AHSS sheets. However, a specific series of material characterization tests must be carried out for a given sheet material in order to determine the parameters in the constitutive model that will describe the actual behaviour of this sheet. As constitutive models become more advanced, they generally have more parameters that need to be determined, which means more sophisticated characterization tests are required.

During many stamping or drawing operations the sheet metal is subjected to successive bending and unbending during the forming process, such as when the blank is formed over a punch or die radius. When a blank is drawn over a die radius one side of the sheet is deformed in tension while the other side is in compression, and a gradient of deformation develops through the thickness of the sheet. But once the sheet exits the curved portion of the tooling it straightens out again, and the side that was in tension becomes loaded in compression, and vice versa for the opposite side of the sheet. When sheet metal is formed through a drawbead the material experiences a series of bending-unbending cycles. Forming operations that make use of drawbeads to control the flow of metal are quite common and lead to cyclic loading and unloading in specific areas of the part. It is essential therefore, that the constitutive model in the FEA be able to accurately simulate the actual behaviour of the sheet material when it is cyclically deformed, because unless the strains and stresses are accurately predicted in the virtual forming process the strains and stresses (and the part shape) will obviously not be accurately predicted after springback.

The main objective of this research is to design and build a testing apparatus that will enable us to experimentally determine the cyclic stress-strain behaviour of sheet materials so that finite element (FE) analysts seeking to predict the springback of stamped parts can determine the material parameters in advanced constitutive models from the experimental stress-strain data.

The development of a test to cyclically deform sheet metal specimens involves several steps:

- Selecting the type of deformation to impose on the specimen (e.g. tension/compression, bending/unbending, simple shear etc.).

- Designing and optimizing the specimen geometry with a gauge area in which stresses and strains are uniformly distributed and can easily be measured during a test.

- Designing and building a rigid fixture that can be mounted in a testing apparatus and that can impose the desired type of cyclic loading onto the specimen.

Once the prototype fixture is built and sheet specimens are fabricated, it will be necessary to carry out tests to verify that the specimens, fixture and testing actually provide the desired experimental stress-strain data.

This thesis divides into six chapters. Chapter 2 provides a review of springback and the current constitutive models used to simulate the deformation of anisotropic sheet materials. Moreover, a literature review of various testing facilities that have been used to experimentally determine the cyclic behaviour of sheet materials is also provided. Chapter 3 presents a description of the methodology that was followed to design both the test fixture and the geometry of the sheet specimen. Chapter 4 presents the experimental work that was done to verify the effectiveness of the test, including the different sheet materials that were tested, the testing procedures, the strain measurements and the details of data analysis. Chapter 5 provides the experimental stress-strain response of the sheet materials that were tested. Finally, Chapter 6 presents the observations made throughout this experimental work as well as some conclusions and recommendations.

2. LITERATURE REVIEW

Before one can design a testing apparatus to experimentally determine the cyclic stress-strain behaviour of AHSS sheets it is necessary to first consider the work that other researchers have done to characterize and model the cyclic behaviour of sheet materials. This chapter provides an overview of the literature relevant to this study and divides into four main sections. The first section briefly describes the types of springback that can develop in industrial sheet metal components. The next section provides an overview of some simulative tests that have been developed to experimentally investigate springback. The third section gives a review of constitutive models (anisotropic yield criteria and hardening laws) used to numerically simulate sheet metal forming and springback. And the final section describes various experimental testing facilities that researchers have developed to characterize the cyclic behaviour of sheet materials in view of obtaining material input data for numerical simulations.

2.1 SPRINGBACK IN STAMPED PARTS

In the automotive industry, high strength steel sheets and low density sheet metals have become a necessity in order to reduce the weight of the vehicle body-in-white. However, the increased use of materials with high strength and/or low elastic modulus as well as reduced gauges leads to a significant increase in the amount of springback in stamped parts. Therefore, springback has become a major challenge in regards to manufacturing lightweight automotive components.

During the stamping of a sheet metal component, the sheet material is often subject to bending around a tool radius, and in fact may undergo a series of bends and reverse bends. The

stress distribution in the part after forming, and especially the stress gradient through the thickness, is responsible for the nature and magnitude of springback. For example, Fig. 2.1 shows the stress distribution in a sheet material at different stages throughout the process of being formed into a cup and after the part is allowed to springback. The non-uniform distribution of stress in the part is very evident at each stage.
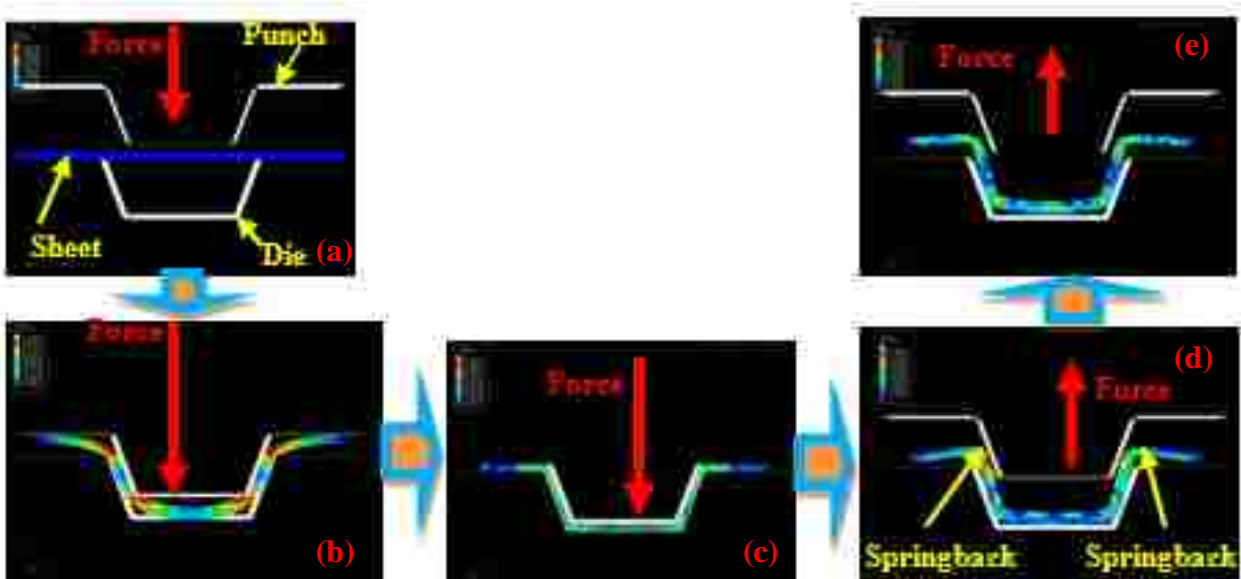
Figure 2.1 Springback simulation of sheet metal cup in stamping

Depending on the type of forming process, the shape of the as-formed part, the sheet mechanical properties, the selection of industrial process parameters and the stress distribution in the formed part, the shape distortions due to springback can manifest themselves in a variety of ways [2]. Because springback is so part and process-dependent, it can be very difficult to control the geometry and dimensional accuracy of stamped sheet metal components. For example, springback can cause twisting of the entire part, stretched areas tend to shrink, bent or flanged edges will unbend to some extent (Fig. 2.2a) and drawn channel sections can exhibit curling of the sidewalls (Fig. 2.2b and Fig. 2.3). Researchers have defined six common classes of springback as follows [2]:

1) Sidewall opening (Figure 2.2a)

2) Sidewall Curl (Figure 2.2b)

3) Edge line warping or bow (Figure 2.2c)

4) Twist

5) Global shape change

6) Surface distortion
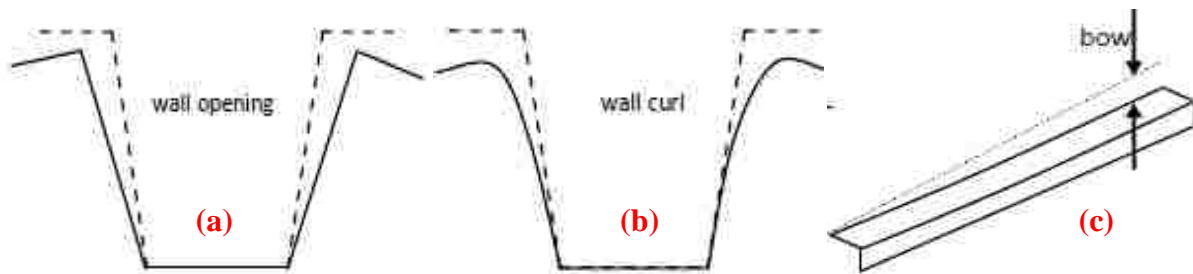
Figure 2.2 Different types of springback (a) wall opening (b) wall curl (c) bow [2]
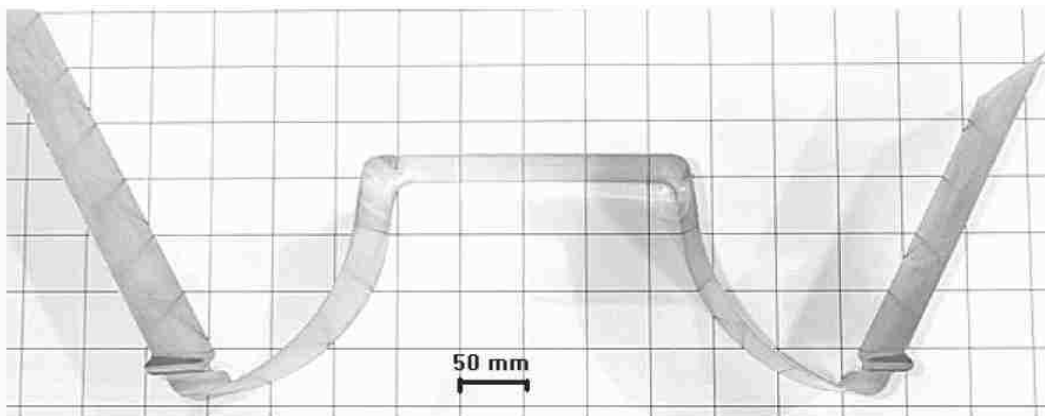
Figure 2.3 Sidewall curl in a drawn channel section [2]

In order to minimize the distortions due to springback, efforts have typically been made on two fronts: *a*) adjustments can be made to critical process factors such as blank holding force, die clearances, ram velocity, lubrication, drawbead restraining force, etc. [3], and *b*) springback is numerically predicted and compensated for at the tool design stage [4, 5]. The first approach is essentially a pragmatic way to minimize springback due to variations in the mechanical

properties of incoming sheets after the stamping dies have been built. This type of springback correction tends to have a limited impact and is only used to make minor adjustments since the stress distribution in the part is largely determined by the deformation history of the sheet metal in the dies. Process changes are rarely sufficient to eliminate springback problems that result from a poorly designed tool. The second approach endeavours to optimize the forming process and the design of the dies before they are built, so that the flow of metal during the stamping process can be as even and uniform as possible and any gradients in residual stresses can be minimized. Nowadays, this is the most cost-effective approach to springback compensation.

2.2 EXPERIMENTAL SPRINGBACK STUDIES AND SIMULATIVE TESTS

The earliest experimental springback studies consist of simple bending tests. Ogawa et al. [6] performed V-bending tests to predict the springback of the high strength steel sheets and observed that springback drastically decreases with increasing bottoming force. Fu and Mo [7] conducted air bending test on high strength steel sheets and measured the springback angle and radius. The geometric model of the air bending of sheet metal specimen proposed by Fu and Mo is shown in Fig. 2.4.
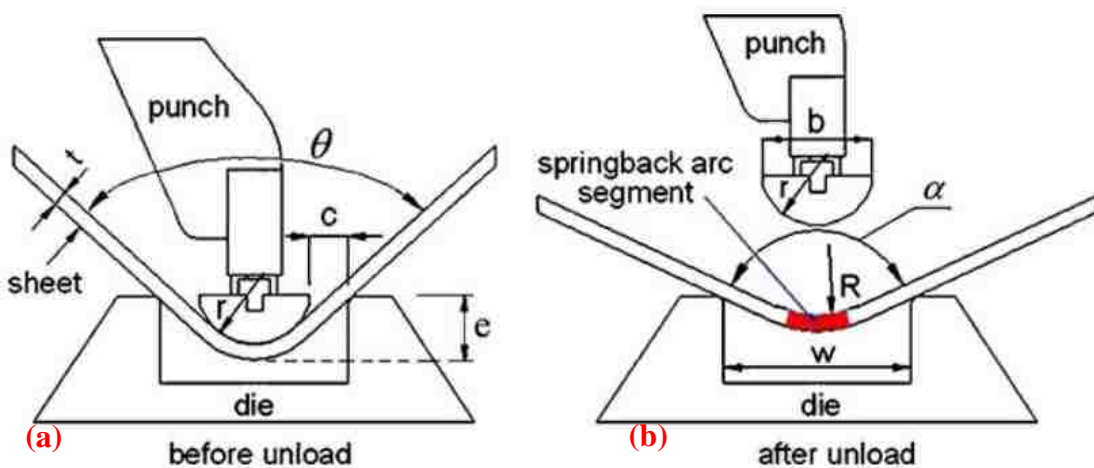
Figure 2.4 Geometrical model of air bending of sheet metal [7]

9

In Fig. 2.4, c is the tool gap, t is sheet metal thickness, w is the die opening, r is the punch radius, R is the bending radius, b is punch width, e is the punch displacement, and the springback arc segment is defined by the bending arc segment of sheet metal after removal from the punch. It is important to mention that in air bending springback can lead to changes of bending radius, bending arc segment, and bending angle. The difference between the bending radius of a sheet after unloading (R), and the punch radius (r) is defined as springback quantity of the bending radius ($\Delta\rho = R-r$). The springback angle ($\Delta\beta = \alpha-\theta$) is the difference between the unloaded bend angle (α) and the bend angle before springback (θ).

In many stamping operations, it is common for the sheet metal to be deformed in a plane strain mode as a result of combined bending and tension. For instance, when sheet metal is drawn through a drawbead and over the die shoulder radius as a result of the punch action (Fig. 2.5), it becomes subject to bending under tension. In order to thoroughly understand the springback behaviour of sheet materials that have been deformed in this way a number of researchers [7, 8] have developed simulative tests that reproduce bending-under-tension deformation modes, and then have attempted to model the springback behaviour that was observed experimentally.
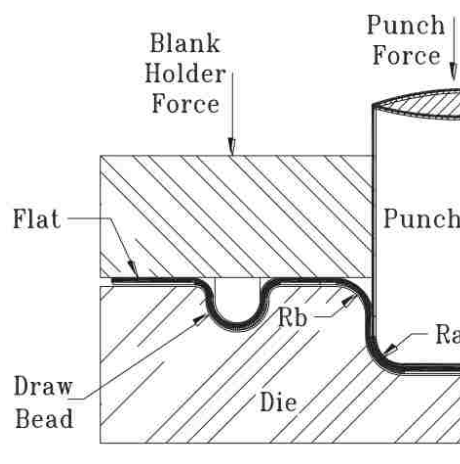
Fig. 2.5 Bending under tension in a typical stamping (drawing) operation [8]

Sanchez [8] developed a drawbead simulation testing apparatus that can apply both bending and tension to a sheet specimen using three pin rollers. During testing the sheet metals are bent, un-bent and bent in the reverse direction in a three-cycle sequence. A schematic of Sanchez' experimental binder geometry and theoretical model is shown in Fig. 2.6. During his experiments, Sanchez observed that springback decreased with increasing tension and became negligible for tensile forces approaching the tensile strength of the material. He reported that if the coulomb friction on the pins increases by about 0.01, it would result in noticeably greater tension forces and smaller curvature after springback [8].
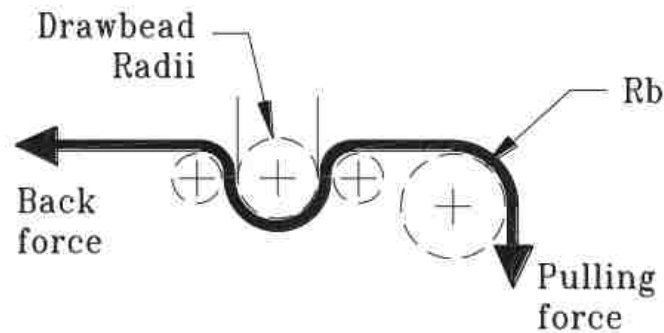
Figure 2.6 Schematic of Sanchez' three pin roller set-up for cyclic bending of sheet metal [8]

Schilp et al. [9] investigated the effects of three different factors on the springback response after stretch-bending tests: the stretching method, the stretching length and the stretching direction. They showed that when the bending radius to the sheet thickness ratio (R/t) increases, the springback gradually increases and reaches a maximum when the ratio is R/t = 10, with a 45° bending angle. In order to investigate the stretching effect, Schilp et al. [9] compared four processes: bending without stretching (WS), pre-stretching and bending (PB), pre-stretching plus simultaneous stretching and bending (PSB), and simultaneous stretching and bending (SB). They compared the springback factor maintained a fixed R/t and changed the bending angles of 15°, 45° and 90°. It was observed by them when the bending angle decreases, especially in WS

11

process the amount of springback increases drastically. The springback remained regular values regardless of bending angle in SB process. As, R/t increases and the bending angle becomes smaller, the SB process produces less springback than other process. They concluded that, simultaneous stretching and bending can reduce the springback, and the variation of stretching length has no distinct effect in the simultaneous stretching and bending process.

Lim et al. [10] conducted an experimental study using a draw-bend test (Fig. 2.7) to determine the time-dependent springback at room temperature of four AHSS sheets, (DP600, DP800, DP980 and TRIP780), and three conventional steel sheets (AKDQ, DQSK and HSLA). After drawing the test strips over the tool radius and unloading them, they measured the springback angle at regular time intervals up to 6 months after the test; the instantaneous springback angle was called the time-independent springback angle. When the springback angle continued to increase over time, it would eventually reach a saturation value; the difference between the saturated angle and the instantaneous angle was called the time-dependent springback angle. It was observed that both AHSS and conventional steels showed a decrease in the instantaneous springback angle with increasing back force and tool radius. In addition, AHSS with higher yield stress showed larger instantaneous springback angles compared to conventional steels [10]. All AHSS demonstrated angle changes during the 6 months after testing, but the conventional steels did not. It was observed that for DP800, DP980 and TRIP780 steels the maximum time-dependent angle was attained only 2 weeks after testing, but for DP600 steel, the angle change saturated a long time after testing (Fig. 2.8). Lim et al. also observed that the time-dependent springback angle increased with yield strength as did the time-independent angle [10].
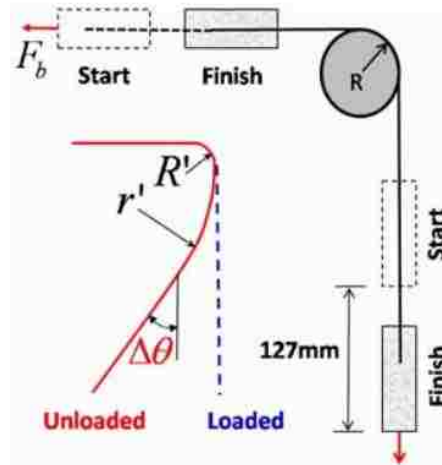
Figure 2.7 Schematic of the draw-bend test [10]. R is the roller radius, F_b is the back force, and $\Delta\theta$ is the springback angle
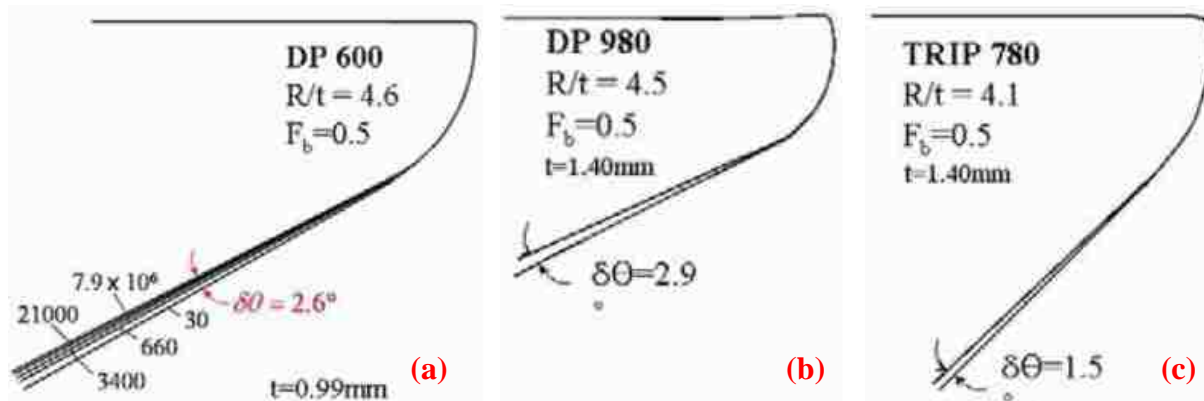
Figure 2.8 Time-dependent springback in (a) DP600 (b) DP980 (c) TRIP780 strips subject to bending under tension [10]. R/t is the roller radius to sheet thickness ratio, F_b is the back force, and $\delta\theta$ is the time-dependent springback angle

In order to understand the time-dependent springback of AHSS, Lim et al. investigated two mechanisms: an elastic deformation and residual stress driven creep. They used a simple finite element model based on residual stress-driven creep model to simulate their experiments, but found that the model over-estimated the experimentally measured springback angles by a factor of two.

Wagoner et al. [11, 12, 13, 14, 15, 16] carried out extensive research on springback prediction using draw bend tests. In order to determine the springback effect, Wagoner et al. [11] performed two-dimensional stretch draw bend tests adjusting three process parameters: tool radius, friction and back force. They found that the applied back force dominated the springback sensitivity that R/t had a modest effect and friction had a minor effect on springback. The springback decreased with increasing R/t ratio and increasing back force. The springback can be decreased up to about 90% and 25% by increasing the tensile stress and the R/t ratio, respectively [12].

Wagoner et al. [14] devised draw-bend tests to measure and predict springback under controlled conditions. They observed a discrepancy between the simulation and experimental results. It might have been due to the use of the isotropic hardening model that does not reproduce the Bauschinger effect. The springback angle is very sensitive to the hardening model. In order to generate a mixed hardening law that could describe the active yield surface and bounding surface, Wagoner et al. [15] devised a tension-compression-type model. They showed that the springback angles were reduced by using a compression-tension or tension-compression model instead of the isotropic hardening model. The modified nonlinear hardening model developed by Wagoner et al. [16] showed that the predicted springback angle tends to linearly decrease with an increasing back force. They concluded that accurate springback simulations might obtained by a judicious combination of material properties, R/t, and sheet tension.

Carden et al. [17] conducted bending and un-bending tests to measure 'sidewall curl'. They reported that the curl is minimized for a variety of steels when R/t = 2, and smaller R/t values might produce a curl in the reverse direction.

14

2.3 PREDICTION OF SPRINGBACK

As mentioned earlier, the most efficient way to build stamping dies that accurately compensate for springback is to numerically simulate the forming operation and the subsequent elastic unloading of the part. Such numerical simulations are generally performed with a finite element code in which the sheet material behaviour is described by an appropriate constitutive model. In the classical theory of plasticity, a constitutive model is comprised of a flow curve that defines how the material hardens during plastic deformation, and a yield criterion and a hardening model. The yield criterion is a function that represents the stress states at which the material starts to yield, i.e. when the transition from elastic to plastic behaviour occurs, and these stress states form a convex surface, called the yield surface. The hardening law describes how the yield surface evolves in stress space as a function of plastic deformation. In this section, the yield criteria and hardening rules that are most commonly used to simulate sheet metal forming and springback will be presented.

2.3.1 PLASTICITY AND ANISOTROPIC YIELD FUNCTIONS

The two simplest yield criteria were proposed by Tresca [18 and von Mises [19 and determine the onset of yielding of isotropic materials [20]. Since most sheet materials display some level of anisotropy (through the thickness or in the plane), many researchers (Hill 1948, 1979, 1990, 1993, Hosford 1979, Barlat1989, Barlat1991, Barlat1994, Barlat1996, Barlat 2000, Karafillis1993, Cazacu & Barlat 2003, Banabic & Balan 2003) have proposed plane-stress anisotropic yield criteria to represent the behaviour of orthotropic sheet materials. Among all these criteria, Hill's (1948, 1990), and Barlat's (1991, 2000) yield criteria are the most widely used for simulating sheet metal forming operations [21].

Hill's Yield Criteria

Hill [22] was the first to propose a yield criterion for anisotropic materials. Hill's 1948 yield criterion is an extension of von Mises' criterion for isotropic materials and describes the yielding of anisotropic materials using additional material constants. Due to its mathematical simplicity, Hill's 1948 quadratic yield function continues to be widely used for metal forming simulations of orthotropic steel sheets [23]. One of Hill's more recent yield criteria (1990) is also used when additional precision is required, such as for the prediction of earing in drawn cups.

Barlat's Yield Criteria

To properly describe the yield and anisotropy of aluminum alloys Barlat et al. [24,25] proposed a plane-stress yield criterion in 1989 that has been successively modified in 1991, 1996, 2000, and 2003. These yield criteria are widely used for modelling the behaviour of FCC materials such as, aluminum alloys [26]. Barlat's Yield 2000 criterion also accurately predicts the behaviour of sheet steels e.g. DP600, HSLA [27].

These various yield functions describe the initial stress states at which yielding begins but do not account for the evolution of material anisotropy during on-going plastic deformation [26]. A hardening law is required to model the evolution of the yield surface.

2.3.2 HARDENING LAWS

At a given material point the yield surface evolves in stress space as a result of work hardening, and it is important to accurately describe the way in which it evolves because, in the numerical simulation. The shape of the yield surface determines the direction of the plastic strain increments (normality rule), which in turn determines the prediction of strains in the virtual part.

The hardening law models the possible changes in shape, size and orientation of the yield surface at each increment during the plastic deformation.

As was pointed out earlier, cyclic loading is a very common type of loading in sheet metal forming processes. Since reverse loading can lead not only to elastic unloading but also to plastic deformation in a reverse direction, the hardening rule should be able to accurately predict the hardening behaviour for cyclic loading. Over the past few decades, researchers have developed several hardening models and the most important ones will be described below.

Isotropic Hardening

When the expansion of the yield surface is uniform in all directions in stress space, the hardening is referred to as isotropic [28]. Indeed, many materials can be considered isotropic in the annealed state, and the Bauschinger effect and the anisotropy developed due to deformation may be neglected [29]. This hardening law has been widely adopted in the industry since it is easy to implement (i.e. it does not require any cyclic testing to be carried out), although it may give large errors under reverse loading [30]. The yield function equation for isotropic hardening is written as:

$$f(\sigma, p) = \sigma_e - \sigma_y(p) = 0 \qquad\qquad 2.1$$

where σ_e is the effective stress, p is the accumulated effective plastic strain, and $\sigma_y(p)$ is the yield stress which might be of the form :

$$\sigma_y p = \sigma_{y0} + r(p) \qquad\qquad 2.2$$

where σ_{y0} is the initial yield stresses and $r(p)$ is called the isotropic hardening function.

Fig. 2.9 schematically shows the relationship between the uniaxial stress-strain curve and the evolving yield surface with isotropic hardening [28]. Because of the uniform expansion of the

yield surface, the yield stress in the reverse loading is equal to that in forward loading. Therefore isotropic hardening is not able to describe the Bauschinger effect which is often observed under reverse loading.
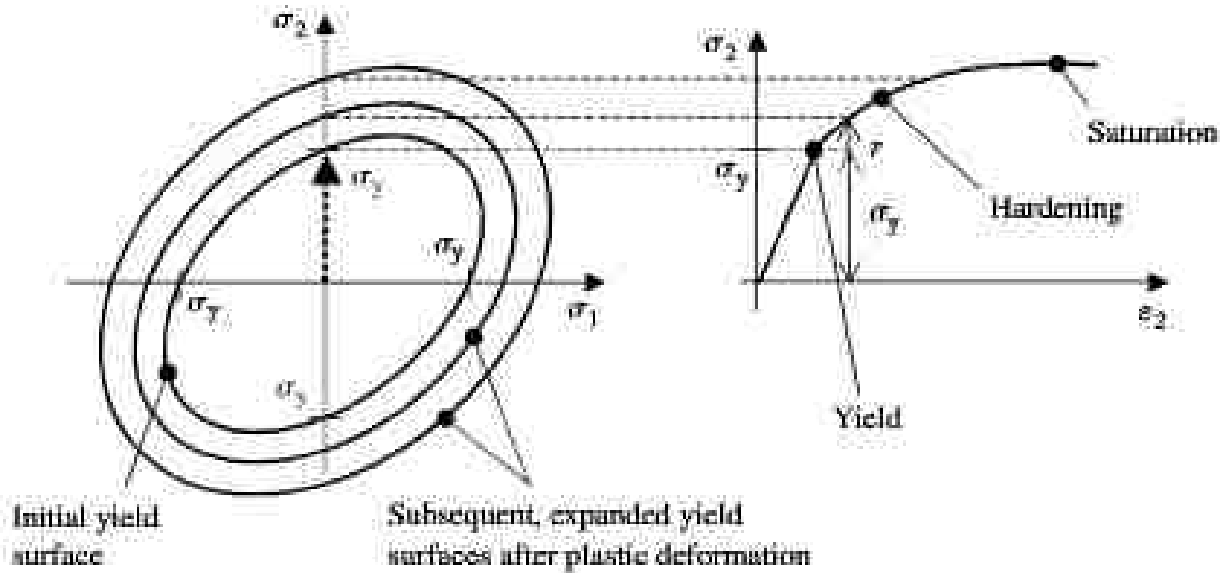
Figure 2.9 Isotropic hardening of the yield surface with plastic deformation, and the corresponding uniaxial stress-strain curve [28]

Kinematic Hardening

Kinematic hardening was developed to model the work hardening behaviour of materials that exhibit the Bauschinger effect (a decrease in the yield stress in compression as a result of previous loading in tension). Kinematic hardening assumes that the yield surface merely translates in stress space during plastic deformation (Fig. 2.10), and the translation in one direction results in a reduction of the yield stress in the opposite direction [31]. Therefore, the shape and size of the subsequent yield surface do not change during plastic deformation. Fig. 2.10 (a) and (b) show that the stress increases until the yield stress is reached.
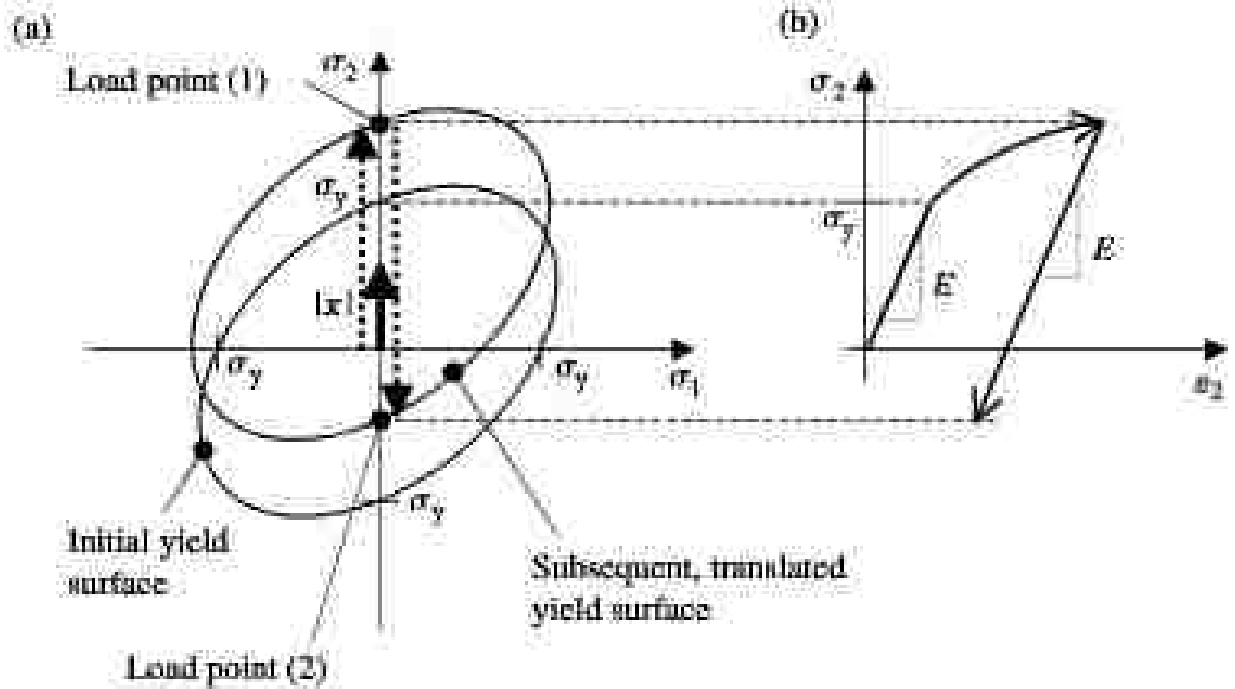
Figure 2.10 Kinematic hardening showing (a) the transitions, $|x|$ of the yielding surface with plastic strain, and (b) the resulting stress-strain curve with shifted yield stress in compression-the Bauschinger effect [28]

With continued loading, the material deforms plastically and the yield surface translates. When load point (1) is achieved the load is reversed, so that the material deforms elastically until point (2) is reached, when the load point is again in contact with the yield surface. Therefore, the elastic region is much smaller than that predicted with isotropic hardening. In the case of kinematic hardening, the equation of the yield surface is written as:

$$f(\sigma - \alpha) - \sigma_y = 0 \qquad\qquad 2.3$$

where α is called the back stress tensor which determines the location of the centre of the yield surface.

Prager [32] and Ziegler [31] were the first to develop kinematic hardening rules. However, the classical kinematic hardening model tends to over-predict the Bauschinger effect, and it is not able to model other characteristics of materials when they are subject to cyclic

19

loading, such as the smooth transient re-yielding behaviour, work hardening stagnation or the creep (ratchetting) effect under cyclic stress [33].

Non-Linear Kinematic Hardening

Armstrong and Frederick [34] developed a nonlinear kinematic hardening (NKH) model by modifying the linear hardening law proposed by Prager [32]. Chaboche [35] also predicted the smooth transient behaviour by introducing an additional nonlinear back-stress term to Prager's linear kinematic hardening model which could not account for the permanent softening behaviour during the reverse loading. Li [36] developed a pure nonlinear kinematic approach with finite element implementation to perform a shakedown analysis of materials. The experimental and simulated cyclic behaviour of a DP600 sheet steel is shown in Fig. 2.11 developed by Taherizadeh et al. [2, 37] using a NHK hardening model.
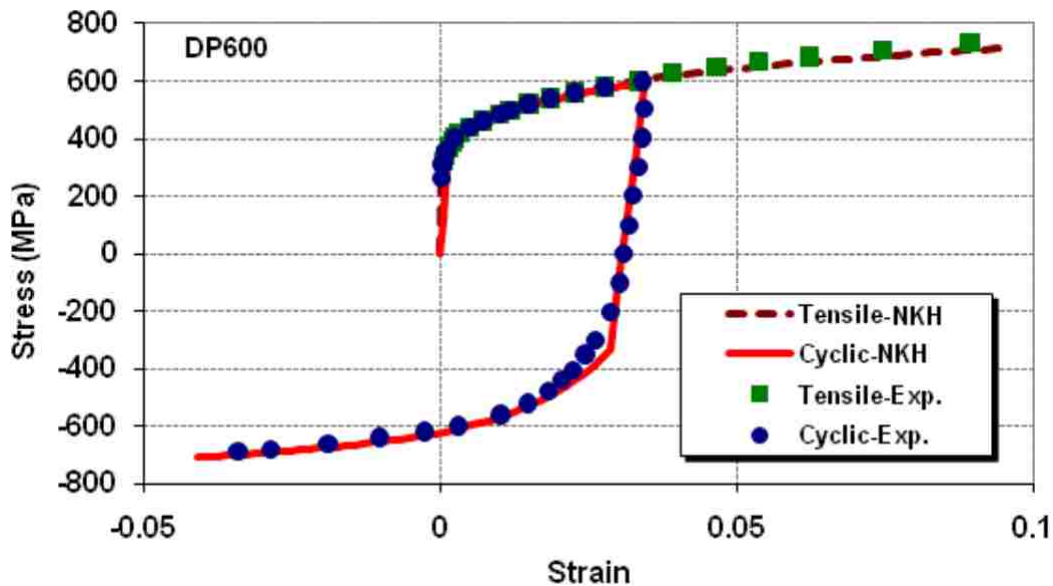
Figure 2.11 Comparison of the experimental cyclic stress-strain data for DP600 sheet steel and that predicted with the NKH model [2, 37]

20

Yoshida et al. [38] identified the material parameters for the NKH model using an iterative multipoint approximation of the data obtained from uniform bending tests. Chun et al. [39, 40] and Vladimirov et al. [41] used NKH to determine the anisotropic parameter of sheet metals. Brunet et al. [42] extended the NKH to the plastic anisotropy and identified the material constants based on four point bending experiments and a Sequential Quadratic Programming algorithm.

Mixed Hardening

Many researchers now use a combined isotropic-kinematic hardening (mixed hardening) model in order to take advantage of both models and more accurately predict the cyclic behaviour of certain sheet materials. For instance, Yoshida and Uemori [43], Geng et al. [44], Chaboche [35], Chaboche and Rousselier [45], Khan and Jackson [46] used the mixed hardening model, since it can reproduce the Bauschinger effect, the smooth elastic-plastic transition upon re-yielding and the isotropic hardening effect. A schematic of the mixed hardening model is shown in Fig. 2.12.

In order to improve the prediction capability of reverse loading and springback behaviour, a modified Chaboche-type combined isotropic-kinematic hardening model was developed by Chung et al. [47] and Lee et al. [48] to effectively describe the Bauschinger effect and the transient behaviour. However, Kim et al. [49] reported that the modified Chaboche model cannot account for the permanent softening behaviour during the reverse loading. Chow et al. [50] proposed a generalized mixed isotropic kinematic hardening plasticity model coupled with anisotropic damage for sheet metal forming.

21
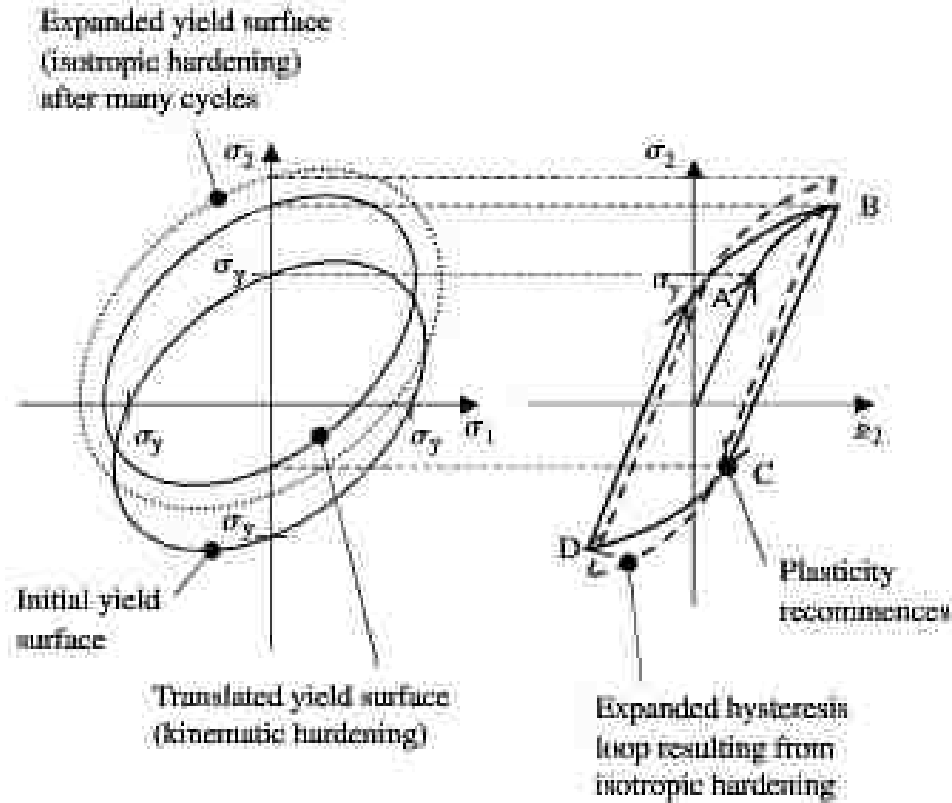
Figure 2.12 Schematic illustrations of combined kinematic and isotropic hardening [28]

Taejoon et al. [51] analyzed the time dependent springback behaviour of a 6022-T4 aluminum alloy sheet using a visco-elastic/plastic constitutive law. They also used the combined isotropic-kinematic hardening law to represent the Bauschinger behaviour and transient hardening, and the non-quadratic anisotropic yield function Yld2000-2D was applied to account for anisotropic yield behaviour. Using the results of draw bend tests, they showed that this constitutive law and formulation are valid for time dependent springback.

Taherizadeh et al. [23] developed a non-associated flow rule (NAFR) with mixed hardening. They showed that the non-associated mixed hardening model significantly improved the prediction of springback in the sidewall of drawn channel sections and the prediction of earing in the cup drawing process. Taherizadeh et al. [37] also suggested that the mixed isotropic-nonlinear kinematic hardening framework is more suitable for cyclic loading. Collin et

22

al. [52] proposed a combined isotropic and kinematic hardening model and used an inverse approach to identify parameters using the monotonic tensile and cyclic experimental indentation curves.

A Rotational-Isotropic-Kinematic (RIK) hardening model was developed by Choi [53] to transform the major effects of micro-mechanical deformation behaviours to a phenomenological model. The proposed RIK model allows the yield surface to grow (isotropic), to translate (kinematic) and even to rotate (rotational) as the deformation progresses. The RIK model was formulated based on the Armstrong-Frederick type kinematic hardening model and on the rotation of the symmetry axes of anisotropy with the plastic spin theory. The ability of the model was demonstrated by the multi-path loading of 'tension-shear' and 'reverse-shear' to reveal the 'crossing' and 'Bauschinger' effects [53].

Multi-surface Hardening Models

The use of multiple-surface models instead of the single yield surface is an alternate way to describe the permanent softening and non-symmetric reloading behaviours. Dafalias and Popov [54] analyzed two-surface kinematic hardening models through complex loading that was developed by Krieg [55]. Yoshida and Uemori (YU) [43] proposed a two-surface plasticity model that assumes kinematic hardening of the yield surface within a bounding surface that expands isotropically and their two-surface model is capable of reproducing the transient Bauschinger effect, permanent softening and work hardening stagnation in large elasto-plastic deformation. The YU two-surface model is schematically shown in Fig. 2.13. The inner surface, or yield surface, determines the elastic domain of the material in stress space and translates in stress space without expansion.

23
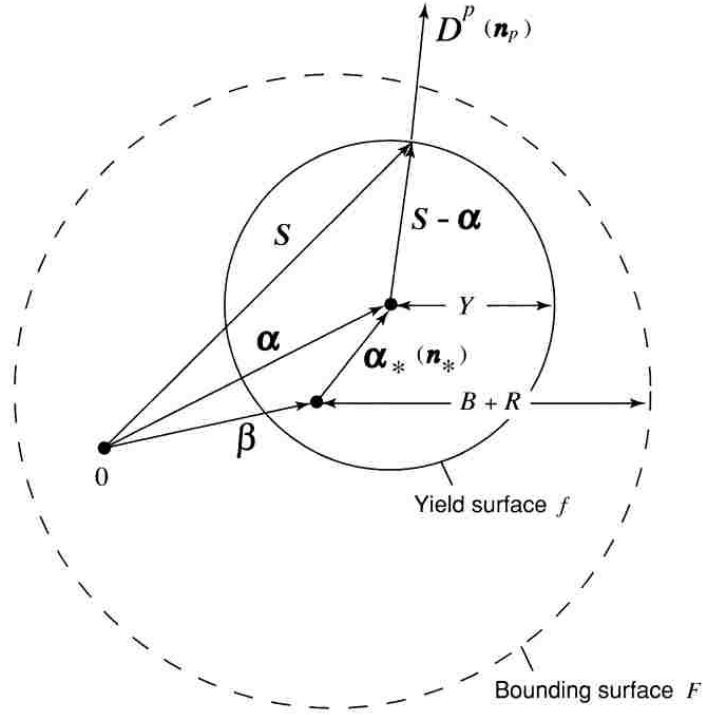
Figure 2.13 Schematic illustration of Yoshida-Uemori two-surface model [43]

In Fig. 2.13, D^p is the rate of plastic deformation, n_p is the unit vector direction of plastic strain rate, S is the Cauchy stress deviator, α_b is the back stress deviator, Y is the radius of the yield surface in deviatoric stress space, β is the center of the bounding surface, B is the initial size, R is the isotropic hardening component, α_* is the relative kinematic motion of the yield surface with respect to the bounding surface and n_* is the unit vector direction of relative kinematic motion. Fig.2.14 shows how these particular material responses appear on a stress-strain curve after a load reversal [56].
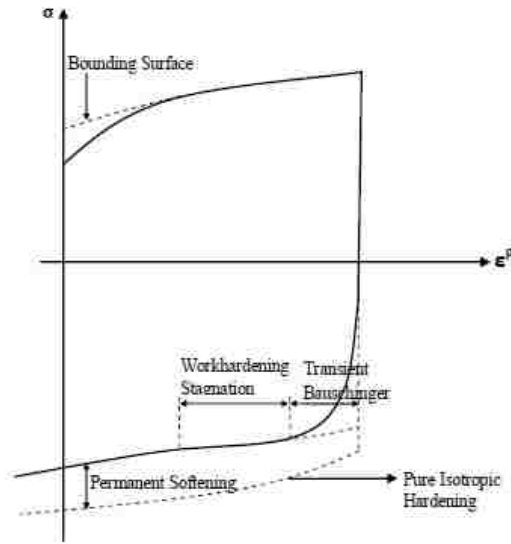
Figure 2.14 Schematic illustration of the stress-strain behaviour of certain materials [56]

McDowell [57] and Lee et al. [58] defined two independent hardening parameters for the kinematic evolution of the yield and bounding surfaces in the YU model. Cardoso and Yoon [59] proposed another two-surface kinematic hardening model. Hashiguchi [61] used a three-surface model; Hassan et al. [61, 62], and Mroz [63] used a model with multiple yield surfaces to describe the cyclic loading. Multi-surface models are capable of describing the Bauschinger effect and the nonlinear transient behaviour, but require a large number of yield surfaces to obtain the smooth transient behaviour.

2.3.3 NUMERICAL SIMULATION OF SPRINGBACK

The complexity of predicting springback in stamped components is such that many researchers around the world have been working for the last few decades to develop numerical tools and methodologies that enable them to predict springback in a rigorous and reliable manner. As was discussed in the previous section, the selection of a constitutive model that is capable of reproducing the cyclic behaviour of sheet materials is an important first step.

25

However, the accuracy of simulation results depends on many other parameters, such as the numerical implementation of the constitutive model into a finite element program, the accuracy of the forming simulation with its specific challenges of modeling contact and friction, as well as the selection of a host of numerical parameters. In this section, the work of various researchers will be presented with a view to highlighting the most important aspects of numerical simulation of springback.

Hußnatter and Merklein [64], Thuillier et al. [65], Lee et al. [48] and Oliveira et al. [66] reported that springback prediction strongly depends on the accurate simulation and realistic modeling of the forming operation. To predict springback, Thuillier et al. and Oliveira et al. [65, 66] emphasized that the accuracy of the stress state at the end of the forming simulation is critical to the accurate prediction of springback. They mentioned that constitutive models should have a reliable description of the material behaviour, especially in terms of anisotropy and work hardening during loading and unloading.

Cao [67] reported that springback is connected with several factors such as, tool structure, sheet material properties, sheet material geometries, friction etc. The relationships among those factors are complex and non-linear. Therefore, it is difficult to find a mathematical model that can predict the springback perfectly.

Verma et al. [68] reported that the accuracy of springback prediction depends on the yield surface shape, the number of integration points, the type of element used in numerical simulations, the incorporation of permanent softening, and the strain-dependent elastic modulus. Moreover, it is difficult to conclude with certainty the reasons for inaccuracies since the effects of these parameters are coupled.

Oliveira et al. [66] used several constitutive work hardening models such as classical isotropic, non linear kinematic and Teodosiu's micro structural model in order to predict the springback of DP600 and mild steel (DC06). They used Swift's power law to describe the classical isotropic work-hardening, the Lemaitre and Chaboche law [69] to describe the non-linear kinematic hardening model and Teodosiu's micro structural work-hardening model. However, the effect of drawbead penetration was not studied in their work.

Many researchers such as, Hußnatter and Merklein [64], Lee et al. [48], Banu et al.[70], Oliveira et al.[66], Vladimirov et al.[71], and Yoshida[72] have shown that the Bauschinger effect (straining in one direction reduces the yield stress in the opposite direction) has a strong influence on the prediction of springback. Zhang and Hu [73] calculated the springback by using three different cyclic material models such as, isotropic, kinematic and directional hardening, and observed a remarkable difference in results. Campana et al. [74] used a combined isotropic-kinematic hardening model to predict the forming and springback behaviour of various AHSS sheets.

Arwidson [75] reported that when the sheet material was subjected to cyclic loading conditions springback prediction must consider the Bauschinger effect. He showed that the prediction of springback depends on the accuracy of reproducing both the Bauschinger effect and plastic shakedown using a combined isotropic/non-linear kinematic hardening (NKH) material model. He concluded that applying tension drastically reduced springback and the friction in the normal range encountered in sheet metal forming had little effect on springback [75].

Chun et al. [76, 77] used finite element simulations associated with an anisotropic non linear kinematic hardening (NKH) model to predict springback and Bauschinger effects after cup

drawing in the presence of draw beads. However, their drawbead model predicted an excessively large compressive stress at the surface of the sheet at the level of the exit bead.

Taherizadeh et al. [78] showed that the springback results are significantly dependent on the type of hardening model when one compares between pure isotropic hardening (IH) and combined isotropic-nonlinear kinematic hardening. They also reported that the prediction of springback is more sensitive to the hardening model than to the yield function [37]. Taherizadeh et al. [2] conducted further studies to see the effect of drawbead penetration and restraining force on the prediction of springback (Fig. 2.15). Comparing simulation results with experimental springback data obtained from straight channel sections drawn in plane strain they showed that the IH model generally overestimates the amount of springback due to the high stresses derived by this model. On the other hand, the NKH model was able to predict the springback significantly more accurately than the IH model. In this work, the channel sidewall profiles predicted by all models were somewhat different from the experimental springback data because the hardening parameters used in the hardening model were identified from the cyclic tension-compression tests in which the amount of reverse strain was fairly small compared to the amount of plastic strain that the sheet metal underwent during channel forming. These authors recommended that a large reverse strain in the cyclic characterization test would enable more realistic hardening parameters to be determined.
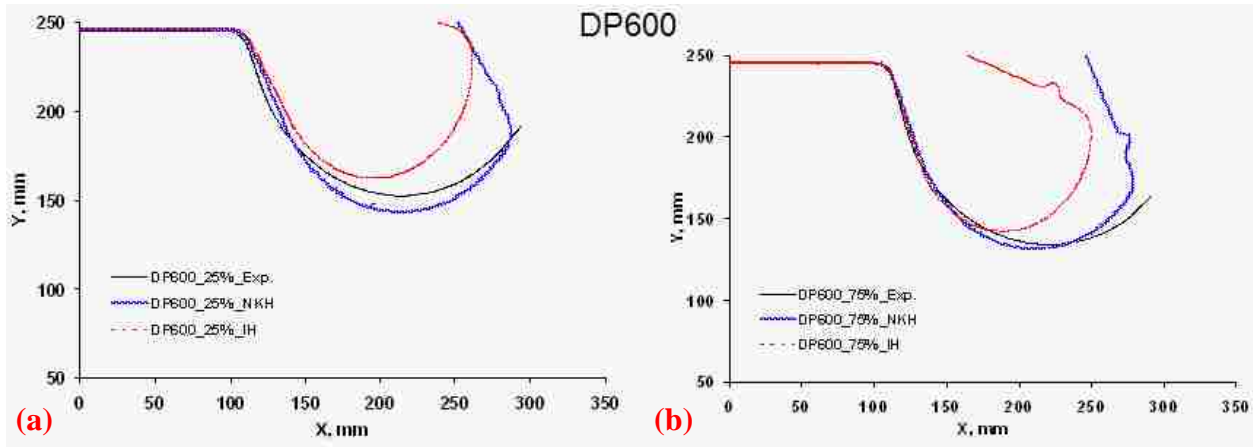
Figure 2.15 Effect of hardening model on the simulated profile of DP 600 channel section (a) at 25% (left) and (b) 75% (right) drawbead penetration [37]

2.3.4 OPTIMIZATION OF SPRINGBACK PREDICTIONS

In addition to developing a finite element model to simulate the forming and springback of stamped or drawn parts, many researchers have also investigated the use of optimization algorithms in conjunction with the numerical simulation tools. Indeed, an optimization algorithm can be set up to run a series of numerical simulations with different input parameters (i.e. product and process design parameters). The results from each simulation can then analyzed to determine the optimum forming conditions that will minimize springback. This section will provide a review of some of the springback optimization research that has been carried out in recent years.

Inamader et al. [79] developed an artificial neural network to predict springback in air bending. Lepadatu et al. [80] proposed a concept of experimental design and response surface methodology for optimum prediction of springback. The main challenge with this approach is the complexity of linking the finite element code to the optimization algorithm. Gassara et al. [81] developed a Gauss-Newton method coupled to ABAQUS standard finite element code and Python to optimize the springback of sheet materials. They optimized three process parameters such as, die entry radius, punch-die clearance, and the blank holder force of an L bending

process and ignored the effect of stroke, lubrication and friction. Their studies showed that clearance, die radius, and blank holder force have significant effects on the springback response.

Fu and Mo [7] conducted air bending tests on high strength steels sheets and used a genetic algorithm (GA) and a back propagation neural network (BPNN) to establish a model to predict springback: they predicted the springback angle and radius using the GA, and the punch radius using the BPNN approach. Artificial neural networks have the ability of associative learning, parallel processing, and a certain degree of fault tolerance. They found that the mechanical properties of the sheet metal and the punch radius have significant influence on springback in air bending. Moreover, the tool gap and the punch displacement only have a minor influence on the springback radius, but have a major effect on the springback angle. They concluded that the springback error can be reduced by selecting materials with lower yield strength, greater Young's modulus, greater thickness, lower tool gap and greater punch displacement [7].

Ruan et al. [82] also used the GA and BPNN, to predict springback of complex sheet metal parts. They found that springback predictions using the GA-BP model were quite accurate. The relative error of GA-BP model was lower than that of the BP and the regression model [82].

Liew et al. [83] developed a neural network model and used an Integrated Neural Network Evolutionary Algorithm to minimize springback for constrained, unconstrained, single and multiple objective problems arising in process design. To minimize the springback problem they used three methods: Random Search (RS), Evolutionary Algorithm (EA) and Integrated Artificial Neural Network Evolutionary Algorithm (ANN-EA). They showed that ANN-EA neural networks is capable of predicting springback reasonably well (within ±2%) and led to more accurate springback results than the EA method. Moreover, they reported that the presence

of draw beads during the forming process can also help to minimize stress gradients and springback [83].

2.4 EXPERIMENTAL CHARACTERIZATION OF THE CYCLIC BEHAVIOUR OF METAL SHEETS

The numerical simulation of sheet metal forming and springback has been shown to depend on the ability of advanced constitutive models to predict the actual behaviour of the sheet when it is deformed and unloaded. Prior to performing numerical simulations, however, the parameters in the constitutive models must be determined from experimental material data [84]. For instance, the anisotropy, the work hardening behaviour and the strain rate sensitivity of a particular sheet material are determined from a series of material characterization tests, and the more advanced the constitutive model, the more characterization tests are generally required.

The uniaxial tensile test has been extensively used to obtain the characteristic behaviour of a given sheet material, since it provides both the yielding and the work hardening behaviour. However, it only supplies data for unidimensional stress states, therefore additional tests are needed to experimentally determine sheet mechanical properties. For example, the hydraulic bulge test is often used to determine work hardening behaviour under a biaxial stress state. But it has already been pointed out that the cyclic work hardening behaviour of a sheet material has the most significant effect on the springback behaviour of a stamped or drawn component. Indeed, it is essential to obtain experimental cyclic stress-strain data that can exhibit the Bauschinger effect as well as the transient and permanent softening behaviour during reverse loading. Several types of test methods have been proposed to generate experimental cyclic stress-strain curves, but the purpose of this section is to review the test methods that are based on tension-compression, cyclic bending and cyclic shearing, since these are applicable to testing sheet materials.

31

2.4.1 TENSION-COMPRESSION TESTS

Many researchers have developed experimental testing facilities to determine the response of sheet materials during cyclic loading in uniaxial tension-compression. However, it is a challenge to carry out cyclic tension-compression tests on thin sheet specimens because of the tendency for buckling during compression. To overcome this problem researchers have taken various steps, such as, joining two or more sheets, changing the geometry of the test specimen and using anti-buckling devices.

Yoshida et al. [85] successfully bonded a few thin sheets of metal to provide greater support for the specimen during uniaxial compression. They also attached a special device (specimen holder) to the specimen by coil-springs to prevent buckling. They reported that cyclic stress amplitudes strongly depended on cyclic strain ranges and mean strains, and the larger the strain ranges, the larger the saturated stress amplitudes. They observed that during unloading Young's modulus decreased with plastic strain and finally saturated to a particular value after a large amount of plastics strain. Uemori and Yoshida [86] used the same technique to determine the cyclic plastic behaviour of copper sheets in cyclic tension-compression tests. To prevent the buckling, five pieces of sheet were bonded together with an adhesive. To minimize the effect of the adhesive layer on the stress-strain response the thickness of each adhesive layer was kept as thin as 0.01 mm which has extremely low deformation resistance.

Kuwabara et al., [87] and Lee et al. [48] reported that conventional tension-compression tests are difficult to set up due to buckling of the sheet specimen when the sample does not have an appropriate ratio of width to height. Masendorf and Zenner [88] reported that buckling can be prevented by means of friction minimized supporters. Kuwabara et al. [87] used fork shaped dies and developed a device with two pairs of sliding combs to reduce the unsupported area and

32

prevent buckling. Cheng et al. [89] used two pairs of wedge plates clamped together with a spring to eliminate the unsupported area and thus prevent buckling. Wang et al. [90] and Lee et al. [48] conducted compression-tension unloading tests by positioning the specimen between two flat plates on which a lateral force was applied to avoid buckling. Teflon was used in the anti-buckling device to reduce the friction between the specimen and the flat plates. Lee et al. [48] reported that good alignment of the specimen was required to prevent early buckling.

To prevent a sheet specimen from buckling when it is subjected to a tension compression cyclic load, Cao et al. [33] developed a fixture which can be used in a regular tensile-compression machine. They used a pre-loaded spring to hold the sheet specimen between four wedge-shaped blocks. The sheet specimen was designed with two sets of lateral fins that protrude from the wedge blocks and the relative displacement of the fins was used to calculate the strain in the gauge area. During a test, the upper fixture remains fixed while the lower fixture is allowed to move with a constant velocity. During reverse loading, they observed the common phenomena such as the Bauschinger effect, smooth elastic-plastic transient behaviour. The test fixture developed by the Cao et al. is shown in Fig. 2.16
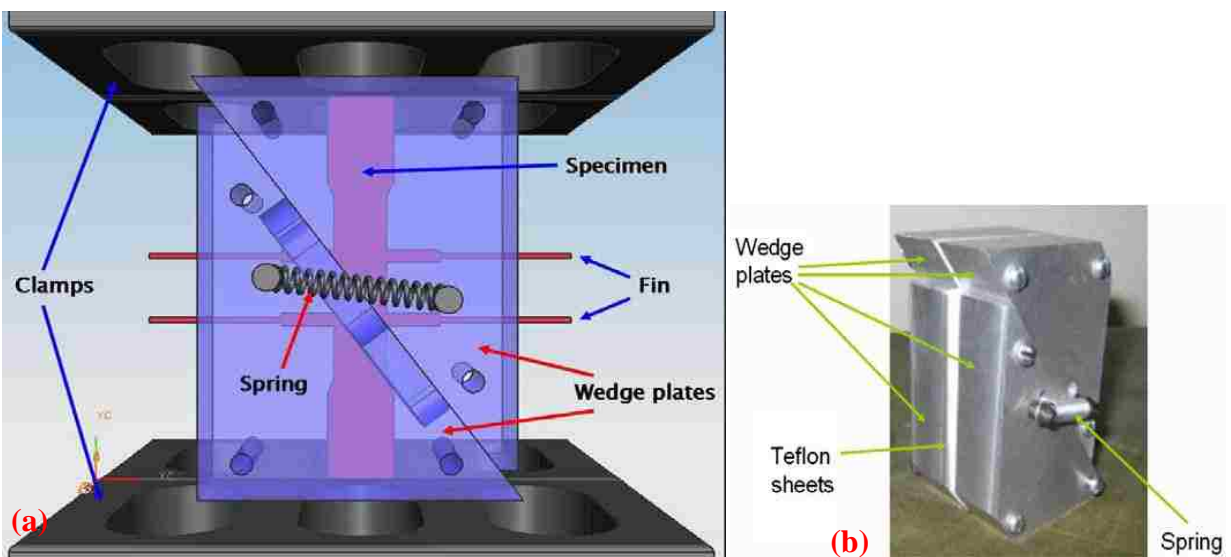
Figure 2.16 Schematic of double wedges uniaxial tension-compression test device [33]

Boger et al. [91] used solid flat plates as buckling constraints and applied a normal pressure through a pneumatic clamping system; this device is shown in Fig. 2.17. Boger et al. [91] also designed specimen geometry with a larger width to gauge length ratio than specified by the ASTM standard to further minimize buckling. Because of the testing conditions, the experimental test data required corrections for friction and off-axis loading. These researchers were successful in carrying out a continuous strain reversal to compressive strains greater than 0.20.

Figure 2.17 Schematic of the cyclic tension-compression device developed by Boger et al. [91]

2.4.2 CYCLIC BENDING TESTS

The cyclic bending test is another method to determine the cyclic behaviour of sheet metals that has been widely used by researchers because of its simplicity. Brunet et al. [42] performed cyclic loading of sheets using a pure bending device and proposed an inverse identification technique based on bending-unbending experiments for anisotropic sheet-metal

strips. They reported that the stress-strain behaviour can be determined numerically, without the use of FEA, by using a constant bending moment over the length of the specimen.

Zhao and Lee [1, 92] conducted three-point bending tests on mild and high strength steels to obtain the hardening characteristics during cyclic loading. They used a typical rectangular specimen of 203 mm x 25 mm. They neglected the strain-rate effects and only controlled the speed and displacement. Jiang [93] also performed three-point bending tests for springback investigations through cyclic bending of sheet metals. His experiments were not perfectly stable upon load reversal, and the measured punch loads vs. punch stroke curves were not continuous due to the lack of rigidity of the bending apparatus. Shen [94] carried out similar work with a modified equivalent three-point bending apparatus and improved the results. Eggertsen and Mattiasson [95] conducted three-point cyclic bending tests and used an inverse procedure based on response surface methodology to determine the parameters from the experimental load-displacement curve.

Urriolagoitia-Sosa et al. [96] conducted experiments on rectangular bars subjected to four-point bending and were able to observe Bauschinger effects. Compressive strains from bending were compared with compressive strains under uniaxial compression for strains on the order of 0.0006. The results showed that the tension and compression flow curves can be reasonably determined from bending tests.

Zhang and Hu [73] studied the stress distributions after bending, unbending and reverse bending in order to find out the differences in springback prediction results among different researchers with the same input. In this regard, they adopted three cyclic models such as: the kinematic model, the directional work hardening and isotropic work hardening model. Yoshida et al. [97] designed a bending machine to conduct uniform bending tests. The cyclic bending

tests were conducted to determine the stress-strain response of sheet metals including the Bauschinger effect and transient and permanent softening.

In spite of its simplicity, the bending test has some limitations in terms of providing cyclic stress-strain data for input into numerical simulations. The stress-strain curve is generally obtained by numerically simulating the bending test and comparing the output data with the experimental force vs. displacement data or bending moment vs. curvature data. The cyclic stress-strain data used as input in these simulations must then be optimized until the predicted bending data coincides with the experimental bending data. This inverse approach is not considered as reliable as direct stress and strain measurements. Moreover, higher strength materials tend to develop a plastic hinge when they are repeatedly bent and unbent, and therefore the strain amplitudes that can be achieved with this test are somewhat limited, particularly for less formable sheet materials.

2.4.3 CYCLIC SHEAR TESTS

The simple shear test has also become an effective way to characterize the yielding and work hardening behaviour of sheet metals. Unlike the uniaxial tension-compression test, the simple shear test does not present the same risk of buckling in compression nor does it lead to plastic instability and strain localization [84] which cause premature failure in tension. Moreover, the shear test can be performed on conventional tensile testing machines by using an appropriate fixture for gripping and loading the specimen. Also, the simple shear test can be used to provide yielding data for input into advanced yield criteria as well as cyclic work hardening behaviour up to large strains.

Two types of simple shear tests have been developed: the one-sided shear test and the symmetrical shear test. The one-sided shear test is the most basic way to perform a shear test in which the two clamped sides of the specimen move parallel to each other to generate a shear deformation in the gauge area. Meyer et al. [98] conducted simple shear tests to determine the yield stress of a sheet metal in simple shear, and they measured the shear strains using a digital image correlation technique (ARAMIS). Schikorra et al. [99] reported that the planar simple shear test appeared to be the most promising test for cyclic testing of sheet metals due to the facility with which the stress-strain relations can be determined and because of the absence of frictional influences. They developed a cyclic material testing equipment to determine work hardening behaviour with a view to predicting springback more accurately. Genevois [100], Rauch [101] and Barlat et al. [102] also successfully used the simple shear test for reverse loading at large strains. Although, this test seems simple, special attention is required to design a loading fixture that does not superimpose a bending moment on the specimen [45]. For shear tests conducted to high levels of strain, it appears that some slipping of the specimen in the clamps cannot be completely avoided [45]. Finally, Zhao [103] reported that out-of-plane wrinkling or buckling will occur after significant shearing.

The symmetrical shear test was first developed by Miyauchi [104,105,106] who presented a specimen geometry which consists of three clamped areas and two shear zones between them, as shown in Fig. 2.18. By displacing the middle section parallel to the two outer sections, the gauge areas between the clamped sections are deformed by simple shear. The load and displacement are continuously measured to determine the shear stress (τ) vs. shear strain (γ) curve.
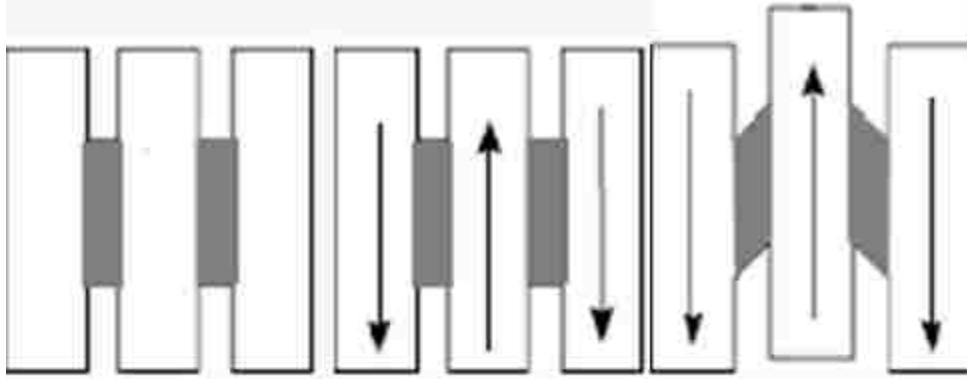
Figure 2.18 Schematic of the simple shear test sheet specimen developed by Miyauchi [104]

Initially, Miyauchi used sheet specimens with sharp corners and slots at the edges which made it more difficult to measure stresses and strains. Because the test was difficult to perform and the shear strain measurements were difficult to carry out using conventional methods [106], therefore, this test was not widely used. However, several researchers have modified Miyauchi's test to achieve more uniform stresses and strains up to large deformations. Merklein el al. [84], G'Sell et al. [107], and Bae et al. [108] emphasized the importance of using an appropriate specimen geometry that enables to generate simple shear over a relatively small gauge area. Boger et al. [91] showed that appropriately shaped specimens provide relatively uniform stress-strain distributions at low strains. However, as the deformation increases, shear bands may develop and end effects tend to become problematic. In addition, the strain levels at which the strain concentrations become a problem depend on both the material and the geometry of the specimen. An et al. [109] reported that the strain distribution in the gauge area is dependent on the specimen geometry and that the shear strain and stress usually increase rapidly from the edges but decrease toward the specimen centre [109]. For this reason, they adopted a mostly rectangular specimen with a long and narrow gauge area, as shown in Fig. 2.19.
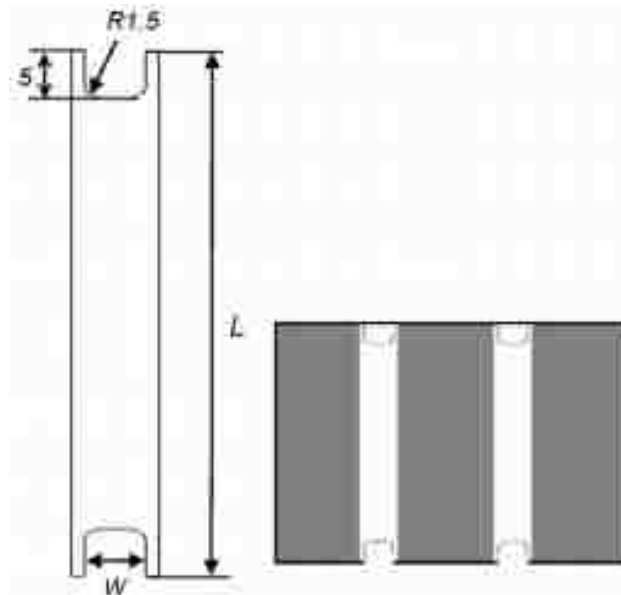
Figure 2.19 Symmetrical shear test specimen geometry used by An. et al. [109], in which L and W are the dimensions of the gauge area; the white areas are the shear zones and the grey areas are the clamping zones

The gauge area in a shear specimen always tends to have a non-uniform strain distribution. The influence of edges, borders and clamps may lead to locally significant deviations from the average shear strain. With increasing deformation, failure may be induced by crack initiation as a result of superimposed tensile stresses. In order to reduce non-uniform stress distributions in the gauge area, Bouvier et al. [110] recommended that the ratio of the gauge length to gauge width be at least 7 to 10, depending on the material. They conducted simple shear tests to characterize the plastic anisotropy of low-carbon steel and ultra-high strength steel sheets, and found that accurate shear strain measurements cannot be easily achieved with a conventional extensometer [110]. It was also observed that specimens with slots showed less stress concentrations, whereas plain rectangular specimens showed high local stress and strain concentrations. Bouvier et al. [110] reported that for most low-carbon steels, local strain concentrations are not a hindrance to achieving large shear strains, but for high strength steels

such with tensile strengths of 600 MPa or greater, premature failure occurred due to stress concentrations.

In sheet forming processes, reverse loading occurs wherever bending and unbending take place, such as when a sheet is pulled over a die radius and straightened after leaving the die radius. Therefore many researchers have carried out shear testing with one or more load reversals. For instance, Rauch [101], Bouvier et al. [110] conducted shear tests to estimate the anisotropy in sheet materials and characterize the hardening behaviour of sheet metal after a single strain reversal.

Thuillier and Manach [65] designed a shear test device and used it to characterize the cyclic hardening of sheet metals. The experimental set up of the testing apparatus used in the shear test is shown in Fig. 2.20. The device is directly connected to a tensile testing machine. A rectangular shaped sheet specimen, having a total area of 50 mm x 18 mm and a gauge area that is 4.5 mm wide, was used to perform monotonous shear tests. One side of the specimen is clamped in a fixed grip and the other side in a movable grip. The clamping of a specimen in the grips is achieved by tightening six screws with a torque wrench, and an optimal torque was determined to avoid slippage of the specimen in the grips. The movable grip is displaced at a constant speed. The simple shear strain was calculated by the ratio of the longitudinal displacement over the gauge width. The strains were measured with a commercial non-contacting optical strain measurement system named ARAMIS. The cyclic shear tests were performed in order to highlight the Bauschinger effect and to measure the kinematic hardening parameters.
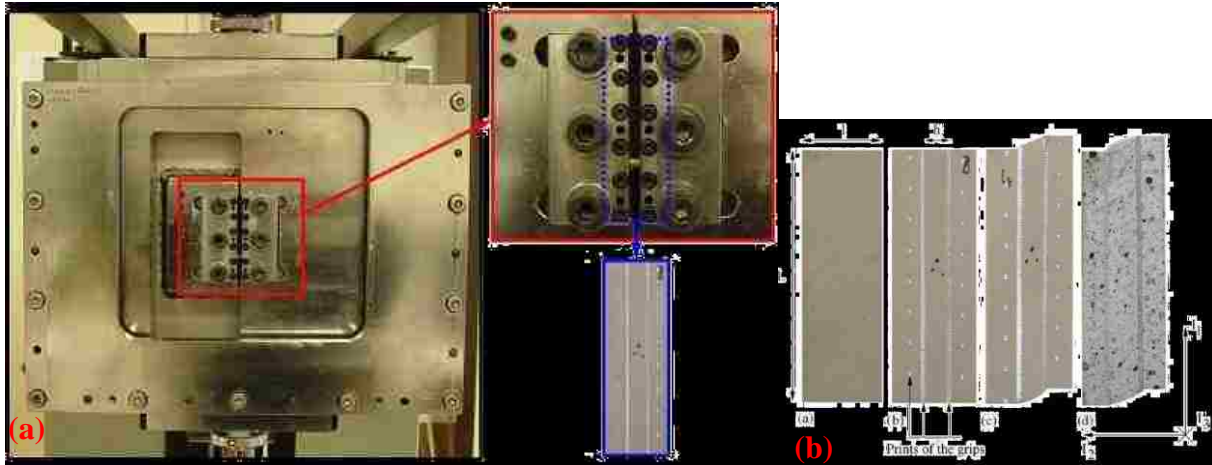
Figure 2.20 Photograph of the simple shear device developed by Thuillier and Manach [65] with a close-up of the grip system

Merklein el al. [84] performed simple shear tests based on a Miyauchi-type specimen to determine the plastic properties of Al-Mg sheets at large strains. They machined their specimens to reduce the thickness of the sheet metal in the shear zone: the initial sheet thickness was 1mm, and the thickness in the gauge area was reduced to 0.5 mm. The gauge area was 33 mm x 3 mm [84]. They reported that the optimal length to width ratio should be greater than 10 to minimize the unwanted normal stress along the loading direction. Also, the shear zone should be sufficiently large to avoid buckling due to grip constraints. In order to reduce edge effects that cause the state of stress to deviate from simple shear, these researchers designed the specimen with a corner fillet radius that was half the width of the gauge area that is 1.5 mm [84].

Zang et al. [27] conducted cyclic shear tests on DP500 and DC04 sheet materials. They also used rectangular specimens with a gauge area of 50 mm x 4 mm to determine the Bauschinger effect in these sheet materials. A digital image correlation system was used to determine the average shear strain across the rectangular gauge area. The specimen used in their experiments and the homogeneity of the strain distribution is shown in Fig. 2.21.

41
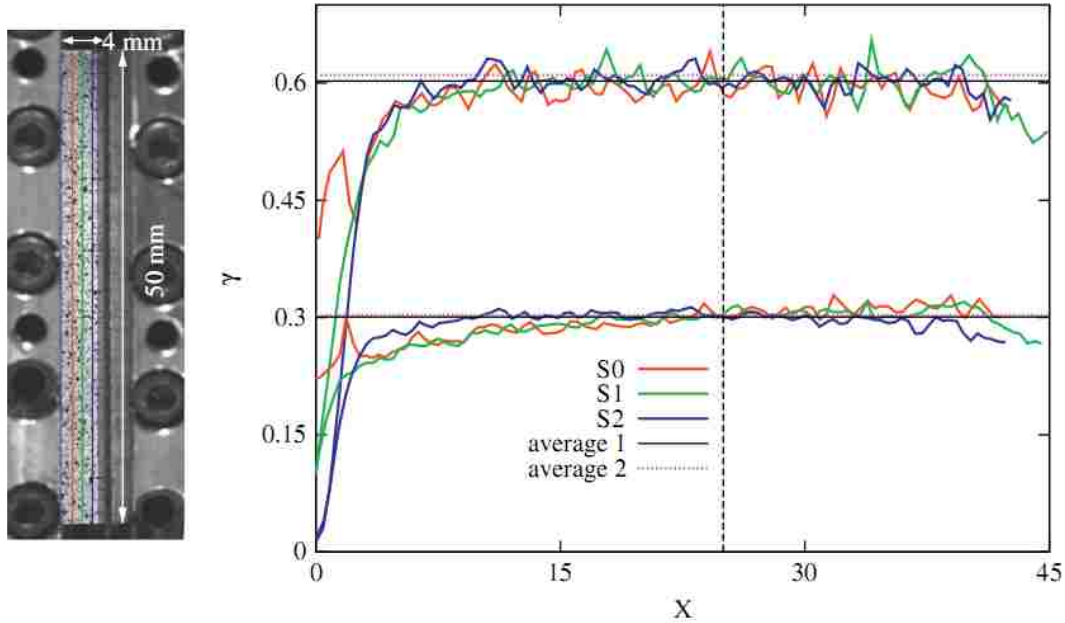
Figure 2.21 Simple shear test specimen developed by Zang et al. [27] showing the homogeneity of the strain distribution along three sections of the gauge region (S_0, S_1, S_2) parallel to the shear direction, for $\gamma = 0.3$ and 0.6, average 1 indicates the entire gauge surface and average 2 indicates the reduced area in the specimen center, and X denotes the sample length

Wack and Tourabari [111] conducted shear tests on sheet specimens and emphasised the design of the test specimen. They reported that the ratio of the width to the thickness in the gauge areas should be small enough to avoid buckling of the sheared zone, and the ratio of the length to the width should be sufficiently large to minimize the error due to non-uniformity of the shear stress and strain at the two ends of the specimen.

Meyer et al. [98] also developed a cyclic shear test facility based on Miyauchi-type specimen geometry, as shown in Fig. 2.21. A specially designed fixture was used that can allow to measure wide range of strain through the ARAMIS system. They conducted their shear tests at strain rates up to 2 x $10^2 s^{-1}$. The test jig and the rectangular specimen with two shear zones are shown in Fig. 2.22 (a) and (b), respectively.
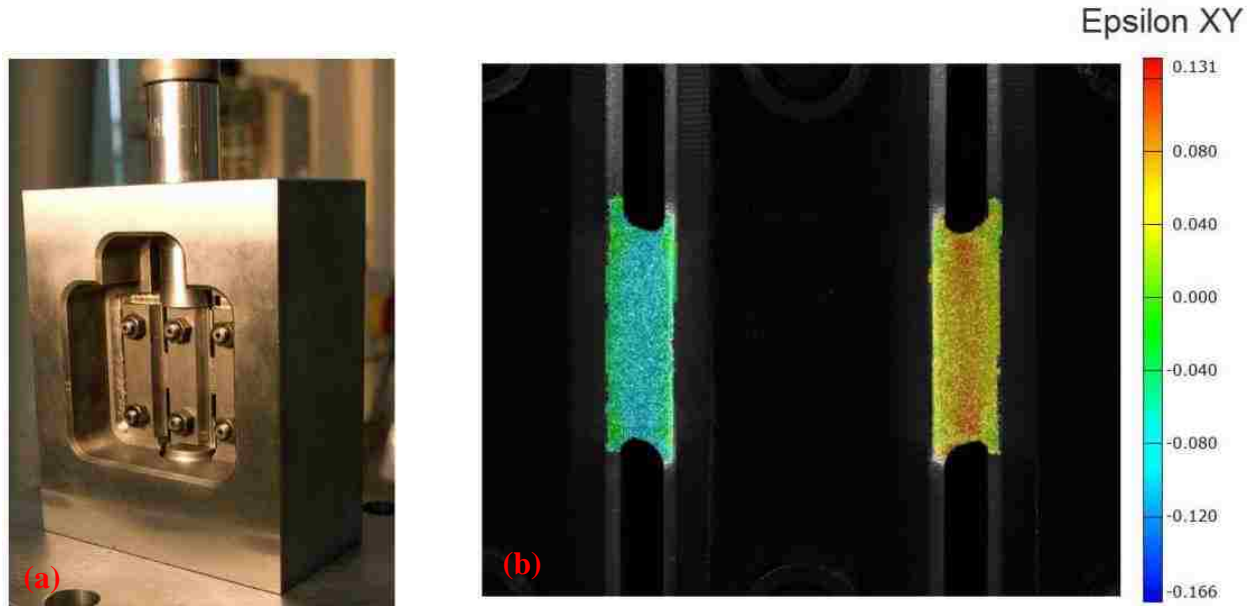
Figure 2.22 Shear test facility developed by Meyer et al. [98] showing (a) the jig and specimen (b) the strain field in the shear zones measured with the ARAMIS system

Schikorra et al. [99] reported that the typical sheet metal thickness in the stamping industry varies from 0.4 mm to 2.0 mm. In order to avoid buckling in the gauge area they designed a shear zone that was 5 mm wide for the sheet metals which were thicker than 0.5mm. An et al. [108] also analyzed the geometry of different sheet metal specimens using finite element simulations and concluded that the length to width ratio in the gauge area should be kept between 5 and 10. They observed that the corner radius 'r' in the slots have a minor effect on the strain distribution, while the effect of specimen geometry was significant. They found that the average shear stress was approximately 2.5% lower than the maximum shear stress for a gauge area with an aspect ratio of 10. For the specimen with an aspect ratio of 5 the maximum shear stress was about 5% greater than the average shear stress. Based on simulation results, An et al [53] concluded that the specimen geometry was the most important factor that determines the uniformity of the shear stress in the gauge area.

Measurement of the shear strain is quite complex using conventional strain measurement techniques. During a simple shear test the principal axes of stress and strain may tend to rotate if the specimen slides in the grips. Because of the relative motion of the specimen in the grips, Rauch and G'Sell [112] calculate the shear strain with respect to the relative grip displacement. Yoon et al. [113] used a correction factor being measuring the shear strain since the specimens were sliding during the shear test. However, it has been highly recommended that an optical strain measurement technique be used to measure the local shear strains instead of calculating them from the displacement of the grips [114] as it eliminates the undesirable contribution of the relative deformation between specimen and grips. Many researchers have used optical strain measuring systems to accurately determine the strains during experimental shear tests. Bouvier et al. [109] used a video camera to measure the shear strain. Merklein and Biasutti [84], Thuillier and Manach [65], Meyer et al. [98] and Liewald et al. [115] all used optical measurement techniques based on the digital image correlation method to track the displacement of randomly distributed speckle points in the shear zone and to measure the strains and strain rates based on these deformations.

2.4.4 ADVANTAGES OF CYCLIC SHEAR TESTS

This literature review has shown that the conventional tension-compression test is difficult to conduct with sheet specimens as it requires an anti-buckling device and generally requires post-analysis to eliminate the effects of friction and of biaxial stress states induced by the anti-buckling system. Cyclic bending tests can easily lead to the development of a plastic hinge, particularly in higher strength sheet specimens, and are therefore limited to lower strain amplitudes.

The shear test, on the other hand, can generate cyclic stress-strain curves up to large strain amplitudes, provided the specimen geometry is designed with a gauge area that has a suitable aspect ratio, and provided the loading fixture can minimize undesirable bending moments and slippage of the specimen in the grips. Indeed, the effectiveness of the shear test is somewhat dependent on achieving a relatively uniform stress and strain distribution in the gauge area. Although, there are boundary effects that tend to generate stress concentrations in the corners of the shear zone [65], researchers have shown [107] that these stress concentrations can be minimized by using a long and thin shear zone. Therefore a careful selection of the ratios between the length, the width and the thickness of the shear zone can lead to a uniform strain distribution. Based on this literature review, it was decided that the shear test is probably the most promising type of test for experimentally determining the cyclic behaviour of sheet materials.

This review of prior research also points toward developing a shear test that is based on a symmetrical shear specimen as originally proposed by Miyauchi. The objectives of this work are to design an appropriate specimen geometry and a loading fixture that is simple, rigid, easy to set up and cost effective in comparison to the existing fixtures which have been developed by the other researchers. Some specific objectives of the proposed shear test are listed below:

1) The specimen design should lead to a uniform strain distribution in the gauge region

2) Tests must be performed in a conventional or universal testing machine

3) The loading fixture should be apply a balanced centric loading structure

4) The loading fixture should be simple in its design

5) The loading fixture should be suitable for testing sheets with a thickness up to 3.0 mm

6) The loading fixture should be sufficiently rigid to test sheet materials with a tensile strength up to 1000 MPa

7) The loading fixture should be easy to fabricate, assemble and set up

8) The specimen should be visible throughout the test to permit the use of an optical strain measurement system based on DIC techniques

3. DESIGN OF THE CYCLIC SHEAR TEST FIXTURE AND SPECIMEN

This chapter provides a detailed description of the cyclic shear test fixture, the test specimen, and the methodology which was used to complete the design. The chapter consists of three sections: Section 3.1 presents the design methodology, and Section 3.2 describes the design, modelling and optimization of the cyclic shear test fixture and its various components. Finally, the design of cyclic shear test specimen, its numerical modelling and optimization of the specimen geometry are presented in Section 3.3. The individual fixture components and assembly drawings with the bill of materials are provided in Appendix A.

3.1 DESIGN METHODOLOGY

The main objective of this work was to design a cyclic shear test facility (i.e. a test fixture with corresponding test specimens) with a view to experimentally determining the cyclic stress-strain behaviour of sheet metals, using a universal testing apparatus. During the design process the geometry of the test specimen was chosen in such a way that it would be fully supported both during the loading and the reverse loading. The length-to-width ratio of the specimen gauge area was selected so that large strain amplitudes can easily be reached without failure. Special attention was given to design a specimen that exhibits a uniform strain distribution in the gauge area, and the effects of the applied loads on the strain distribution were determined using numerical simulations of the cyclic test.

A numerical analysis was also performed to design a test fixture that allows for free movement of sheet metal specimens in the machine loading direction, but prevents wrinkling or

tearing under cyclic loading conditions. Once the design parameters were optimized the fixture was fabricated and the test specimens were prepared in order to conduct cyclic shear tests.

The design was completed by considering a set of design related stages which are: concept generation, modelling using computer aided design (CAD) software, analysis, numerical simulation of cyclic testing using the finite element code LS-DYNA, design optimization, development of the final design. The steps involved in the design process of a cyclic shear test are shown in the flow diagram in Fig. 3.1.
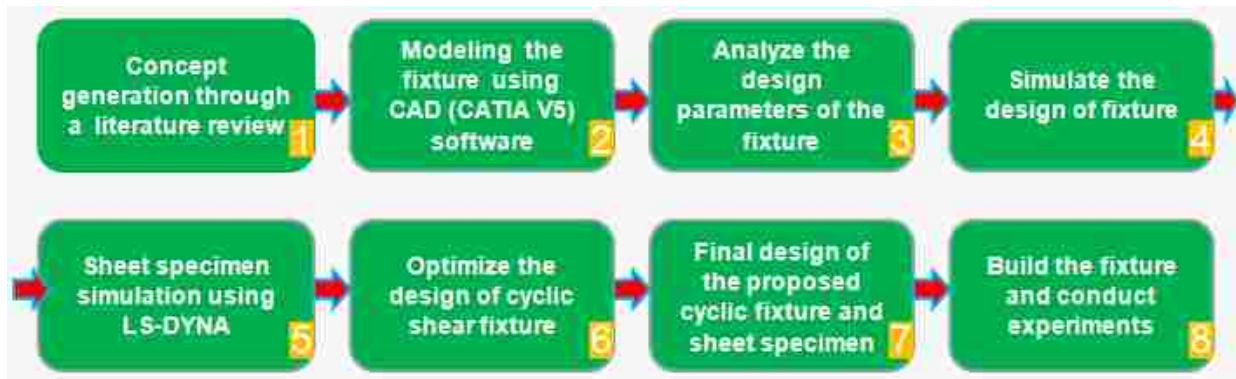
Figure 3.1 Flow diagram of the design processes for a cyclic shear test facility

3.2 DESIGN OF A CYCLIC SHEAR TEST FIXTURE

This section provides the detailed description of a CAD model, which relates to the design of the cyclic shear test fixture and its components. To create 3D models and 2D drawings and to conduct FEA simulations of the test fixture and its components, FEA software CATIA V5, was used in this research. The load bearing capacity, deflection, deformation, stress-strain distribution of the fixture and its components were also analyzed by using this software. This section consists of three subsections. Section 3.2.1 describes the design of the test fixture components and Section 3.2.2 discusses the necessity for design optimization of the cyclic shear

test fixture. Finally, Section 3.2.3 presents a finite element analysis of the fixture to determine the maximum deflections that will occur during testing.

3.2.1 DESIGN OF THE CYCLIC SHEAR TEST FIXTURE

The cyclic shear test fixture was designed following a literature review that highlighted the advantages of the facilities developed by different researchers. To complete the cyclic shear test design, a set of design related issues were considered, such as the purpose of these tests, the most extreme material properties that would be encountered, sheet material behaviour during tests, and other test related issues. Prior to modelling the cyclic shear fixture it was also necessary to determine the type of testing machine that would be used, the capacity of the machine, the types of sheet specimens, and the shape and geometry of the specimens. It was also important to understand the fixture and specimen installation process, the experimental data to be measured during the tests, the testing duration, and the way of conducting experimental tests. A CAD model of the test fixture was developed using CATIA V5 software. The CAD model of the cyclic shear test fixture and the INSTRON universal testing machine in which it is to be mounted are shown in Fig. 3.2.

The proposed cyclic shear test fixture was designed in such a way that it can fit between the upper (fixed) and lower (movable) flange of the INSTRON universal testing machine, which is available in room 203 of Essex Hall, at the University of Windsor. The total length of the fixture is 610 mm, and an additional supporting flange 45 mm thick is required to adjust the travelling length during testing.

49
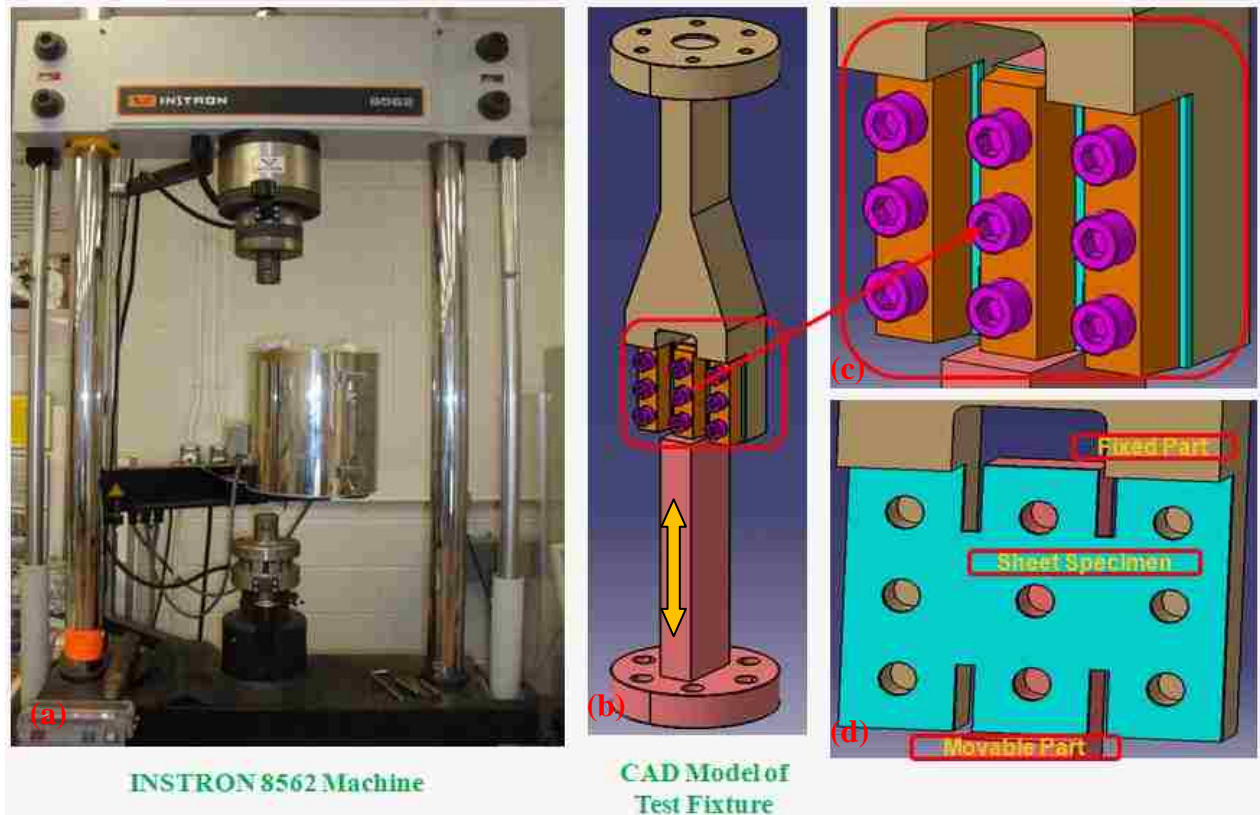
Figure 3.2 Photograph of (a) the INSTRON 8562 universal testing machine, (b) a CAD model of the cyclic shear test fixture, and (c) the details of holding blocks and bolts (d) the sheet specimen positioned in the testing fixture

The travelling distance of the lower, movable fixture was determined to be 80 mm in both the upward and downward directions to allow for large strain amplitudes during testing. The fixture was designed so that the specimen will remain in the same plane when it is clamped in the upper and lower testing fixtures. A gap of 0.5 mm was designed between the edges of the sheet specimen and the nearest surfaces of the upper and lower fixtures, so that the acting forces would be transmitted from the fixtures to the specimen via the flat specimen surfaces rather than through the sheet edges. Moreover, this allows for easy installation of the sheet specimen prior to testing. A description of the various components of the cyclic shear test fixture is presented in the following paragraphs.

50

<u>Fixed Upper Part</u>

The fixed upper part of the fixture is a 'Y' shaped piece and can be attached to the upper head of universal testing machine through bolts. The 'Y' shape geometry was chosen to provide minimum deflection at maximum load and to withstand the maximum admissible load. The fixed upper part is 360 mm in length, 100 mm wide, and 30 mm in its thickness. One end of the fixed upper part has a flange having dimensions Ø140 mm x Ø38 mm x 30 mm. The thickness of the fixed upper part geometry was determined so as to prevent buckling during compressive loading. The detailed drawing of this part can be found in Appendix A.

In the parametric modelling of the upper fixture it was specified that it would be built from a solid bar to ensure more rigidity and straightness, and prevent distortion or excessive deflection during cyclic loading. Therefore it was specified to be made from AISI 1040 chromium-molybdenum annealed steel which has excellent machinability properties and superior strength. The CAD model of the upper part of the fixture and a photograph of the actual part are shown in Fig. 3.3a and Fig. 3.3b, respectively.
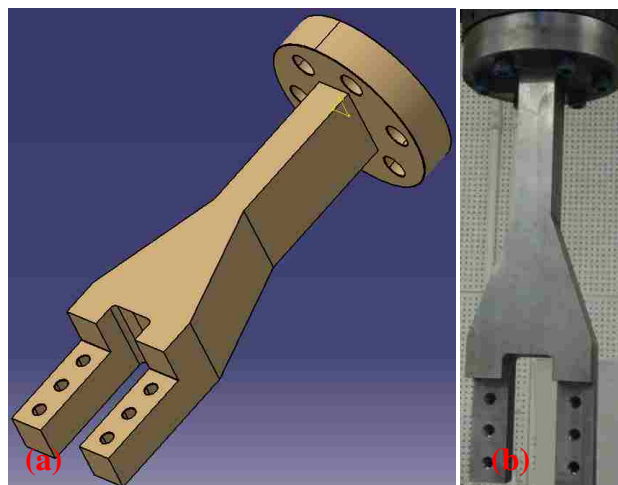
Figure 3.3 (a) CAD model of fixed upper part of cyclic shear fixture (b) photograph of fixed upper part of cyclic shear test fixture

Movable Lower Part

   The lower movable part of the fixture is an 'I' shaped component, which is fastened to the lower hydraulic actuator of the universal testing machine with six bolts. It is designed to move up and down along the loading direction of the machine. This lower part is 330 mm long, 100 mm wide and 30 mm thick. It has a circular flange at one end having dimensions $\emptyset$140 mm x $\emptyset$38 mm x 30 mm. The detailed drawing of this part is provided in Appendix A. This part was designed in such a way that it can easily withstand a maximum specified load of 100 kN, and provide minimum deflection at maximum load. The lower movable part was specified to be built from a machined, solid bar which ensures its rigidity, perpendicularity, and straightness during cyclic loading. It might have been easy and cost effective to fabricate this lower part as a welded sub-assembly, but a welded part was not considered because the welding itself typically causes distortion of the components. The CAD model of lower movable part of cyclic shear fixture and a photograph of the actual fabricated part are shown in Fig. 3.4a and Fig. 3.4b, respectively.
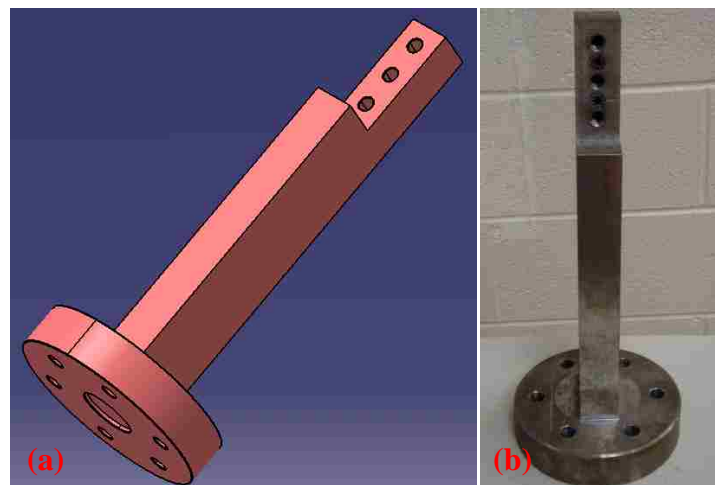
Figure 3.4 (a) CAD model of movable lower part (b) photograph of movable lower part of cyclic shear test fixture

Holding Blocks

The fixture is designed with three blocks that can be bolted to its upper and lower parts to hold the sheet specimen in place. Each holding block is 80 mm long, 25 mm wide and 15 mm deep. A detailed drawing of a holding block is attached in Appendix A. The height of the blocks was chosen so that the fixture can bear maximum compressive load and can prevent buckling satisfactorily. The width of each block was reduced from 25 mm to 20 mm to allow light to shine on the gauge areas of the specimen during testing. The blocks were also designed with a tapered side to ensure that the gauge areas of the specimen are visible to an optical strain measurement system. Moreover, the dimensions of the blocks were determine in such a way that they would not contact the upper and lower parts of the fixture even at maximum load. Finally, a chromium-molybdenum annealed AISI 1040 medium carbon steel was chosen to fabricate the holding blocks. A CAD model of one holding block and a photograph of actual blocks are shown in Fig. 3.5a and Fig. 3.5b, respectively.
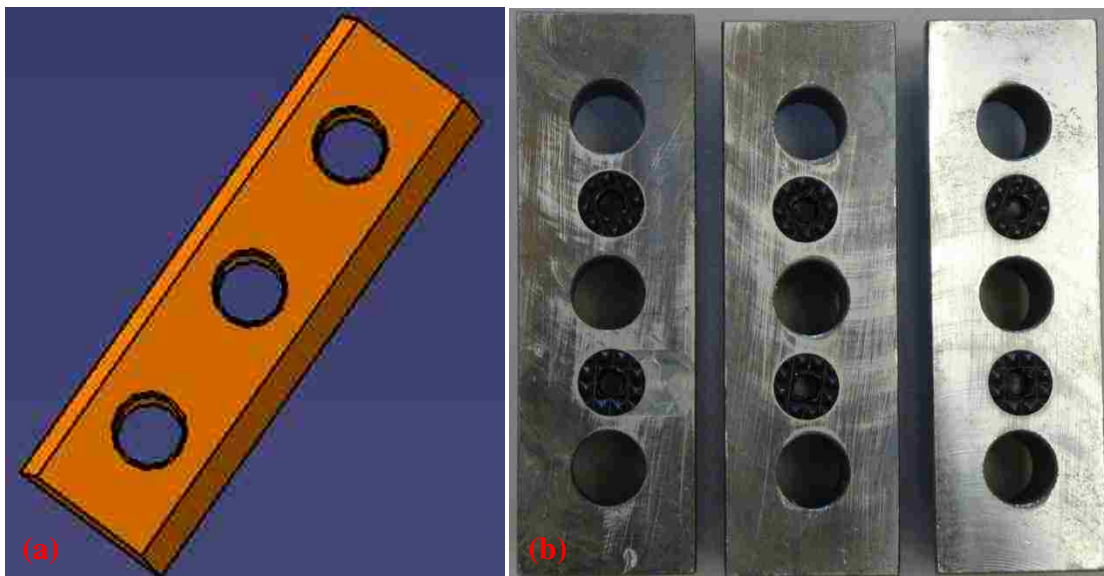
Figure 3.5 (a) CAD model of holding block (b) photograph of holding blocks of cyclic shear test fixture with inserted circular knurled blocks

Standard socket head cap screws were used to fasten the sheet specimen between the blocks and the upper and lower parts of the loading fixture.
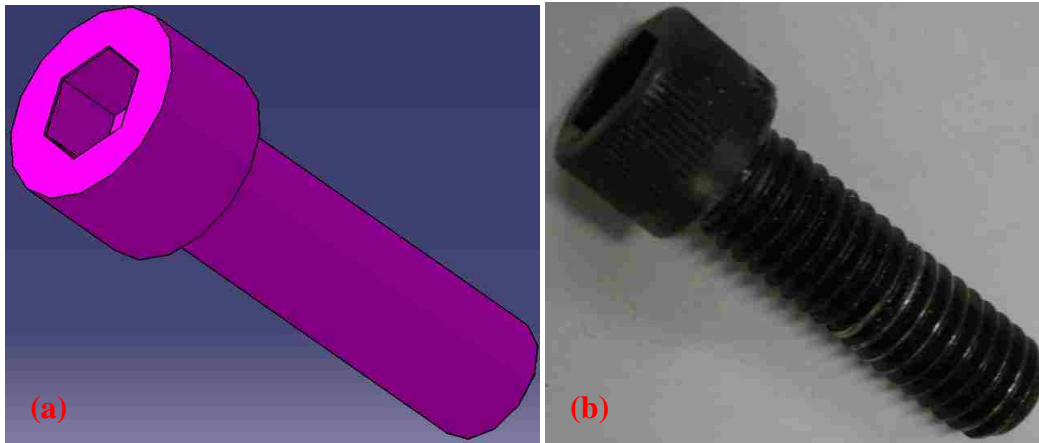
Figure 3.6 (a) CAD model and, (b) photograph of a socket head cap screw

The strength and load bearing capacity of bolts were considered during the design: the bolts can bear a torque of 140 N-m and have a minimum tensile strength of 1200 MPa, although a torque no greater than 70 N-m was applied when mounting the specimen prior to testing. The length of each M10 x 1.25 bolts is 30 mm, with a class of fit 5g6g. A CAD model of a bolt and a photograph of an actual bolt are shown in Fig. 3.6a and Fig. 3.6b, respectively.

3.2.2 OPTIMIZATION OF THE CYCLIC SHEAR TEST FIXTURE DESIGN

Design optimization is essential when considering the design of a new product. The optimization was performed in regards to the geometry of the proposed fixture. Other objectives considered during the optimization process were to reduce the weight and the cost. Optimization also helps to improve the quality and performance of the fixture. The integration of optimization

techniques with FEA and CAD was considered during the product design stage. Engineering expertise is required in order to identify the design variables and to reach an optimal design.

The World Auto Steel Organization, which is responsible for design and development of future generation vehicles, has emphasized that new generation car models should be optimized according to 3G [116, 117]. 3G signifies the part geometry, the grade, and the gauge of sheet metals. The 3G system was also followed in order to optimize the cyclic shear fixture and cyclic shear sheet specimen. The parameters of the fixture which were optimized are: the length, width, and the thickness of the upper and lower parts of the fixture, including the diameter and thickness of flanges. In addition, the gap between the specimen and the upper and lower parts of the fixture, different profile radii, the number of bolts required to clamp the specimen, their sizes and positions, the geometry of holding blocks, the load bearing capacity of the fixture, the stress concentrations and deflections due to applied load were also optimized. CATIA V5 knowledge tool was used as a design optimizer to accomplish the optimization of this shear test fixture. However, the CATIA knowledge tool has some limitations: it does not allow the optimization of multiple objectives and variables as do other commercial optimization packages.

3.2.3 DEFORMATION OF THE TEST FIXTURE

In order to optimize the design of the test fixture, however, it was necessary to ensure that it would not deform excessively during testing, as this would impose an undesirable bending deformation mode on the test specimen. The maximum deflection of the cyclic shear test fixture was therefore determined numerically by carrying out a FEA of the deformation of both the virtual fixture and the sheet metal specimen. This numerical analysis was performed using the linear finite element analysis available in CATIA V5.

The displacement of the lower movable fixture was seen to have an effect on the entire fixture, since the load is applied to the specimen through the lower fixture during testing. Although, the upper part is essentially fixed, it nevertheless undergoes some deflection during cyclic loading due to the transfer of loads through the sheet specimen. The FE model showed that the deflection of the 'I' shaped lower movable part of the fixture was negligible in comparison with that of the 'Y' shaped upper fixed part.

The maximum deflection of each arm of the fixed upper part of the cyclic shear test fixture was found to be 0.157 mm when the testing machine was operating at maximum capacity (100 kN) in tension, as shown in Fig. 3.7a. Each arm of the upper fixture also deflected by 0.046 mm during the compression cycle of the machine (−100 kN), as shown in Fig. 3.7b. The maximum von Mises effective stress developed in the upper fixture was 208 MPa at maximum load; this is half the value of the yield stress of AISI 1040 steel which was used to build the fixture. The maximum von Mises stress was 372 MPa in the lower fixture at maximum load, which is again significantly less than the yield stress of this grade of steel. It can be concluded that the upper and lower parts of the fixture will satisfactorily withstand the maximum load capacity of this universal testing machine, even under cyclic loading conditions.
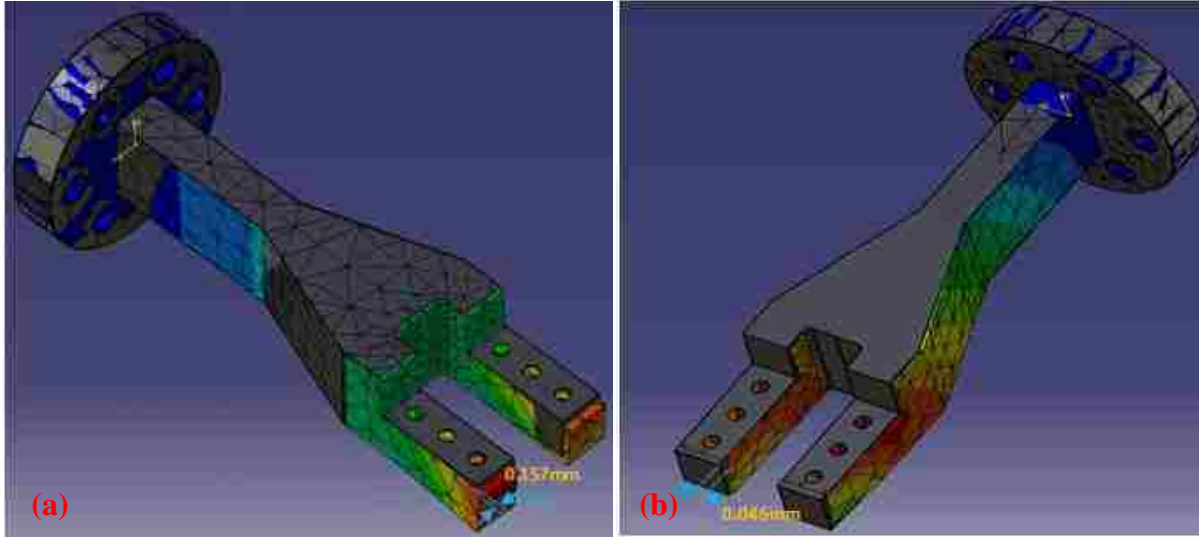
Figure 3.7 Maximum deflection of the fixed upper part of the cyclic shear test fixture (a) during tension and (b) during compression

3.3 DESIGN OF A CYCLIC SHEAR TEST SPECIMEN

Researchers have designed different types of shear test specimens to determine the cyclic behaviour of sheet metals; many of these are described in the literature review of Chapter 2. This section provides a detailed description of the design of a shear test specimen that fits in the testing fixture described in the previous section. The shape of the sheet specimen must meet certain design requirements and should also comply with existing testing standards. In this development work CATIA V5 was used to create a 2D CAD model of a sheet specimen, and the finite element code LS-DYNA was used to generate the 3D model, to simulate a cyclic shear test and to analyze the stress and strain distributions in the sheet metal specimen. This section consists of two subsections: Section 3.3.1 describes the design of the test specimen, Section 3.3.2 describes the finite element simulations of the shear tests to ensure a uniform stress distribution in the specimen gauge and Section 3.3.3 discusses the optimization of the specimen design.

The ASTM has developed a standard B831-05 [118] for shear testing of aluminum alloy sheet products. A schematic of the ASTM standard B831-05 specimen is shown in Fig. 3.8. The shear test specimen has a single shear zone and can be mounted in a universal testing machine without extensive modification. Because of the arrangement of the slots, the area between the fillets is sheared when a tensile force is applied to the ends of the specimen. The ASTM specimen is not suitable for cyclic shear tests because it would buckle under reverse (compressive) loading [119].
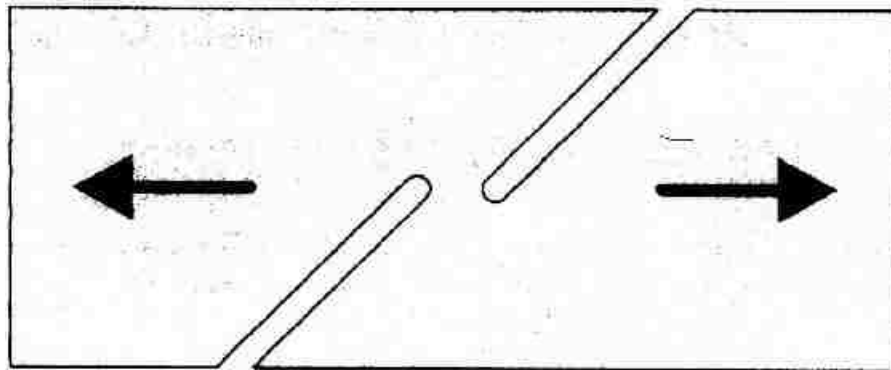
Figure 3.8 ASTM B831 shear test specimen for sheet materials [118]

3.3.1 DESIGN OF THE CYCLIC SHEAR TEST SPECIMEN

To the best knowledge of the author, there is no standard for the design of AHSS sheet specimen for cyclic shear tests. Therefore a new shear specimen was designed partly on the basis of the literature review and partly as a result of original ideas developed during this project. In addition, numerical simulations and design optimization led to further improvements in the design of a sheet specimen suitable for cyclic shear tests.

Special attention was given to the design of this shear test specimen, and many design-related factors were considered, such as geometry, material type and sheet thickness as they have

an influence on the stress and strain distributions in a loaded specimen. It has been clearly shown that the geometry of the specimen has a significant influence on cyclic shear test results; therefore the aspect ratio (i.e. the length-to-width ratio) of the gauge area was selected such that a uniform strain distribution developed in the shear zone. The width of the gauge area was chosen so that it would be clearly visible to a stereo optical strain measurement system. The gauge length-to-width ratio and the width-to-thickness ratio which provided the most uniform strain distribution were chosen, as this also prevents from premature failure due to stress concentrations at the edge of the specimen. Moreover, the ratio of the width-to-thickness was kept sufficiently small to avoid wrinkling in the sheared zone. In the final design, a 40-mm long and 5-mm wide gauge region was selected.

Typical sheet thicknesses in the metal forming industry vary from about 0.4 mm to 2.0 mm, and several researchers have adopted a 5-mm wide gauge in order to avoid wrinkling in the shearing zone [99]. Another design requirement was that the test specimens should be made from practically any grade of automotive steel, even the AHSS that are in demand because of a mandate for constant weight reduction. This material factor required that the flat specimen be designed such that significant shear loads could be applied to the fixture and the specimen without wrinkling or twisting out of plane. Therefore the specimen was designed to be clamped into place using nine bolts, which helped to not only ensure a uniformity of stresses and strains in the gauge area, but also increase the clamping force during cyclic loading.

A rectangular specimen without any slots leads to premature failure due to stress concentrations at the edge of the specimen. To avoid this problem, the specimen was designed with two sets of opposing slots. In preliminary designs, slots with sharp corners were considered to facilitate shearing in the specimen gauge. However, there are two problems associated with

sharp slots: this creates stress concentrations and prevents reaching higher strain amplitudes. To achieve high strain amplitudes, to obtain a uniform strain distribution, and to avoid stress concentrations in the corners of the gauge area, corner radii of 2 mm were considered at the end of the slots instead of sharp corners. A detailed drawing of the proposed sheet specimen is shown in Appendix A. A CAD model of the sheet specimen and a photograph of a machined sheet specimen are shown in Fig. 3.9a and Fig. 3.9b, respectively.
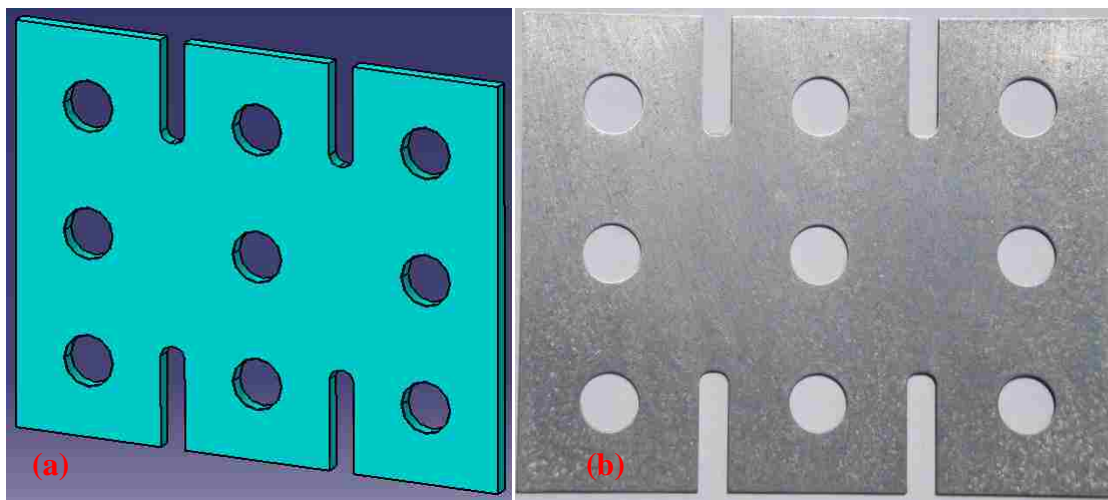
Figure 3.9 (a) CAD model and (b) photograph of the proposed sheet specimen used with the cyclic shear test fixture

3.3.2 NUMERICAL SIMULATION OF THE CYCLIC SHEAR TESTS

A non-linear finite element analysis of the shear tests was carried out in order to predict the stress and strain distributions in the shear specimen when it is under load, and to verify the uniformity of the stresses and strains in the gauge area. This section describes the development of the finite element model as well as the selection of material and numerical parameters that were used in the simulations.

The preparation of the numerical model was done using LS-PREPOST, version 2.4, which is part of the LS-DYNA finite element software package. Due to material symmetry and the symmetry of the applied load, only half the shear specimen was modelled. Belytschko-Tsay 4-noded quadrilateral shell elements were used to build a mesh of a half-symmetry model of the specimen. In order to carry out the simulations, a number of assumptions were made:

1) The sheet metal is considered homogeneous and isotropic and therefore the von Mises yield criterion was used for simplicity

2) The sheet metal work hardens according to a power law function that was approximated using piece-wise linear stress-strain data

3) Loading was applied through the node sets of the model

4) Belytschko-Tsay 4-noded quadrilateral shell elements were used to mesh a half-symmetry model of the specimen

5) Each element had 5 through-thickness integration points

6) Boundary conditions were applied as they exist in the experimental shear test

The holding blocks and fixture were not included in the numerical model. Tooling was assumed to be rigid, and the load was therefore applied directly through the node sets of the sheet specimen model. The translation and rotational movement of the nodes along the symmetry plane of the specimen were completely constrained. Translational constraints were also applied to the nodes that lie around the circumference of the bolt holes, which allowed them to rotate around the Z-axis (normal to the sheet surface) and translate in the Z-direction, but not to translate in the X- and Y-directions.

The commercial finite element code LS-DYNA version 971, revision R4.2 was used to carry out the simulations of the shear tests. The numerical analysis was based on a rigorous Lagrangian elastic-plastic finite strain formulation. The mechanical properties and work hardening behaviour of each sheet material can be found in Chapter 5, Section 5.2. The simulation results show that the cyclic shear test was essentially quasi-static, since the kinetic energy at the end of the simulation was very low; in fact the internal energy was 350 times greater than the kinetic energy.

In order to verify the sensitivity of the model to the mesh density, several models were created with different mesh densities, defined as coarse, average and fine meshes. The element size for the coarse mesh was 1 x 1 mm^2, which led to a model with 3503 elements and 3746 nodes. The model having an average mesh density was made up of 5157 elements and 5479 nodes. The element size was kept at 1 x 1 mm^2 throughout the specimen, except in the gauge region where the element size was reduced to 0.25 x 0.25 mm^2. A fine mesh model was also built to obtain more accurate stress and strain data. The element size was 0.5 x 0.5 mm^2 throughout the specimen, which led to a model with 13700 elements and 14188 nodes.

The influence of the different mesh sizes was analyzed through a series of simulations. The stress and strain distributions in the gauge region were analyzed for each model, and it was observed that the finer mesh led to a more uniform strain distribution. Comparisons of the stress and strain distributions in the gauge region resulting from the three different meshes are shown in Fig. 3.10 and Fig. 3.11.
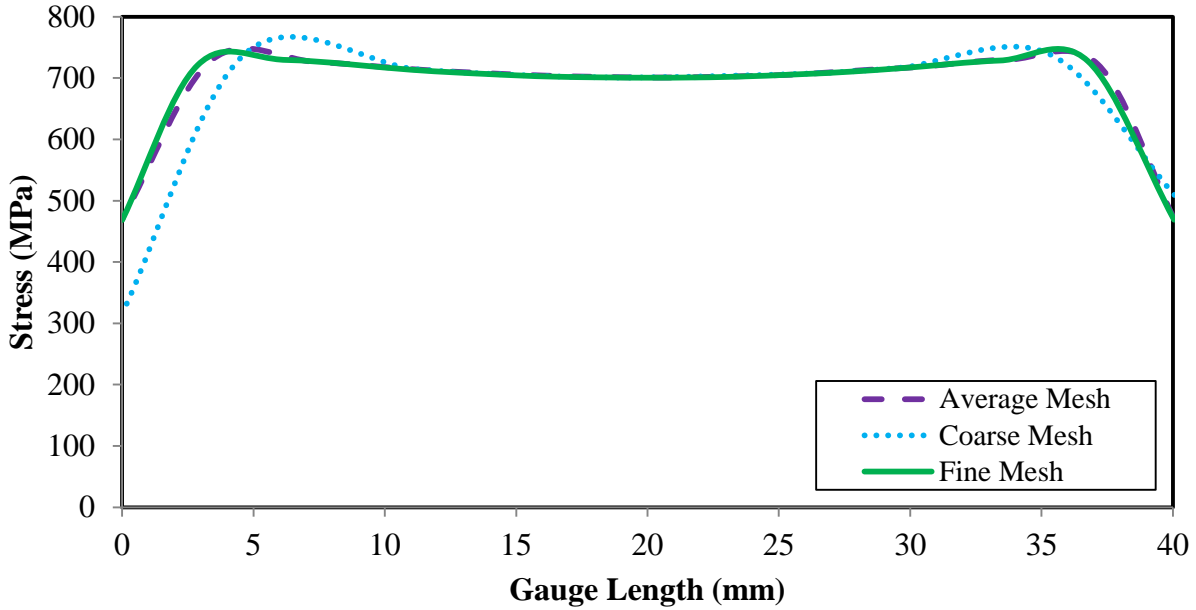
Figure 3.10 Comparison of the predicted stress distribution along the length of the gauge area of the shear specimen for different mesh sizes
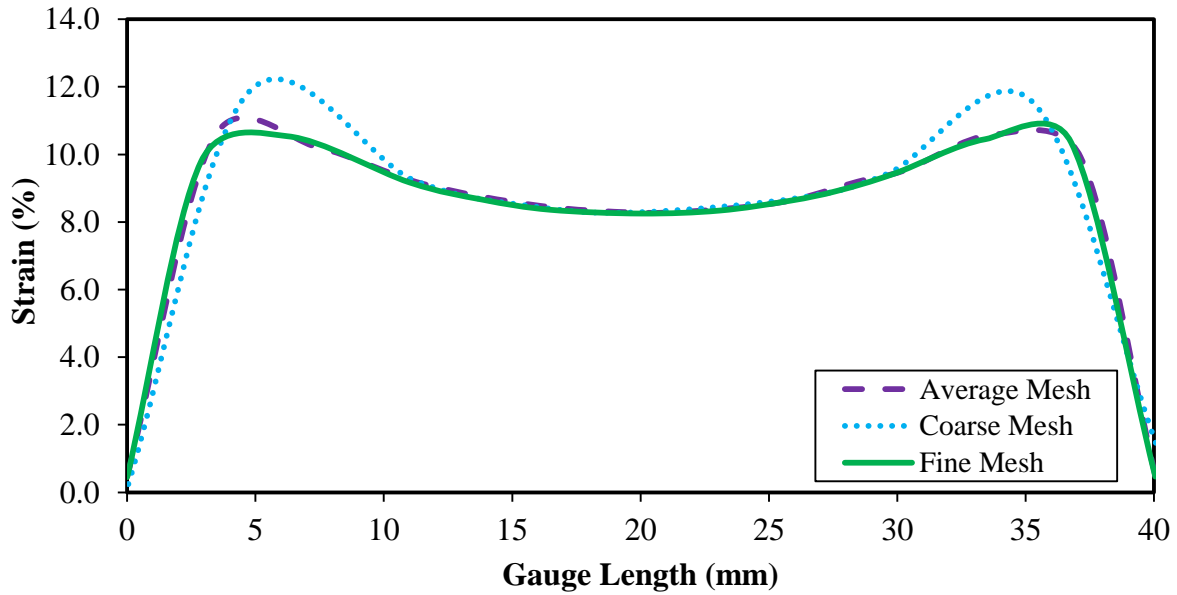
Figure 3.11 Comparison of the predicted strain distribution along the length of the gauge area of the shear specimen for different mesh sizes

The numerical simulations were carried out with a fine mesh on both specimens that have 2-mm corner radii in the end of the slots and specimens that have slots with sharp 90° corners.

Simulation results showed that specimens with sharp corners had significant stress concentrations in the corners at the ends of the slots and rapidly fractured at this location. Therefore, it was not possible to achieve the same strain amplitudes due to crack propagation after a few cycles. Therefore, a specimen with 2-mm corner radii was adopted and the fine mesh for this model is shown in Fig. 3.12.
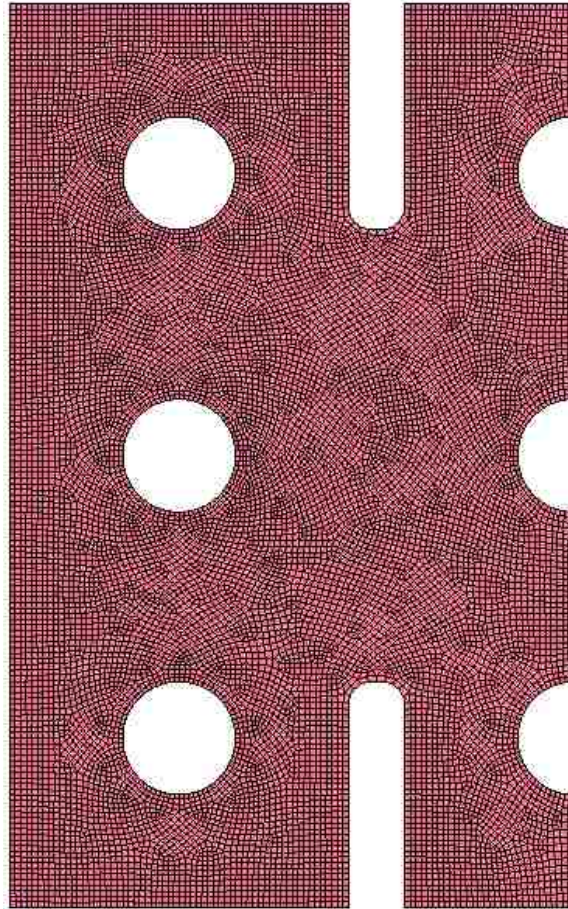
Figure 3.12 Finite element mesh of a half-model of the shear specimen

A personal computer with an AMD Opteron™ processor 248, with 4 GB of RAM was used to carry out the simulations of the cyclic shear tests. The numerical model was run using an explicit integration scheme with a specified simulation time of 1 second. The simulation of the

shear test using the finer mesh model lasted 57 minutes and 56 seconds. A comparison of the different computation times is shown in Table 3.1.

Model Description	Element Size	Number of Elements	Number of Nodes	Simulation Time
Coarse mesh	1 x 1mm^2	3503	3746	12 min 18 seconds (738seconds)
Average mesh	1 x 1mm^2, and 0.25 x 0.25 mm^2	5157	5479	16 min 6 seconds (966 seconds)
Fine mesh with sharp slot corner	0.5 x 0.5 mm^2	13700	14188	47 min 50 seconds (2870 seconds)
Fine mesh with 1 mm radius at the slot corner	0.5 x 0.5 mm^2	15231	15702	59 min 12 seconds (3552 seconds)
Fine mesh with 2 mm radius at the slot corner	0.5 x 0.5 mm^2	14982	15449	57 min 56 seconds (3476 seconds)

Table 3.1 Comparison of the execution times for different mesh densities

3.3.3 OPTIMIZATION OF THE CYCLIC SHEAR TEST SPECIMEN DESIGN

Design optimization is a computational process employed to find the best of all possible designs by modifying several variables in such a way as to satisfy certain constraints. Typical engineering systems are described by a large number of variables and designers need to utilize their knowledge, experience, and judgment to specify these variables in order to obtain an effective design. Engineering expertise is required in order to identify what should be optimized, and which should be the design variables and the parameters that can be changed in order to achieve an optimum design. The following design parameters were selected for optimization:

1) Length and width of the test specimen

2) Number of bolt holes in the test specimen

3) Diameter of the bolt holes in the test specimen

4) Length and width of the slots in the test specimen

5) Number of slots in the test specimen

6) Vertical spacing between bolt holes

7) Horizontal spacing between bolt holes

8) Vertical spacing between slots

9) Horizontal spacing between slots

10) Corner radius at the bottom of the slots

The 'knowledge tool' in CATIA V5 was used to carry out the optimization. This knowledge tool can optimize the geometry of a parametric part and product design by minimizing, maximizing or targeting specific parameter values. This optimization tool uses three basic components such as: an objective function, a set of design variables and a set of constraints to optimize the design. In the optimization of the shear test specimen geometry, the objective was to obtain a uniform strain distribution throughout the gauge region. The parameters that would most affect the strain distribution are the width of the slots, the length of the gauge area, the thickness of the sheet metal and the corner radii at the end of the slots. The main constraint was the width-to-thickness ratio of the gauge area. It should be pointed out, however, that the limitation of this CATIA design optimizer is that it does not allow for multiple objectives and variables.

In order to predict the stress and strain distributions in the gauge area for different specimen geometries, it was necessary to use the commercial finite element code LS-DYNA to simulate the cyclic loading of each test specimen. In these finite element simulations, a half-symmetry

model of the specimen was discretized into 13700 Belytschko-Tsay 4-noded quadrilateral shell elements (0.5 x 0.5 mm^2) each having 5 through-thickness integration points. The sheet material was assumed to be isotropic and therefore the von Mises yield criterion and the isotropic hardening rule were used. The material work hardening behaviour was described using a piecewise linear flow curve. Various node sets were constrained in order to replicate the boundary conditions that would exist during actual loading of the shear test specimen. The details on the finite element model are already presented in previous sub-section 3.3.2 of this chapter.

The selection of an optimum geometry of the cyclic shear test sheet specimen required that many different designs be considered, and each proposed geometry required a separate finite element analysis. For instance, different numbers of bolt holes were considered in different positions to identify which design led to the most uniform strain distribution throughout the gauge region of the sheet specimen: specifically, 6, 7, 8 and 9 holes were considered. It was found that 9 bolt holes provided a reasonably uniform strain distribution but also a much better ability to grip the specimen up to higher loads. The shear strain distribution along the centre of the gauge area of the optimized specimen geometry was predicted using LS-DYNA and is shown in Fig. 3.13.

Different bolt hole diameters were also considered, such as 8, 9, 10, 11 or 12 mm diameters. The analysis results showed that a 10-mm hole diameter provided the best strain distribution compared to other hole sizes.
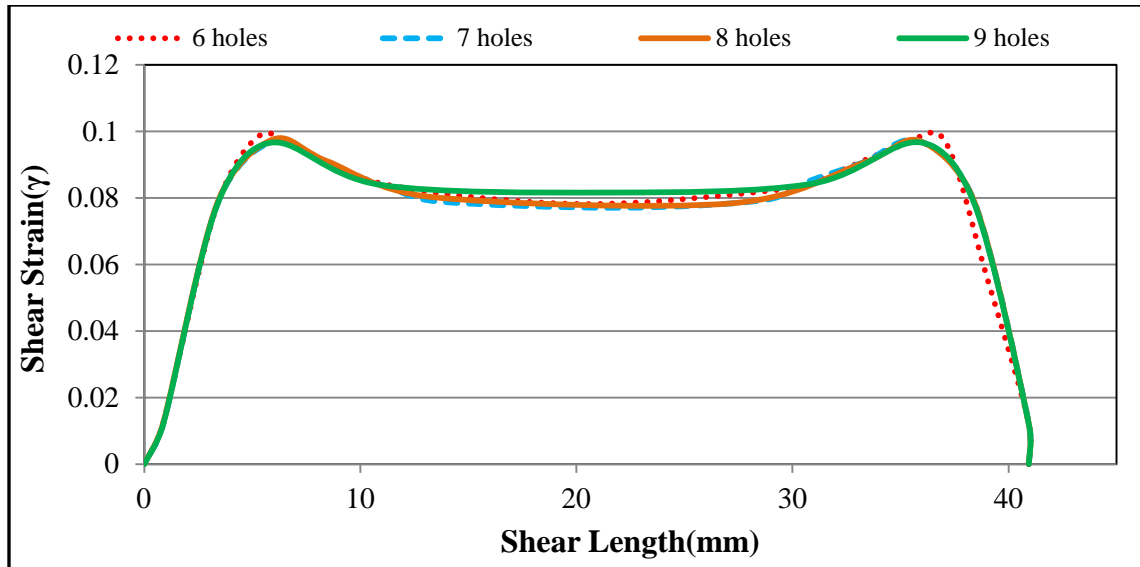
Figure 3.13 Comparison of the shear strain distribution in the gauge area of the sheet specimen for different numbers of bolt holes

The width of the gauge area was varied to observe the effect it has on the stress and strain distributions in gauge region. In this regard, the width of the specimen was changed in 0.25-mm increments from 4.5 mm to 5.5 mm. By comparing the uniformity of strain distribution, it was concluded that the 5-mm gauge width provides a better strain distribution throughout the gauge region.

The vertical and horizontal distances between bolt holes and slots also greatly affected the strain distribution, as observed through simulations. Therefore, based on simulation results, centre-to-centre vertical and horizontal distances of 25 mm and 35 mm were chosen, respectively, and the vertical and horizontal spacing between slots was 40 mm and 30 mm, respectively. Numerical simulations also showed that the specimen with 2 mm radius at the end of the slots achieved greater strain amplitude, compared to that with sharp corners.

The selection of the optimum design variables was based on the design that led to the most uniform strain distribution in the gauge region. For each design considered, a uniformity factor

was calculated for the strain distribution predicted by the finite element simulation, according to Equation 3.1.

Uniformity Factor $= \dfrac{\gamma_{max} - \gamma_{min}}{L_v}$ 3.1

where γ_{max} is the maximum shear strain, γ_{min} is the minimum shear strain, and L_v is the distance between the peaks at both ends of the shear strain distribution plot (see Fig. 3.13). An example of the uniformity factors that were computed for different specimen designs are summarized in Table 3.2, where it can be seen that the 9-hole specimen design leads to the lowest uniformity factor.

Variables		Variable Gauge Length (L_v)	Max Shear Strain (γ_{max})	Min Shear Strain (γ_{min})	Uniformity Factor
Number of Holes	6	30.65	0.0984	0.0824	5.24
	7	29.25	0.0967	0.0770	6.73
	8	29.2	0.0974	0.0783	6.56
	9	30	0.0966	0.0841	4.14

Table 3.2 Comparison of the uniformity factor with respect to the number of bolt holes

The overall dimensions of the optimized test specimen are: 80 mm in width, 100 mm in length and a maximum of 3 mm in the thickness, with a slot width of 5 mm, an effective shear zone that is 40 mm long and 5 mm wide, and corner radii of 2 mm at the end of each slot. The specimen geometry that was finally selected is shown in Fig. 3.14.

The slipping action between the sheet specimen and the contact surfaces of the fixed and movable fixtures and the holding blocks was not considered during the design. But in order to maximize friction, these contact surfaces were machined and left rough. To increase the interface

69

friction in the fixture and provide sufficient gripping force, several circular knurled blocks were

inserted in the clamping areas of the fixture and holding blocks, as shown in Fig. 3.15.
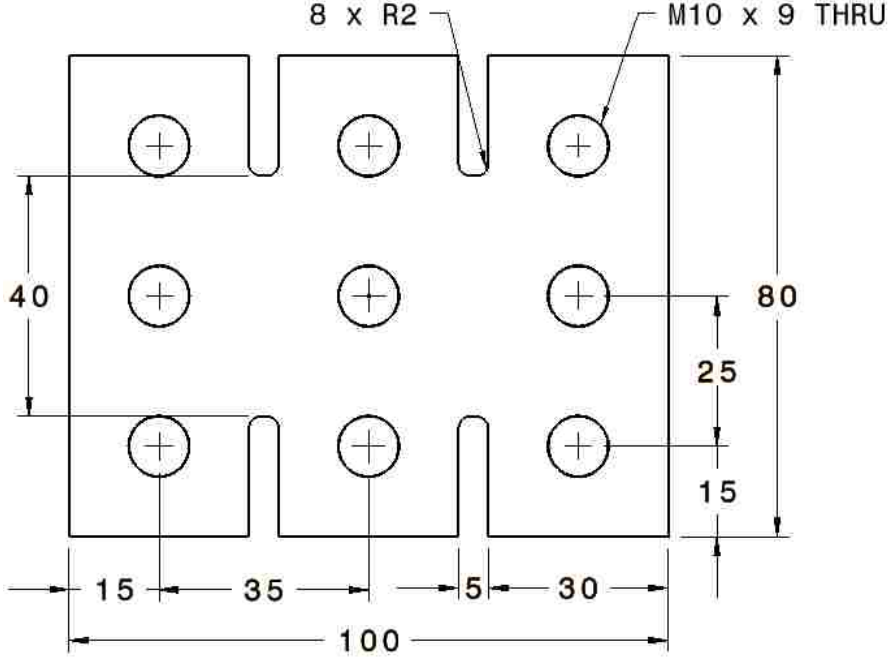
Figure 3.14 Drawing of the optimized cyclic shear test specimen (dimensions are in mm)

Figure 3.15 Photograph of inserted knurled blocks on the surfaces of (a) the upper and lower
fixtures, and (b) the holding blocks of the cyclic shear test fixture

4. EXPERIMENTAL PROCEDURES

This chapter provides a detailed description of the experimental procedures used to conduct cyclic shear tests, the use of the ARAMIS optical strain measurement system, instrument calibration, and the analysis and results of the cyclic testing of certain sheet materials. This chapter consists of four sections. Section 4.1 describes the sheet materials that were tested, and Section 4.2 provides an overview of the specimen preparation for both the tensile and the cyclic shear tests. Section 4.3 is a detailed description of the tensile and the cyclic shear test procedures. Finally, Section 4.4 describes the ARAMIS system, its calibration, the strain measurement, and the accuracy of strain measurements. All the experimental work in this study was performed using an INSTRON 8562 universal testing machine, which is located in Essex Hall Room 203 at the University of Windsor.

4.1 DESCRIPTION OF SHEET MATERIALS

Four different grades of steel sheets were tested in cyclic shear and in uniaxial tension under quasi-static loading conditions: DP600, DP980, TRIP780 and HSLA. The DP980-1.5 mm and the TRIP780-1.2 mm sheet specimens were cold rolled sheets (i.e. uncoated), whereas the DP600-1.0 mm and HSLA-0.8 mm were hot-dipped galvanized (i.e. zinc coating). A general description of each grade of steel is given below.

High Strength Low Alloy (HSLA) Steels: HSLA is a grade of steel that provides better mechanical properties and greater corrosion resistance than conventional low-carbon steel. It is strengthened by the presence of micro-alloying elements such as copper, manganese and

chromium. These alloying elements precipitate into fine carbides and help to refine the grain size [120]. Typically, HSLA has a microstructure of fine-grained ferrite, which is strengthened with carbon and nitrogen precipitates of titanium, vanadium, or niobium [121,122]. This steel can be formed successfully when users area aware of the limitations due to the higher strength and lower formability [121]. To improve the formability and weldability of HSLA, the carbon content is usually kept between 0.05% and 0.25%. The yield strength of HSLA steel is generally in a range between 250-590 MPa and the development of Lüders bands at the onset of yielding causes yield point elongation.

Dual Phase (DP) Steels: Both DP600 and DP980 sheet steels were used in this research. Dual phase steels combine strength, formability, weldability and low cost, and therefore have been increasingly used to produce automotive components. DP steels consist of a hard martensite phase embedded in a soft ferrite matrix which gives them both high strength and formability. The tensile strength of DP steels increases with the volume fraction of martensite [117, 123, 124]. It can be noted that Holloman's stress-strain relation, suitable for most steels, is not adequate for DP steels [120].

DP600 steel has a low ratio of yield strength to tensile strength, a high rate of work hardening, and good energy absorption characteristics. The lower yield strength at a given tensile strength translates to higher elongation values and better formability. DP600 usually shows continuous yield behaviour, i.e. no indication of yield point elongation, giving it better forming characteristics [124].

DP980 has also been used increasingly in the automotive industry because of its high strength, high-energy absorption in crash testing, and good formability. Typically, DP980 is a

combination of about 35% martensite and 65% ferrite. Fig. 4.1 shows typical stress-stress behaviour of different grades of DP steels.
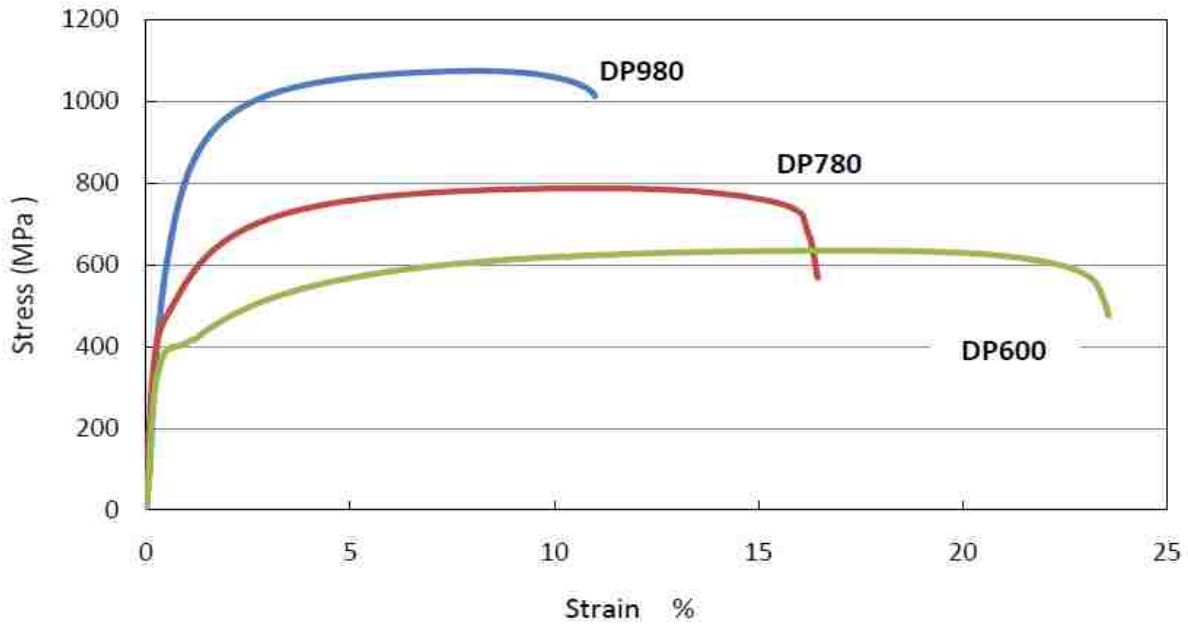
Figure 4.1 Stress-strain behaviour of different types of DP steels [120]

Transformation Induced Plasticity (TRIP) Steels: The development of new steels during the last decade has shown that TRIP steels exhibit even greater formability than DP steels with the same tensile strength. TRIP steels possess a multiphase microstructure, typically consisting of soft ferrite (α-Fe), a combination of bainite, and retained austenite (γ-Fe) in volume fractions greater than 5% [117]. The various levels of these phases give TRIP steels a unique balance of properties. During deformation of TRIP steels, the retained austenite progressively transforms to martensite with increasing strain, thereby, increasing the work hardening rate at higher strain levels.

To illustrate the relative formability of these grades of steel, a comparison of quasi-static stress-strain curves of HSLA, TRIP and DP600 is shown in Fig. 4.2.
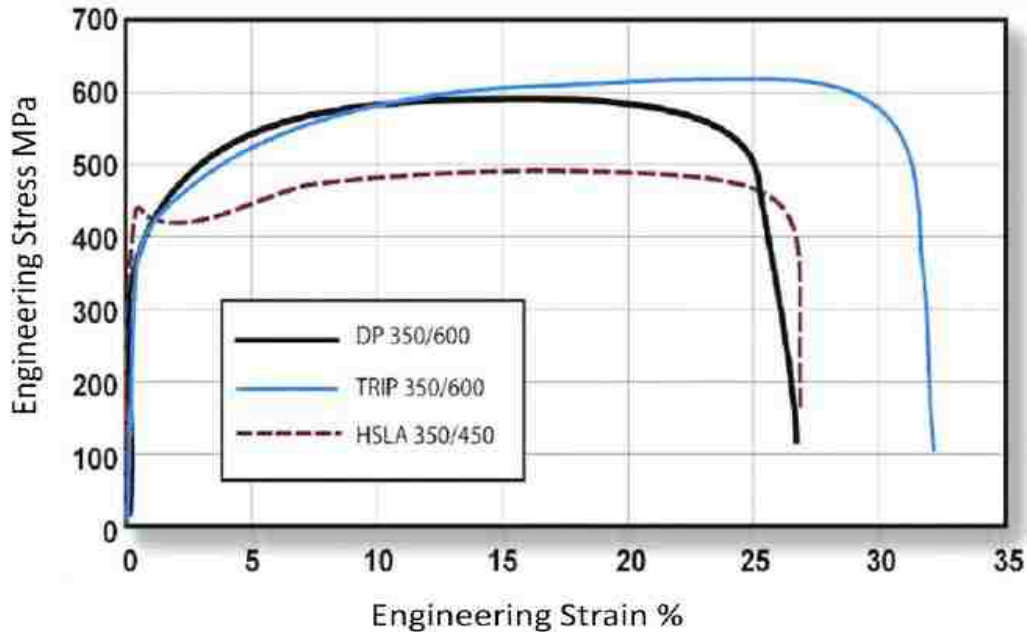
Figure 4.2 Comparison of the typical stress-strain curves of HSLA, DP and TRIP steels [122]

The mechanical properties and work hardening behaviour of these four sheet materials are provided in Chapter 5, Table 5.1 and in Section 5.2.

4.2 SPECIMEN PREPARATION

Uniaxial tension and cyclic shear tests were conducted to determine the behaviour of the four different sheet materials. The experimental results from both types of tests can be used to determine the work hardening behaviour of these sheets and used as input in numerical simulations. In order to get accurate experimental stress-strain data, specimens were prepared in accordance with the existing standards. In this regard, the sheet specimens were cut to shape by the wire-electro-discharge machining process that eliminates any residual stresses. The specimen

preparation procedures for the tension and the cyclic shear tests are described in this section: sub-section 4.2.1 describes the preparation of the tensile test specimen, and sub-section 4.2.2 describes that of the cyclic shear test specimen.

4.2.1 PREPARATION OF TENSILE TEST SPECIMENS

Tension tests were conducted on the four different grades of sheet metal at room temperature to determine their elasto-plastic behaviour. The tensile test specimens were prepared according to the ASTM standard E8M [125], and the geometry of the tensile specimens is shown in Fig. 4.3.
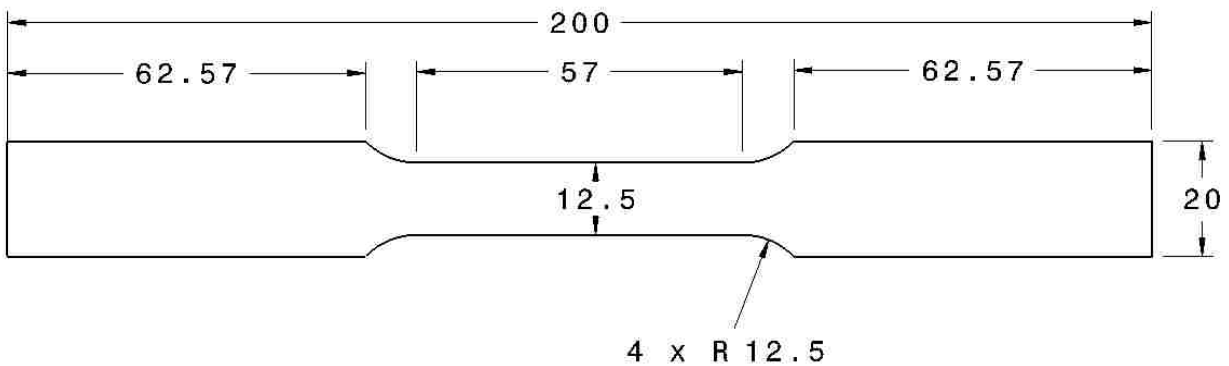
Figure 4.3 ASTM standards E8, geometry for tensile specimens (dimensions are in mm)

The ARAMIS optical strain measurement system was used to measure the strains in the specimen gauge area, and therefore a random speckle pattern was applied to the surface of each test specimen; digital image correlation was used to track the relative movement of the speckled surface and determine the strains. The surfaces of the test specimens were first cleaned with a fine synthetic scouring pad and washed in acetone. Then a flat white paint was applied to the surface of each specimen. To obtain a good contrast, a black speckle pattern was lightly spray-

painted over the white surface after it had dried. Fig. 4.4 shows the black speckle pattern on different tensile specimens that were prepared for testing.
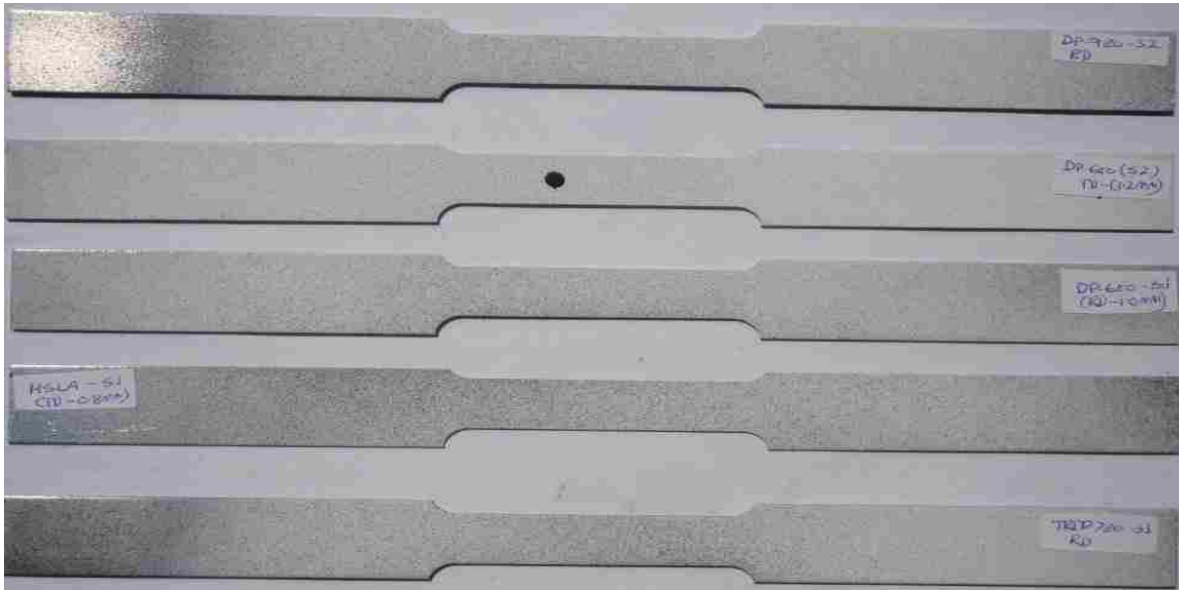
Figure 4.4 Painted tensile test specimens for different grade of sheets with black speckle pattern

4.2.2 CYCLIC SHEAR TEST SPECIMEN PREPARATION

Cyclic shear tests were also carried out on the four different grades of sheet steel and the geometry of the test specimens is shown in Fig. 3.14 in chapter 3. The cyclic shear test specimens were cut parallel to the rolling direction (RD) of the sheet materials. Five specimens of each category were prepared so that the test results would have statistical significance. The bolt holes were first drilled smaller than specified, and then the final specimen geometry was obtained through the wire-EDM process.

Once machined to size, a random speckle pattern was also applied to the shear test specimens according to the same spray-painting procedure that was used for the tensile specimens. An unpainted shear specimen is shown in Fig. 4.5a, and Fig. 4.5b shows a painted

cyclic shear test specimen with the stochastic pattern, which is suitable for measuring strains with the ARAMIS system.
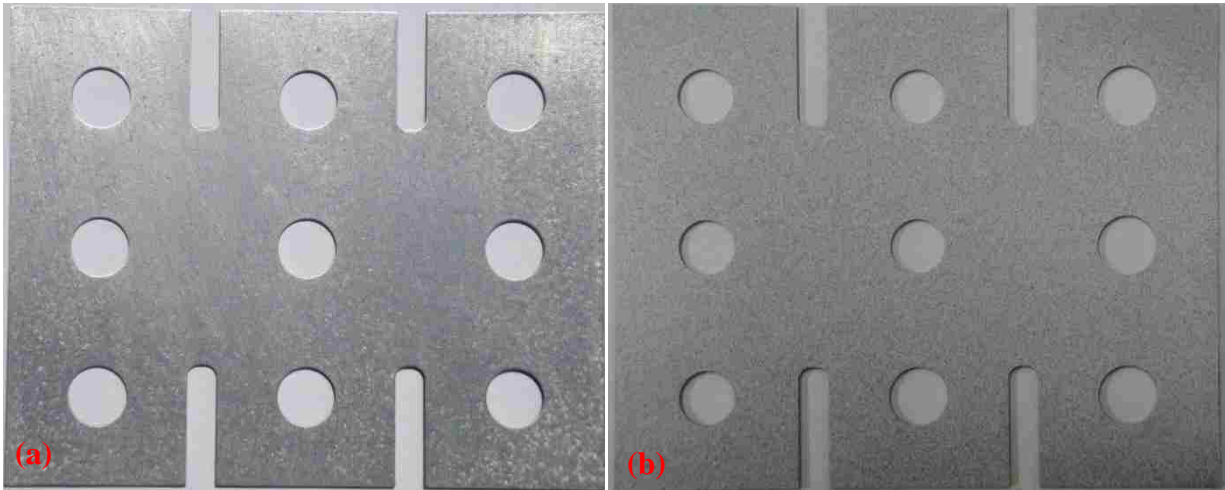
Figure 4.5 Photograph of the cyclic shear test specimens (a) without paint (b) painted with a high contrast stochastic pattern

4.3 TESTING PROCEDURES

One of the objectives of this study is to experimentally determine the cyclic shear stress versus shear strain behaviour, and to investigate the cyclic stress-strain distributions in the gauge region of the sheet specimen during the cyclic loading. Two types of experimental tests, tensile and cyclic shear, were performed on four grades of sheet steel. These tests were conducted under quasi-static loading conditions with a constant cross-head velocity. In order to reach high strains, the extremity of all specimens was allowed to travel a maximum of 2 mm in both forward and reverse loading directions, except for HSLA specimens that had a maximum travel of 1.5 mm to reflect their reduced thickness. Experimental load vs. displacement data were collected during each test and analyzed later.

The cyclic shear and tensile tests were performed on an INSTRON 8562 universal testing machine. This testing apparatus has a capacity of 100 kN, and a maximum travel of 80 mm. A digital controller INSTRON 8500 was used to control the displacement of the moving grip.

4.3.1 TENSILE TEST PROCEDURES

A standard tensile testing fixture, developed by the machine manufacturer, was used to clamp the extremities of tensile specimens. The experimental set up of tensile test specimen is shown in Fig. 4.6a. The two ARAMIS digital cameras were positioned at a specified distance in front of the test specimen (Fig. 4.6b) in accordance with the manufacturer's set-up instructions. The optical strain measurement system was then calibrated. The load and displacement signals recorded by the INSTRON testing machine were also connected to the ARAMIS data acquisition system using BNC cables and connectors. This permitted all the experimental data to be recorded in the same location so that the calculated stresses and strains could be synchronized. Prior to the start of a test, a few digital images of the unloaded specimen were taken, so that strains could be calculated from these reference images.

Tensile tests were performed with a constant displacement rate of 2 mm/min (0.033 mm/sec). During tensile tests the loads were measured with the INSTRON load cell. The images of a deforming specimen were recorded by the ARAMIS system at a frequency of 0.5Hz, and post-processed to determine the strains in the specimen gauge area. The engineering and true stresses were calculated from the measured load, and the strains were computed at the centre of the gauge area with the ARAMIS system. Finally, experimental stress-strain curves were plotted for each tensile specimen.
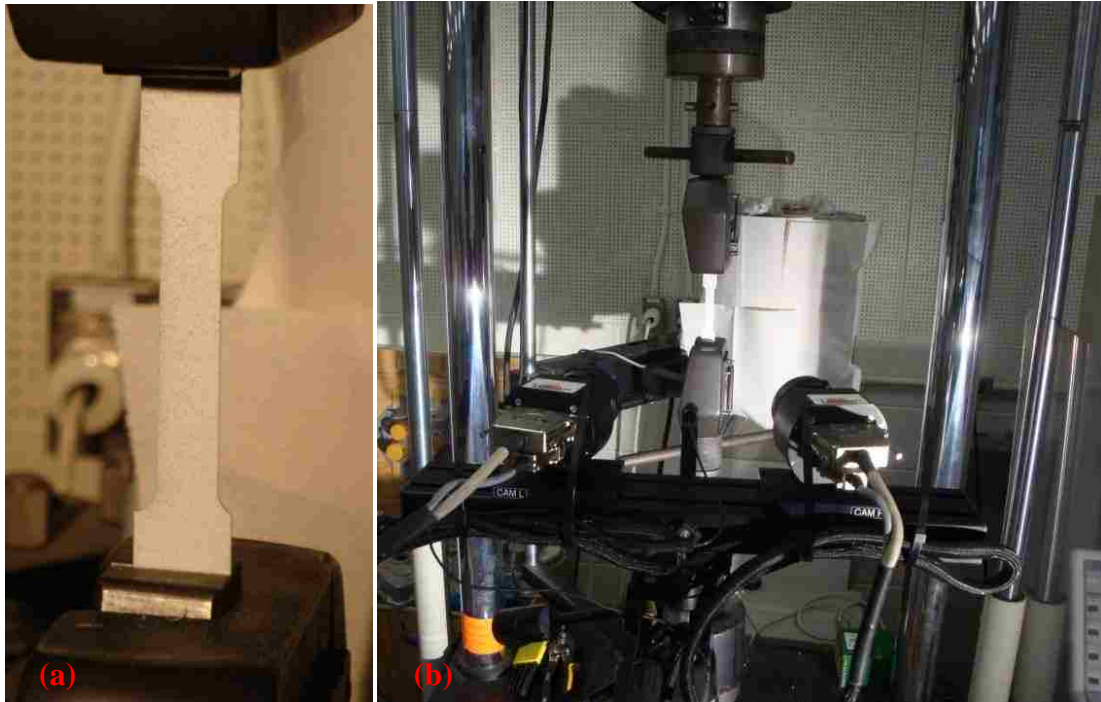
Figure 4.6 Photograph of (a) a clamped tensile specimen ready for testing, (b) the ARAMIS system with stereo cameras focussed on tensile specimen

4.3.2 CYCLIC SHEAR TEST PROCEDURES

The cyclic shear tests were carried out on the four grades of sheet steel using the testing fixture described in Chapter 3. The cyclic shear tests were also performed with the INSTRON 8562 universal testing machine, at room temperature and under quasi-static loading conditions with a cross-head velocity of 1 mm/min (0.166 mm/sec). The upper fixture was bolted to the top head flange of the INSTRON 8562 testing machine, and the lower movable fixture was bolted to the ram flange that is attached to the machine's hydraulic actuator. The fixed upper part and the movable lower part of the fixture were aligned so that the test specimens could be mounted in the fixture without any measurable force being applied to the specimen.

Flat, rectangular specimens with two shear zones were used during this series of experiments, as described in Chapter 3. A sheet specimen was put in place, and bolted between

79

the holding blocks and the fixed and movable fixtures. The experimental set up of cyclic shear test fixture is shown in Fig. 4.7.
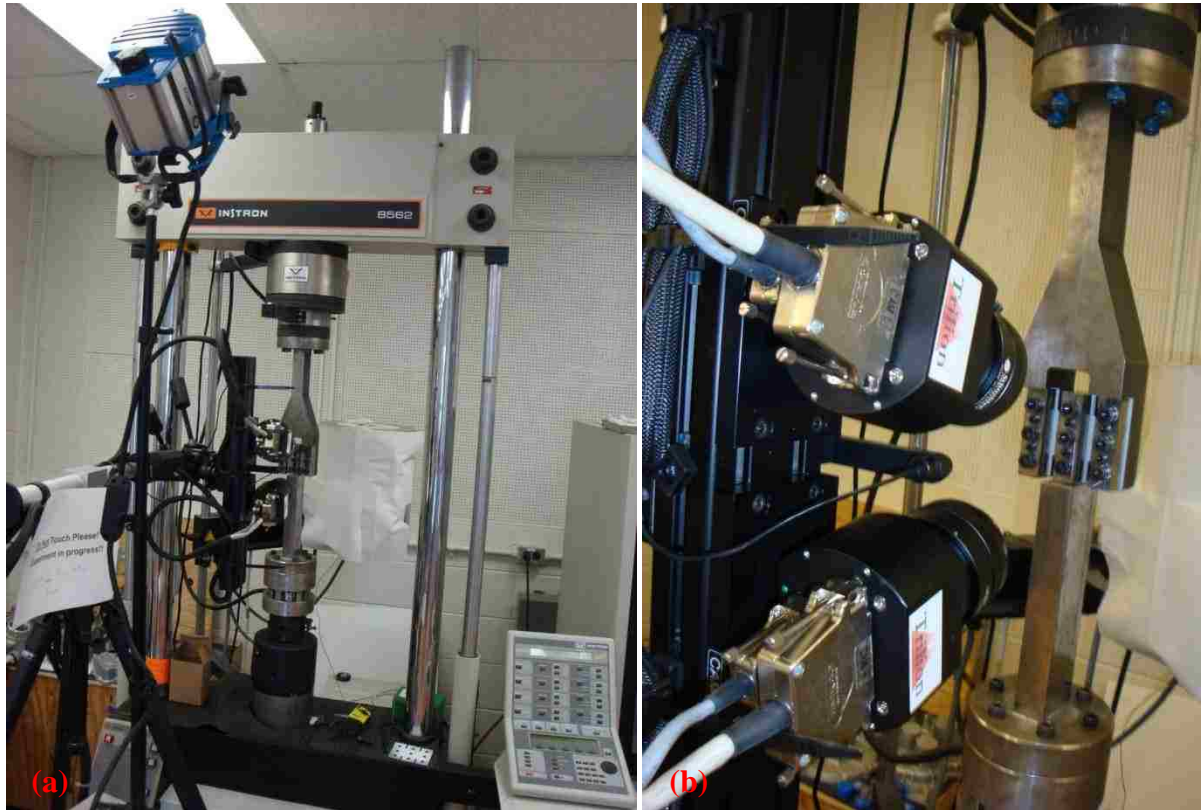
Figure 4.7 Cyclic shear test (a) experimental test set up with ARAMIS system (b) fixture set up

Each shear specimen was clamped into place using nine bolts. To prevent any slippage of the sheet specimen at higher loads, the bolts were tightened to 70 N-m using a torque wrench. The lowest torque that minimized the sliding between the samples and the grips was considered optimal. The presence of knurled blocks in the fixture also helped to prevent slippage of the test specimen at higher loads, therefore, the movement of the specimen was firmly restricted. Photographs of the clamped test specimen are shown in Fig. 4.8.

Figure 4.8 Cyclic shear test (a) specimen set up between fixed upper and lower movable fixture (b) specimen and two shearing gauge zones of the specimen

The two outer regions of the test specimen were securely clamped in the fixed upper fixture, while the middle region of the specimen was clamped to the movable lower fixture. During cyclic shear tests, loads were applied to the sheet specimen by translating the lower fixture up and down in a vertical direction. In this work, the movement of the lower extremity of the shear specimen was controlled so as to reach a maximum displacement of 2 mm, first in one direction, then in the reverse direction. Finally, the specimen was brought back to its original position to complete one loading cycle. As a result of the imposed displacements, a cyclic shear deformation was created in the gauge area of the sheet specimen.

As indicated earlier, the digital images of the deformations in the gauge region were recorded at a frequency of 0.5Hz and analyzed after the test using the ARAMIS digital image correlation software. Therefore the strain distributions were calculated for the entire duration of

81

the test, and the average shear strain in the gauge zone of cyclic shear specimen was determined. Each cyclic shear test was performed three times to verify the reproducibility.

In the cyclic shear test, the load and displacement measurements were not obtained from the load cell of the machine. Instead, the load-displacement data were obtained from a Linux-based data acquisition processor (DAP) written in C. The DAP consisted of four input channels; two were connected to the output channels of the INSTRON 8500 controller via BNC cables and straight plug twin axial BNC connectors. Channel-1 recorded the load voltages and was connected to the output channel (A) of the INSTRON controller. Channel-2 recorded the displacement voltages and was connected to the output channel (B) of the INSTRON controller. At the beginning of each test the load voltage was zero and the displacement voltage was 5.105 volts. The experimental load and displacement data were collected at a sampling rate of 100 samples/sec/channel through the DAP system. The ram load and displacement were electronically monitored using a closed-loop control process of the DAP.

During testing, the INSTRON testing machine, the ARAMIS system, and the DAP system were started concurrently to get synchronized data and images. The load-displacement data were taken from the DAP system, and the images were taken through the ARAMIS system. Finally, the load and displacement voltages of the DAP system were multiplied by a conversion factor of 10 and 5.08 to obtain the applied load and displacement values, respectively. The cyclic shear strains were obtained from the ARAMIS system through computation, and the average cyclic shear stresses and cyclic shear strains were calculated based on cyclic loads and deformations.

4.4 SYSTEM CALIBRATION AND STRAIN MEASUREMENTS

The ARAMIS system was developed by GOM GmbH and was used to measure the strain in the tensile and shear test specimens. Throughout a given test, digital images of the deforming speckle pattern on the surface of the specimen are continuously recorded. Strains are then calculated using a digital image correlation technique. In order to get precise and accurate strain measurements, a number of ARAMIS system parameters require calibration in accordance with the manufacturer's instructions. This section will examine the calibration of the ARAMIS system, the strain measurements and the accuracy of these measurements.

4.4.1 SYSTEM CALIBRATION

The ARAMIS system consists of two cameras to track the displacement of points and measure strains in three-dimensional space. Before recording any images of the specimen, this optical measurement system requires that the displacement of discrete points be calibrated within a volume of space surrounding the test specimen, and the calibration procedure specified by the manufacturer was carefully followed to ensure that the system would accurately measure three-dimensional strains. Several parameters that affect the calibration were considered, such as the distance between the two cameras, the distance from the test specimen to the camera mounting bracket, the angle between the two cameras, and the focal length of each camera lens.

Prior to the calibration, the two cameras were secured to a mounting bracket at an angle of 25° to each other, and the focal length of each camera lens was 50 mm. The base distance between the two cameras and the measuring distance from the cameras to the specimen were set at 240 mm and 510 mm, respectively for the tensile test, and 130 mm and 305 mm, respectively

for the cyclic shear test. Fig. 4.9 shows a schematic of the cameras in relation to the calibrated measuring volume [126].
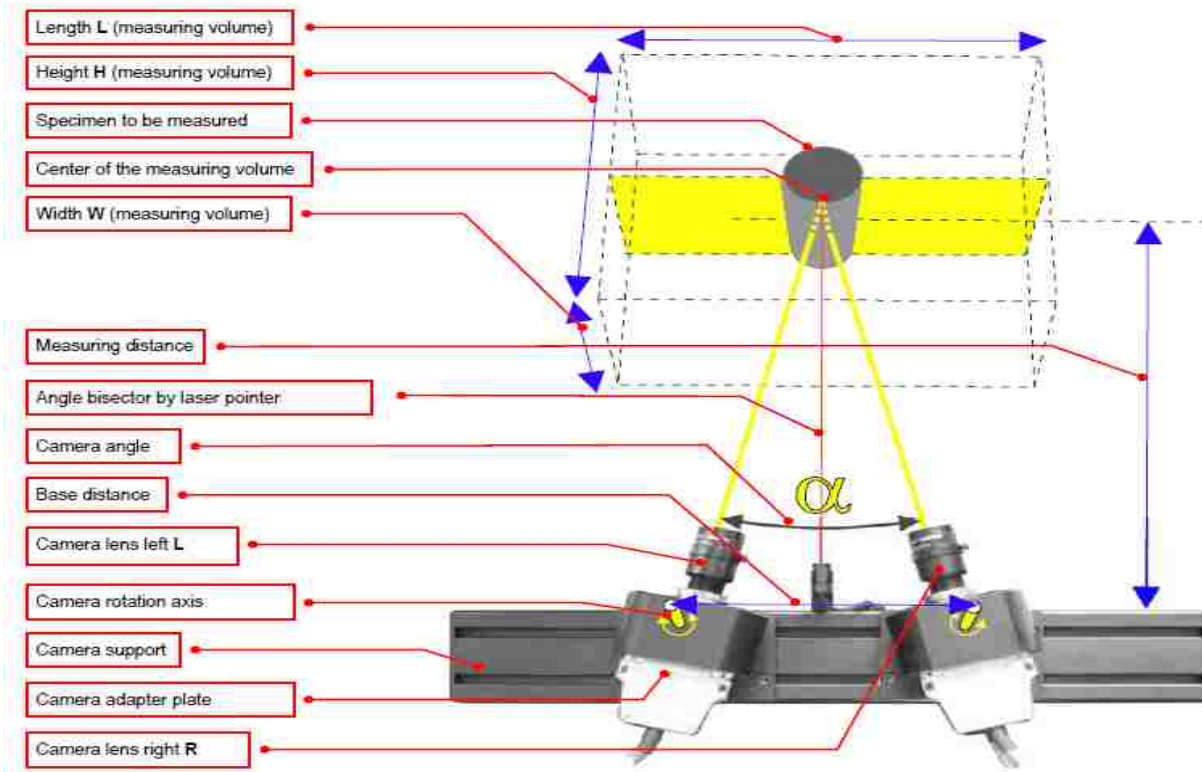
Figure 4.9 ARAMIS 3D sensor unit to measure the volume of calibration panel [126]

The calibration was carried out by taking a series of stereo images of a calibration panel in different positions and locations within the measuring volume. The shutter time was adjusted depending on lighting source. In this research, the cyclic shear test and the tensile test were conducted by using two different calibration panels. The tensile test specimen was calibrated by using a 65 x 52 x 52 mm^3 volume calibration panel, and the cyclic shear test specimen was calibrated by using a 35 x 28 x 28 mm^3 volume calibration panel. Both calibration panels are shown in Fig. 4.10.
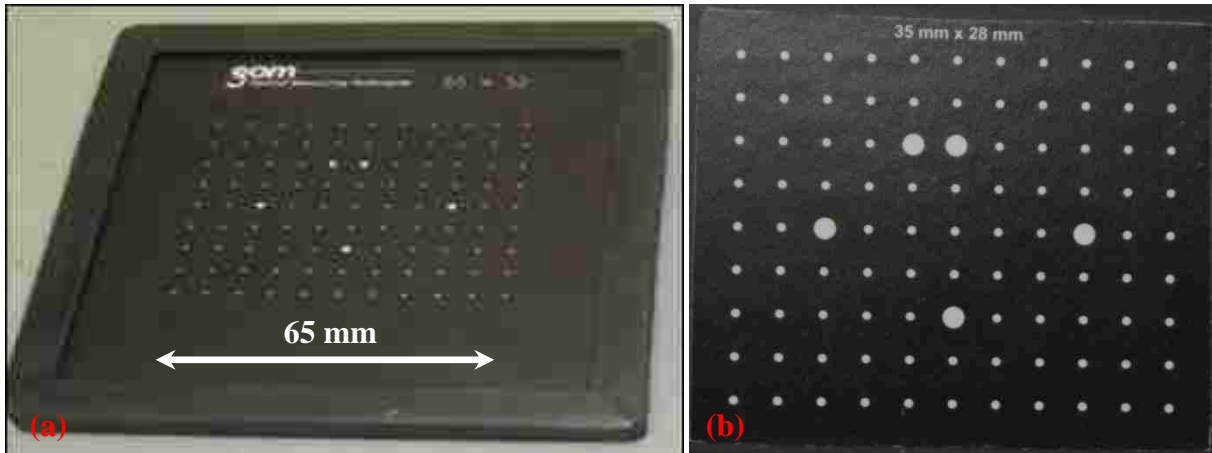
Figure 4.10 Calibration panels for (a) 65 mm x 52 mm x 52 mm volume (b) 35 mm x 28 mm x 28 mm [126]

Once all the calibration images were taken, the ARAMIS software determined an average calibration deviation for each camera; an acceptable calibration value of 0.040 pixels was used throughout the testing.

In order to ensure the quality of the speckle pattern which was applied to the surface of the specimen, a series of images of the test specimen were taken after the calibration and prior to testing. This operation also serves to validate the calibration process. Approximately 5 to 10 images of the un-deformed specimen were taken in the absence of any applied load. The strain values that are measured in this unloaded condition were negligible. The manufacturer of the ARAMIS system reported that if these initial strain values were greater than 0.05%, or the system was unable to measure strains over the entire surface of the specimen, it was an indication that the painted speckle pattern had been incorrectly applied (e.g. insufficient contrast, incorrect dot size, black paint dots are too sparse etc.) and should be redone [126].

4.4.2 STRAIN MEASUREMENTS

Several techniques have been used by researchers to measure strains experimentally: extensometers or strain gauges, photographic techniques, digital imaging on marked specimens, and interferometry or laser speckle techniques [127]. The first technique requires a direct contact with the specimen, whereas the last three techniques are non-contact types. Strain measuring techniques that require contact with the specimen present many disadvantages, such as being able to only measure strains in a single location. In this research, the digital image correlation (DIC) technique was used, which is based on photography and digital imaging.

During each test, a bright light source (ARRI 650 plus, 650 Watt) was used to illuminate the specimen. The two ARAMIS cameras were focused on the specimen gauge area and a computer equipped with the ARAMIS image acquisition software was used to record images of the deforming specimen at a rate of 0.5 Hz.

After the completion of a test, the ARAMIS image analysis software compares each image of the deformed speckle pattern to the un-deformed pattern recorded before the test. The distortions in the speckle patterns are used to calculate the strains at the surface of the specimen [125]. Images of a random pattern before and after deformation are shown in Fig. 4.11.
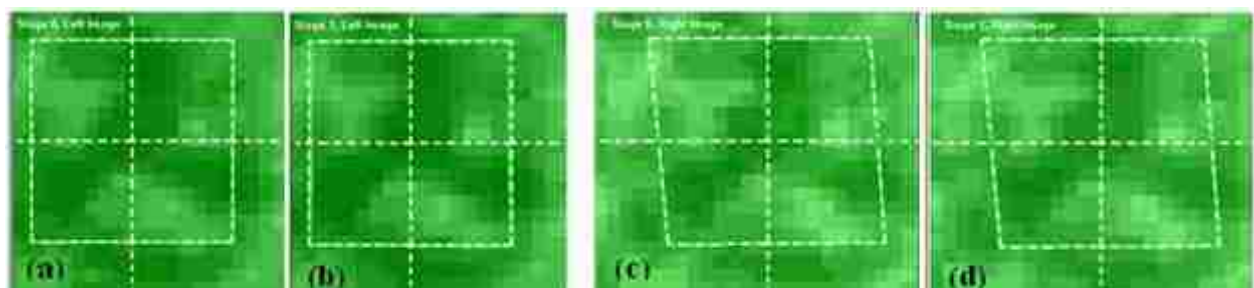
Figure 4.11 Digital images of a random speckle pattern: undeformed pattern as seen from (a) the left and (b) right cameras; deformed pattern as seen from (c) the left and (d) right cameras

The DIC technique therefore provides not only the strain distribution at the surface of the specimen at a given moment in time, but also the entire strain history from the beginning to the end of the test. A photograph of the ARAMIS image analysis software is shown in Fig. 4.12.
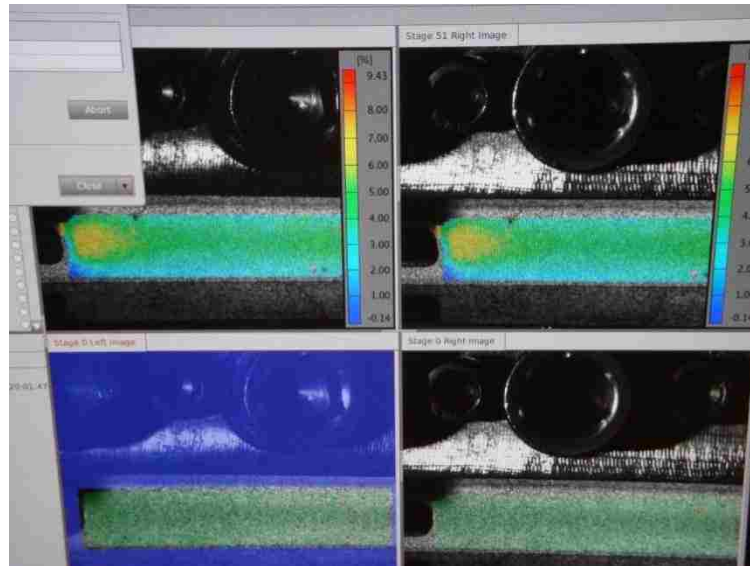
Figure 4.12 Photograph of the ARAMIS digital image analysis software
showing the strain distribution in gauge area of a shear specimen

The ARAMIS system was used to measure strains in both the tensile tests and the cyclic shear tests.

4.4.3 STRAIN MEASUREMENT ACCURACY

The ARAMIS optical strain measurement system was used to measure the surface strains in the test specimens with a high degree of accuracy. According to the manufacturer of the ARAMIS system, the strains can be measured from 0.05% to almost 100% with these calibration panels, with accuracy up to 0.02% [126]. Turton [128] verified the accuracy of the ARAMIS strain measurements by comparing the strains measured with the ARAMIS system and those measured with an extensometer. He compared the strain at different points in the gauge area of

the tensile specimen and found that during the test, the strains measured with the ARAMIS system and those measured with the extensometer were practically identical, and the strains only varied at the end of the test when localized necking occurred. The ARAMIS system can be said to provide very accurate and reliable strain measurements.

5. RESULTS AND DISCUSSIONS

This chapter presents the numerical and experimental results which were obtained during this research. Section 5.1 describes the experimental results of the tensile tests and Section 5.2 presents the numerical and experimental results of the cyclic shear tests on DP600, DP980, TRIP780, and HSLA steel sheets.

5.1 EXPERIMENTAL RESULTS OF TENSILE TEST

This section provides experimental tensile test results for the materials that were characterized in this research. The objective of this research is to experimentally determine the cyclic work hardening behaviour of common automotive sheet steels subject to shearing loads. However, tensile tests were also conducted to determine the yielding behaviour and the mechanical properties of these sheet materials.

During the tensile tests, the forces were recorded as a function of the displacements of the grips. The engineering stress-strain response was calculated from the load-displacement data using Equations 5.1 and 5.2.

$$\sigma_{eng} = \frac{F_i}{A_0} \qquad\qquad 5.1$$

where σ_{eng} is the engineering stress, F_i is the instantaneous tensile load measured by the load cell during testing, and A_0 is the initial area of the gauge cross-section of the sheet specimen. The instantaneous engineering strain ε_{eng} was obtained by using equation 5.2.

$$\varepsilon_{eng} = \frac{L_i - L_0}{L_0} \qquad\qquad 5.2$$

where L_0 and L_i are the initial and instantaneous gauge lengths, respectively. However, the strains in the gauge area were also continuously measured by the ARAMIS system throughout the testing.

Material behaviour was also calculated in terms of true stress – true strain by using Equations 5.3 and 5.4. These calculations were only conducted up to maximum load.

$$\sigma_{true} = \sigma_{eng}(1 + \varepsilon_{eng}) \qquad\qquad 5.3$$

$$\varepsilon_{true} = \ln\left(\frac{L_i}{L_0}\right) = \ln\left(1 + \varepsilon_{eng}\right) \qquad\qquad 5.4$$

The yield stress of each sheet material was obtained for a plastic strain offset of 0.002. It is common to have a 10% variation in the yield stress for specimens tested from the same batch of material [128]. The strain hardening exponent (n) was obtained by regression of the true stress and true strain data using a power law. The hardening exponent 'n' value was calculated for the strain range from 5% to 10%. Holloman's power law equation is given below:

$$\sigma = K\varepsilon_p{}^n \qquad\qquad 5.5$$

where σ is the true stress, K is the strength index, ε_p is the true plastic strain, and n is the strain hardening exponent.

5.1.1 DP600 TENSILE TEST

During the tensile tests, quasi-static loads were applied at a rate of 2 mm/min. It was observed that DP600 sheet specimens fractured in a ductile manner after necking. Continuous deformation was observed until the fracture occurred.
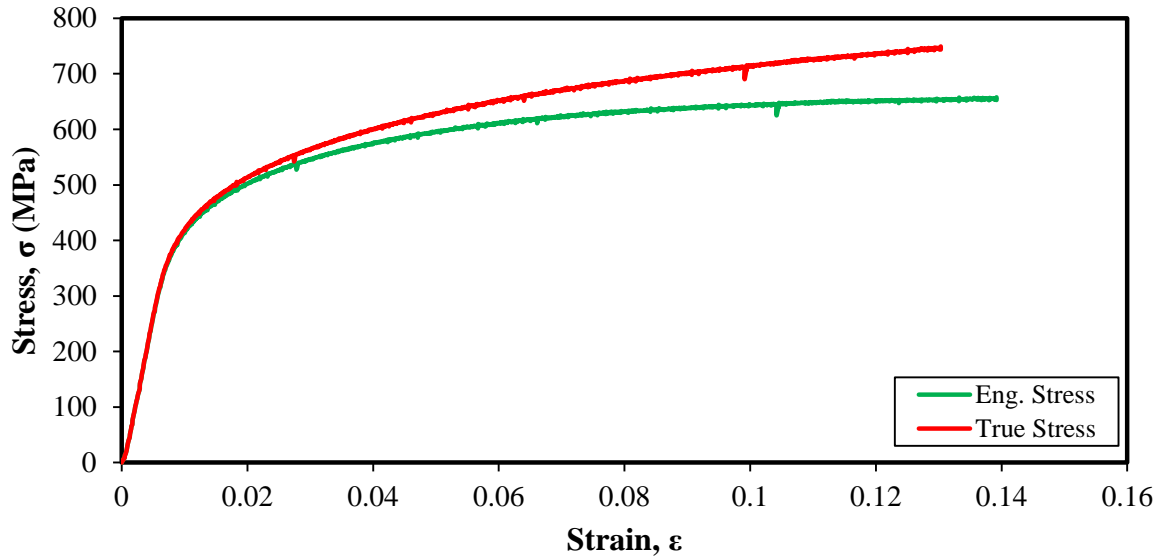
Figure 5.1 Stress-strain behaviour of DP600 steel specimen in tensile test

DP600 exhibits a smooth yielding behaviour, as can be seen from the engineering and true stress-strain curves in Fig. 5.1. This steel has a linear elastic behaviour up to 340 MPa, then exhibits a high initial work hardening rate. A summary of the mechanical properties of this DP600 steel sheet is provided in Table 5.1.

5.1.2 DP980 TENSILE TEST

DP980 also exhibits a smooth yielding behaviour followed by some work hardening, as shown in Fig. 5.2. In the elastic region of the stress-strain curve, the linearity can be observed up to 600 MPa, as shown in the Fig. 5.2. During testing, the DP980 specimens were uniformly deformed up to necking but suddenly broke after necking. Table 5.1 shows that the yield strength and the ultimate strength of DP980 steel are higher than the DP600 steel. However, the total elongation and the strain hardening exponent (n- value) are lower in comparison to the DP600. A summary of the mechanical properties of the DP980 steel is given in Table 5.1.
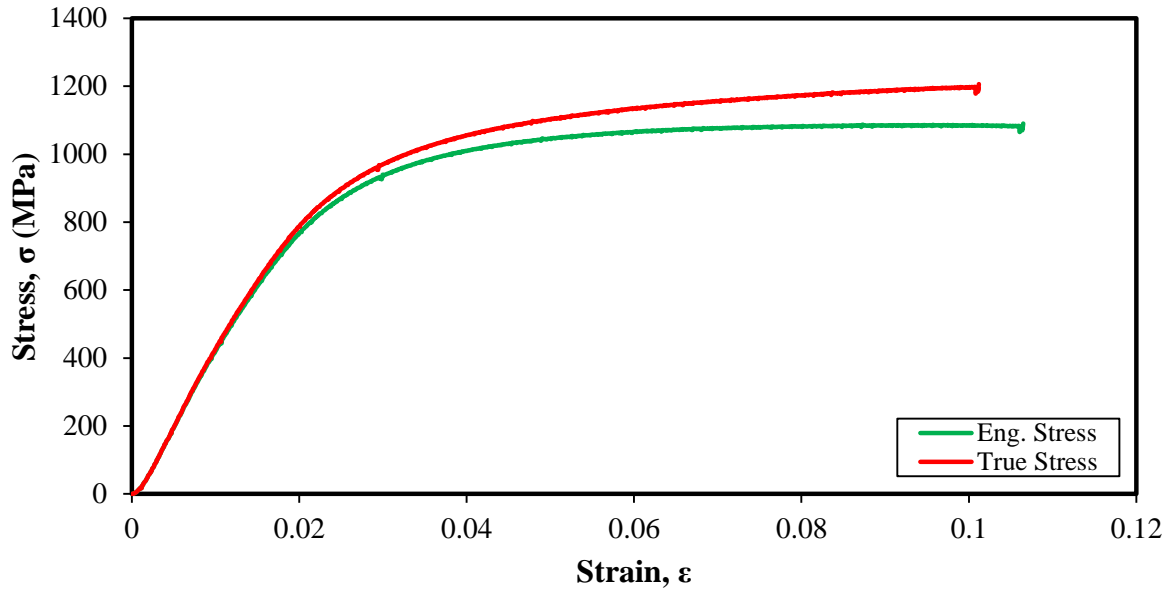
Figure 5.2 Stress-strain behaviour of DP980 sheet steel in tensile test

5.1.3 TRIP780 TENSILE TEST

TRIP780 exhibits a more sudden yielding behaviour, as evidenced by the stress-strain curves in Fig. 5.3. The superior work hardening ability of the TRIP780 was observed during the testing, also depicted in Fig. 5.3. This is due to the dispersion of hard martensite particles in a softer ferrite matrix as well as the progressive transformation of retained austenite to martensite throughout the deformation. It was also observed that this sheet metal deformed uniformly up to the onset of necking, but fractured quite quickly once the ultimate load was reached.
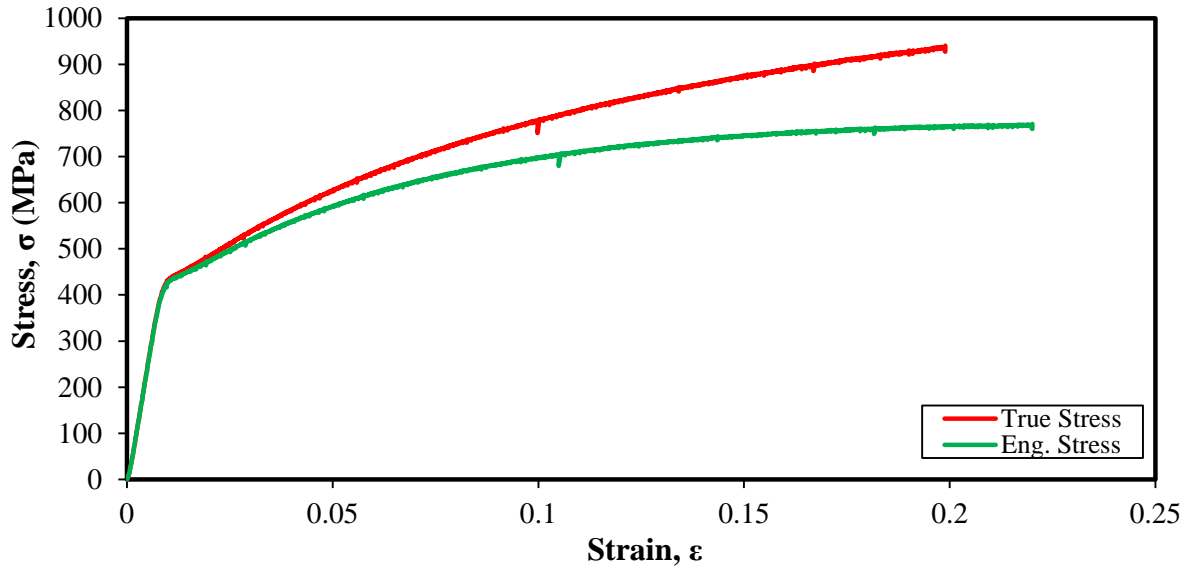
Figure 5.3 Stress-strain behaviour of TRIP 780 steel sheet in tensile test

TRIP780 steel shows a lower initial work hardening rate than DP sheet steels; however, it is comparatively more formable. Fig. 5.10 shows that higher strains can be achieved with this grade of steel. Once again, a summary of the mechanical properties of this TRIP780 steel are shown in Table 5.1.

5.1.4 HSLA TENSILE TEST

The experimental stress-strain curves obtained for the HSLA sheet material are shown in Fig. 5.4. HSLA exhibits a yield point elongation of approximately 0.05, as seen in Fig. 5.4. A linear elastic behaviour can easily be seen up to 370 MPa, and the upper yield point is clearly visible. After the yield point elongation, this HSLA is characterized by a gradual rate of work hardening.
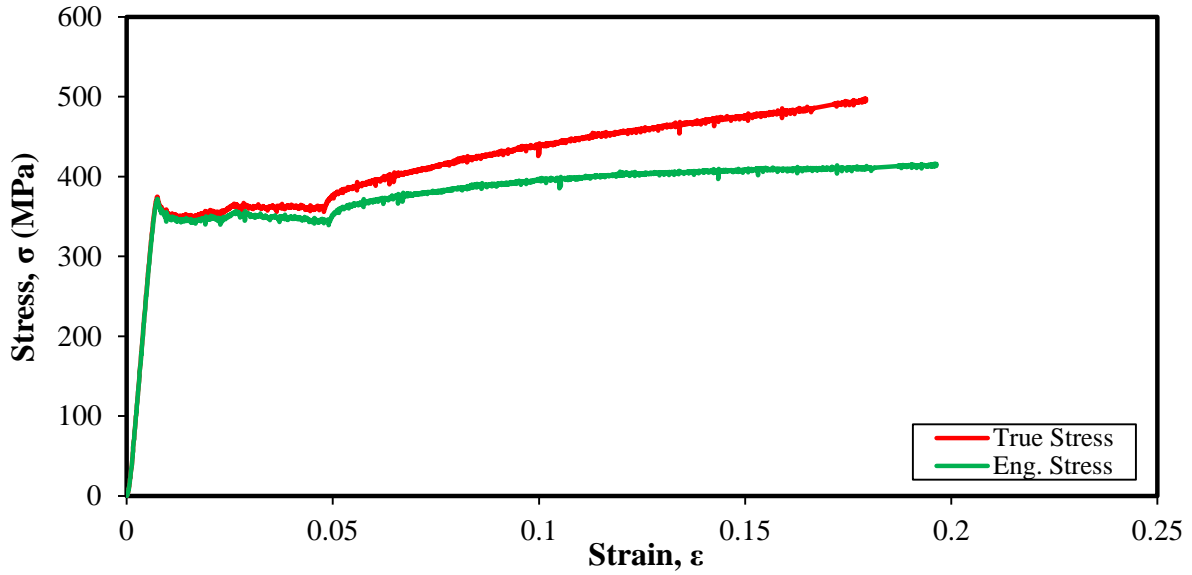
Figure 5.4 Stress-strain behaviour of HSLA steel sheet in tensile test

A summary of the mechanical properties of HSLA steel are given in Table 5.1. For the sake of comparison, the true stress-strain curves of each of the four sheet materials are shown in Fig. 5.5, and a summary of the tensile data is shown in Table 5.1.
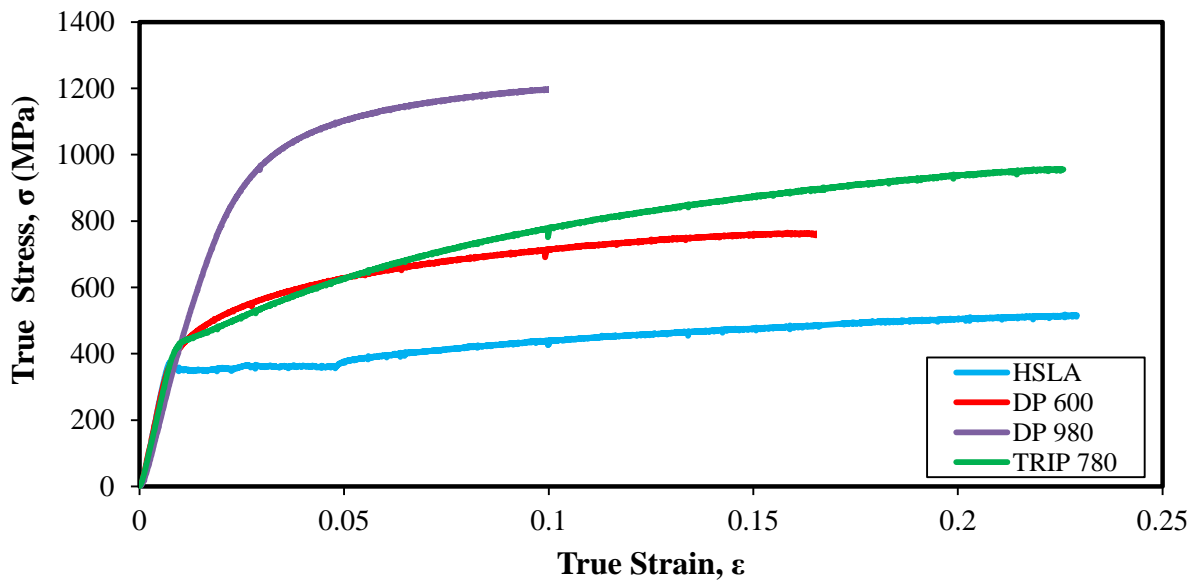
Figure 5.5 True stress-strain curves for different sheet materials in tensile test

Material	Yield Stress MPa (0.2%)	UTS MPa	Yield/UTS	Uniform Elongation (%)	Total Elongation (%)	n-value (5-10)%
DP600	418	665	0.63	14.5	20.6	0.174
DP980	620	1096	0.57	11.0	13.7	0.110
TRIP780	441	777	0.55	22.5	28.4	0.140
HSLA	376	417	0.86	18.7	25.7	0.140

Table 5.1 Summary of the mechanical properties of four different grades of sheet steel

5.2 EXPERIMENTAL AND SIMULATION RESULTS OF CYCLIC SHEAR TESTS

This section provides the numerical and experimental results of the cyclic shear tests that were conducted on the four different sheet steels described earlier. In order to obtain the cyclic stress-strain data, a finite element model of each sheet material was created. The commercial software LS-DYNA was used to apply cyclic load to the model of the shear specimen in order to determine the stress and strain distributions throughout the specimen. The model of the shear test specimen was prepared in accordance with specimen geometry that was proposed in Chapter 3: the gauge length was 40 mm and the gauge width was 5 mm, and the thickness of the various sheet materials varied from 0.8 to 1.5 mm.

During the experimental shear tests, the force was recorded as a function of the displacement of the test grips that were fastened to the hydraulic actuator of the testing machine. The test data were collected by an external data acquisition system, which was connected to the universal testing machine. Experimentally measured strain data showed that the symmetry of the test specimen with respect to the machine loading axis causes the stresses and strains in the two identical shearing zones to be approximately uniform and of the same magnitude. Therefore, the

shear stress in the gauge area was calculated from the measured load taking into account the double shear in the symmetrical test specimen, according to Equation 5.6:

$$\tau_s = \frac{F}{2.l.t} \qquad\qquad 5.6$$

where τ_s is the shear stress, F is the shearing force acting on the two gauge regions, l is the length of the sheared area and t is the thickness of the sheet metal. The shear strains can be calculated from the displacements of the lower fixture according to Equation 5.7:

$$\gamma = \frac{u}{2.w} \qquad\qquad 5.7$$

where γ is the shear strain, u is the displacement of the central part of the specimen, and w is the width of the sheared area. However, the shear strains in the two gauge areas were also measured directly using the ARAMIS optical strain measuring system which continuously maps the coordinates of discrete points in the speckle pattern that was applied to the surface of the specimen. The ARAMIS strains are then computed after the completion of each shear test.

The objective of the cyclic shear tests is to determine the relationship between the shear stress and the shear strain for each sheet material. The experimental stress-strain curves are essential to verify the ability of constitutive models to reproduce the actual behaviour of these sheet materials. In this research, special attention was given to the determination of the shear strains, and their distribution in the gauge region of the test specimens during cyclic loading.

5.2.1 DP600 CYCLIC SHEAR TEST

The predicted stress and strain distributions in the DP600 shear test specimens are presented in this section. Fig. 5.6 shows the von Mises effective stresses and the effective plastic strains predicted by the finite element analysis of the shear test when the maximum displacement (+2 mm) was attained (corresponding to a load of 34 kN). Fig. 5.6 shows that, throughout the

gauge region, the stress and the strain distributions are quite uniform: according to the fringe levels, the effective stress in the majority of the gauge area lies between 571 MPa and 652 MPa, and the effective plastic strain varies from 0.0655 and 0.0873. It can also be seen that peak stresses and strains occur near the edge of the corner radius at the ends of the slots.
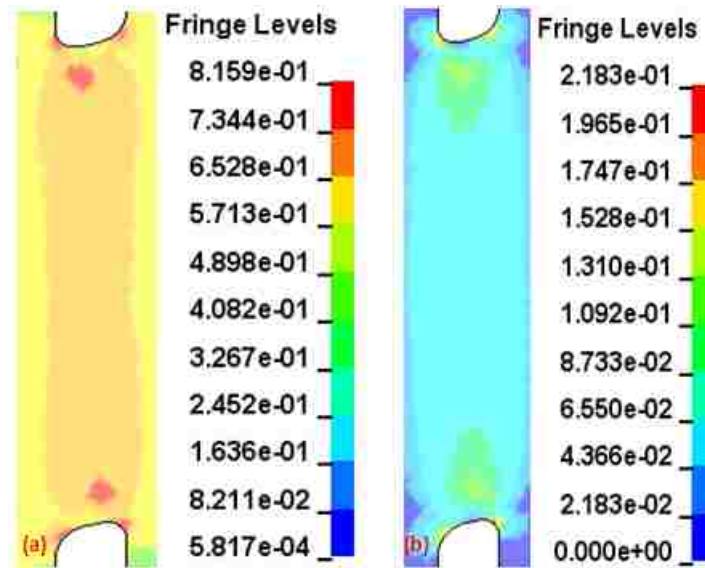
Figure 5.6 (a) von Mises effective stress (in GPa) and (b) effective plastic strain predicted in the gauge region of the DP600 shear specimen after a 2 mm displacement

The uniformity of the stress and strain distributions in the gauge region was further analyzed by plotting the predicted shear stresses and the shear strains along a virtual section (section A-A in Fig. 5.7) at the centre of the gauge region.
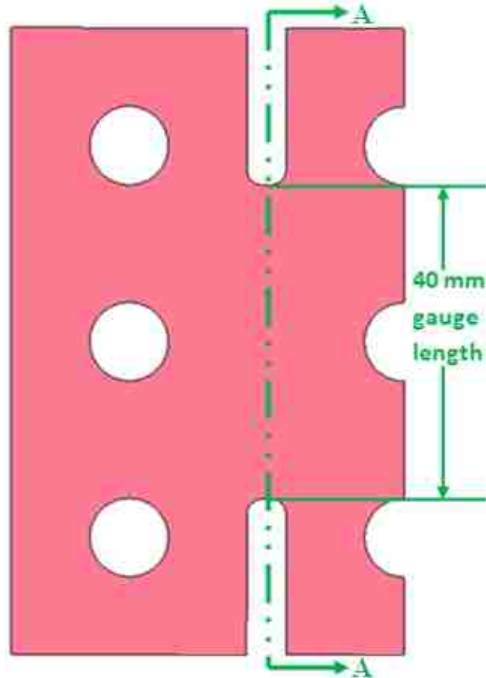
Figure 5.7 Section A-A in the centre of the gauge area of the shear specimen

The shear stress and shear strain distributions along the central section of the gauge area are plotted in Fig. 5.8. It can be seen that the shear stress is very uniform throughout the greater part of the gauge length, although the shear strain does not appear to be quite as uniformly distributed. The values of the shear stress and shear strain in the central part of the gauge area are 408 MPa and 0.0838, respectively, as indicated by the distributions in Fig. 5.8.
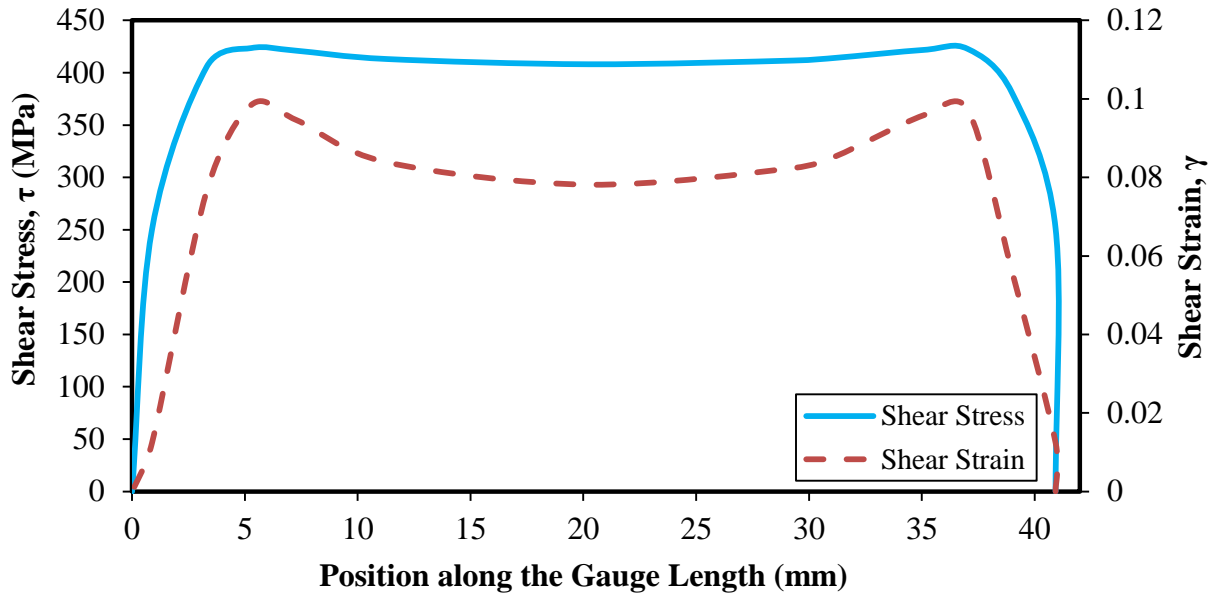
Figure 5.8 Predicted shear stresses and shear strains distributions along the gauge length of the DP600 shear specimen

In the experimental cyclic shear tests conducted on DP600 sheet specimens, the maximum displacement amplitude applied to the central portion of the specimen was ±2 mm, allowing for both forward and reverse loading. The load-displacement diagram and the shear stress - shear strain diagram are shown in Fig. 5.9 and Fig. 5.10, respectively, and the good formability of DP600 steel can be seen in both figures. Fig. 5.9 and 5.10 also show that some work hardening stagnation takes place during reverse loading.
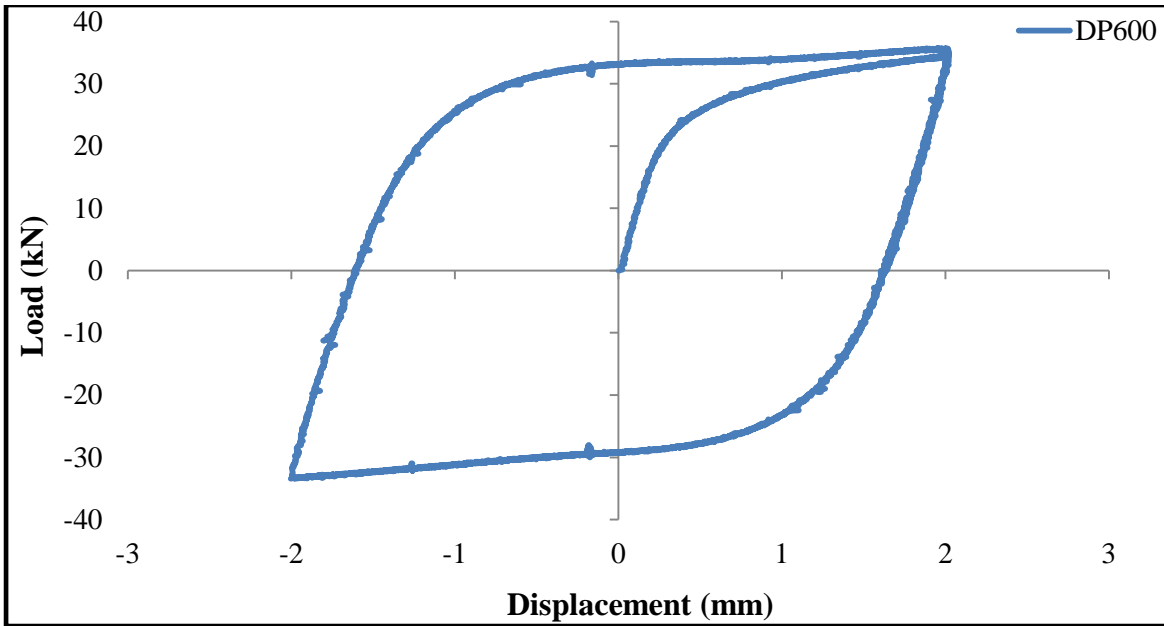
Figure 5.9 Experimental load-displacement curves obtained by cyclic shear for DP600 steel
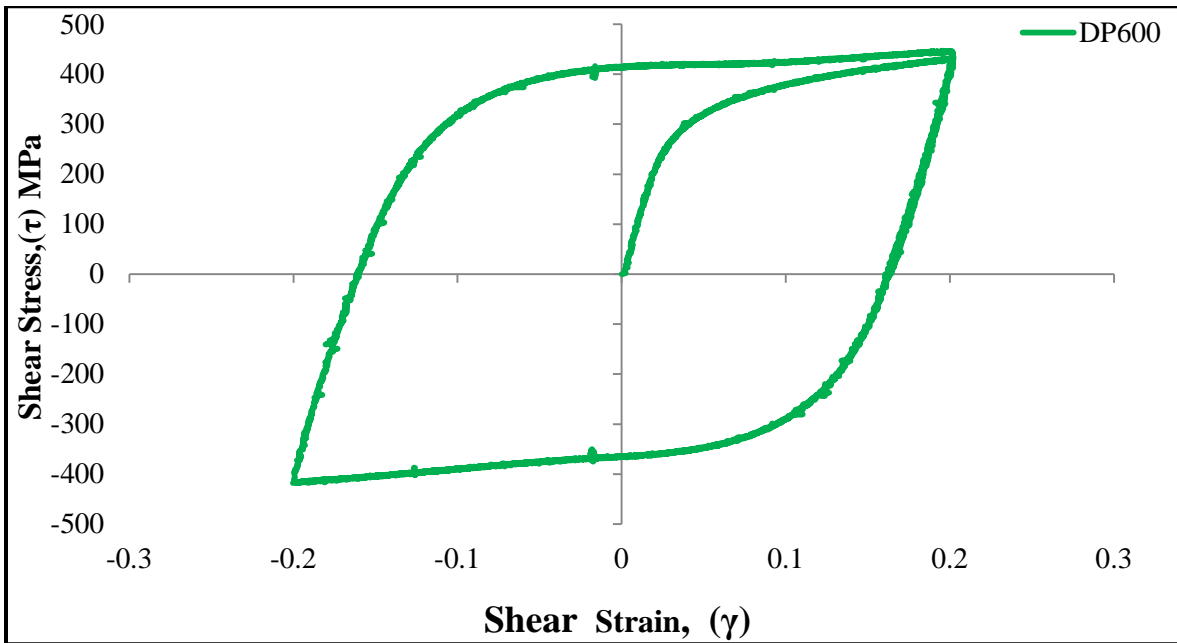
Figure 5.10 Experimental shear stress-shear strain curves for DP600 steel

The strains recorded in the gauge area of the shear specimen using the ARAMIS strain measurement system are shown in Fig. 5.11a, and 5.11b. To verify the uniformity of strain

distributions, the strains were plotted along three different sections. The first section (section 0) was defined 1 mm to the left of the central axis of the gauge area, and is depicted by a black section line in Fig. 5.11a and 5.11b. The second section (section 1) was defined exactly on the central axis of the gauge zone and is indicated by the yellow section line in both figures. The third section (section 2) was made 1 mm to the right of the central axis of the gauge region, and is denoted by the maroon section line in Fig. 5.11a and 5.11b. It can be seen that the strain distributions along each of the three sections are practically identical, as shown in Fig. 5.11b. This signifies that the uniformity of the strains in the gauge region extends to a width of at least 2 mm.
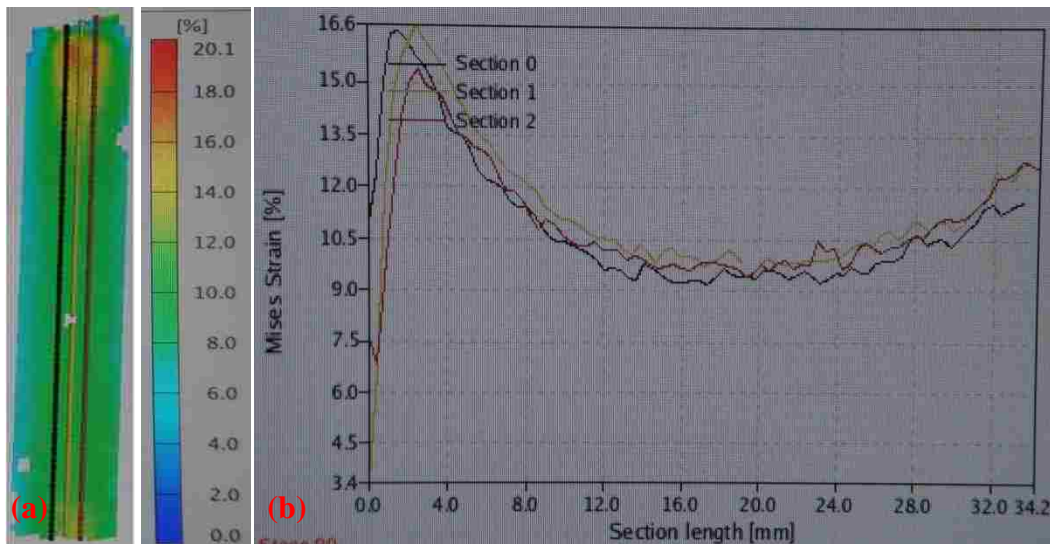
Figure 5.11 (a) three different sections on the gauge region (b) comparison of the gauge sections strain distributions obtained from the ARAMIS system for DP600 sheet steel

The shear strain distributions after loading and reverse loading were almost identical. The strain distribution images obtained from the ARAMIS system in the gauge region are shown in Fig. 5.12a and 5.12b. The shear strain in the centre of the gauge area was lower at the end of the

initial loading (0.084) than it was after the reverse loading (0.09), as shown graphically in Fig. 5.13.
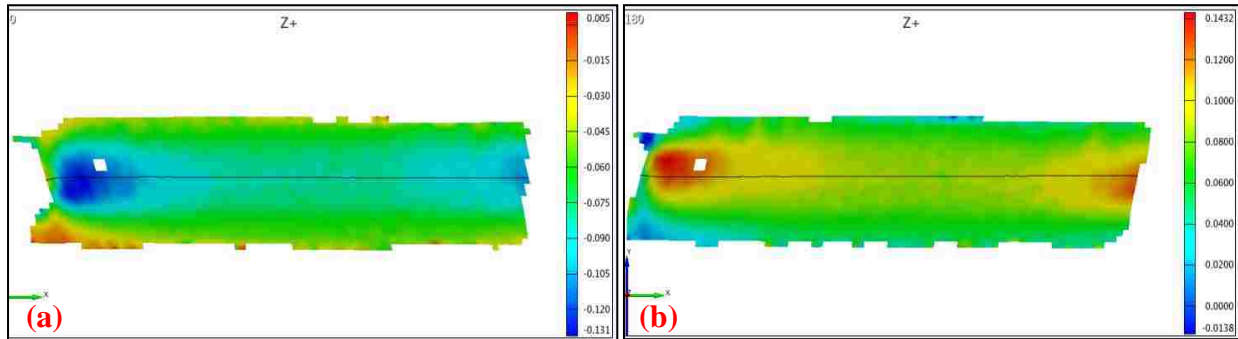
Figure 5.12 ARAMIS images of the shear strain in the gauge of DP600 specimen after (a) forward loading and (b) reverse loading
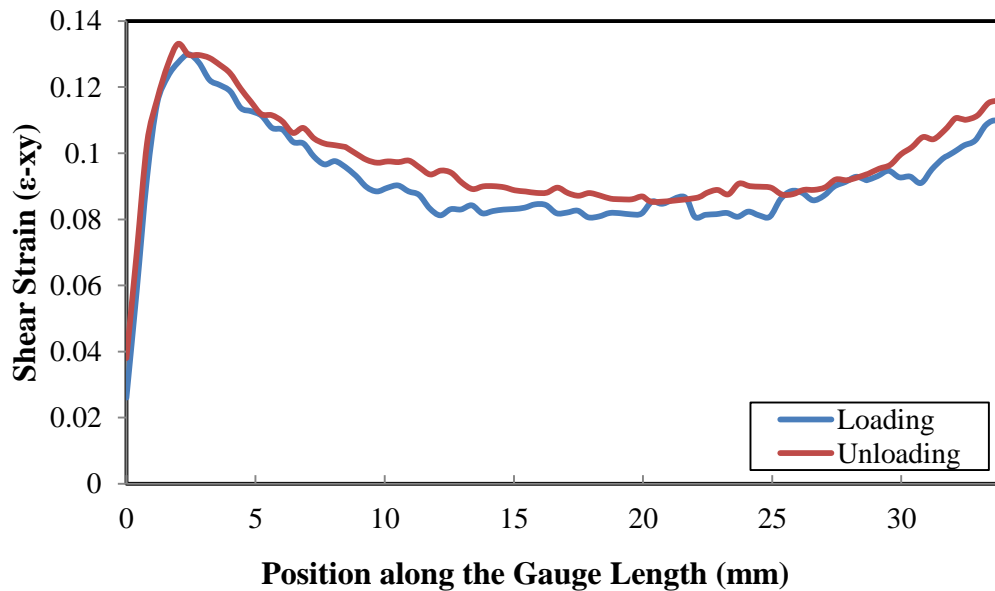
Figure 5.13 Shear strain distributions measured with the ARAMIS system along the centre of the gauge of the DP600 shear specimen after forward and reverse loading

5.2.2 DP980 CYCLIC SHEAR TEST

This section presents the predicted and experimental stresses and strains in the DP980 shear specimens. Fig. 5.14 shows the von Mises effective stresses and the effective plastic strains in the gauge area of the DP980 shear specimen after a displacement of +2 mm, predicted by

numerical simulation. It can be seen that the stress and the strain distributions are quite uniform, except near the two ends of the gauge zone. According to the fringe levels, the effective stress in the majority of the gauge region varies from 1045 MPa to 1219 MPa, and the effective plastic strain varies from 0.0667 and 0.08.

The uniformity of the stresses and strains in the gauge region was further investigated by plotting the shear stresses and shear strains along a section in the centre of the gauge region (section A-A in Fig. 5.7). The shear stress and shear strain distributions predicted by LS-DYNA are shown in Fig. 5.15. It is evident from this graph that the shear stress distribution is almost uniform throughout the gauge region, however, the shear strain exhibits peaks at the extremities of the gauge. The shear stress and the shear strain are approximately 660 MPa, and 0.056, respectively in the central part of the gauge area, as shown on the graph in Fig. 5.15.

Figure 5.14 (a) von Mises effective stress (in GPa) and (b) effective plastic strain predicted in the gauge region of DP980 shear specimen after a 2 mm displacement

103
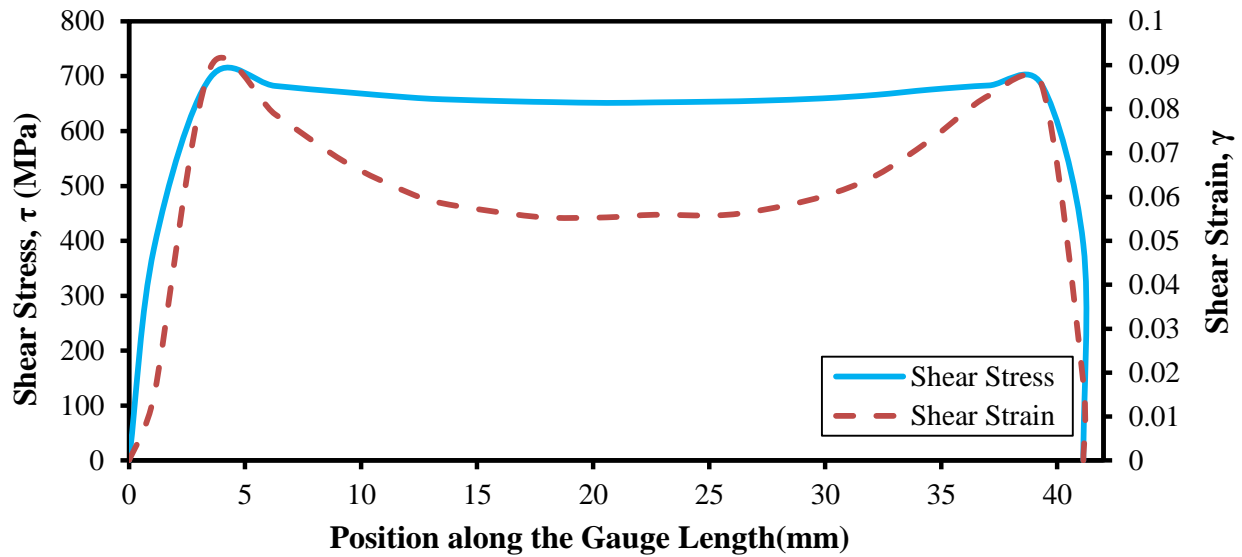
Figure 5.15 Predicted shear stresses and shear strains distributions along the gauge length of the DP980 shear specimen

In the experimental cyclic shear tests conducted on DP980 sheet specimens, the central portion of the specimen was allowed to travel 2 mm in one direction and then in the reverse direction. The load-displacement diagram and the shear stress – shear strain diagram are shown in Fig. 5.16 and Fig. 5.17, respectively. During the cyclic shear testing of DP980 specimens, a small crack was seen to propagate from the end of the slot after some plastic deformation. It can also be observed from the load-displacement curve in Fig. 5.16 (as well as the stress-strain curve in Fig.5.17) that the convexity of the curve changes direction during unloading when the shear strain is approximately zero. This is probably not work hardening stagnation but is more likely due to some slippage of the specimen in the grips. Indeed the higher strength of the DP980 steel leads to higher loads during the shear test, and the torque applied to the bolts in the testing fixture may need to be greater than 70 N-m to adequately grip higher strength specimens.

Figure 5.16 Experimental load-displacement curves obtained by cyclic shear for DP980 steel
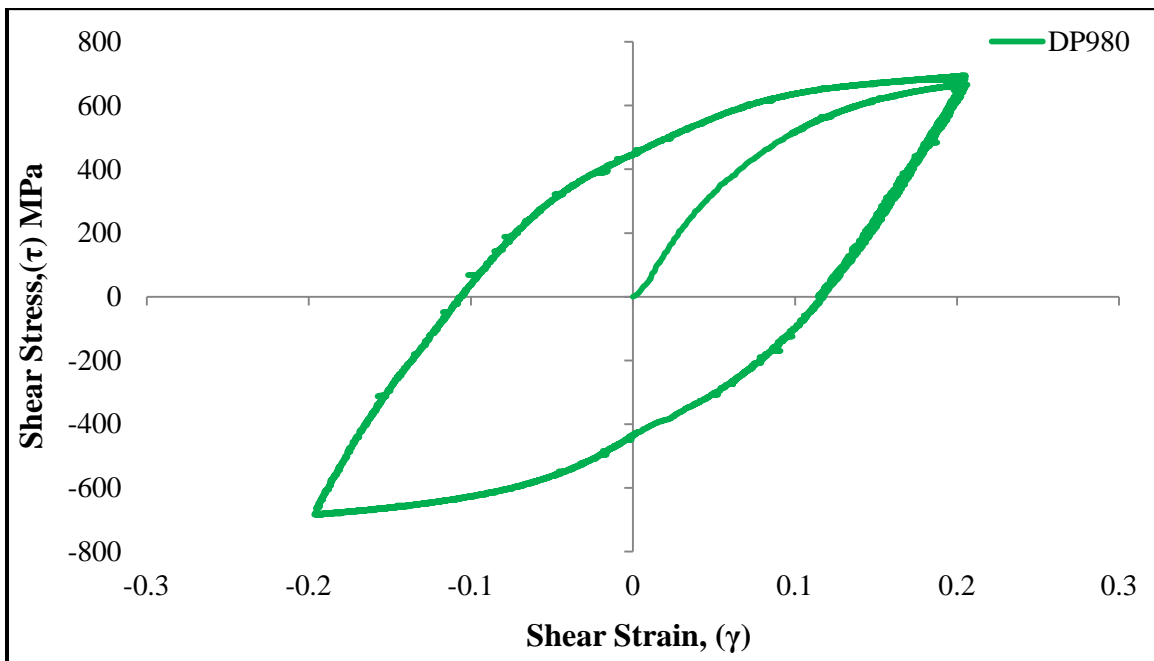
Figure 5.17 Experimental shear stresses - shears strain curves for DP980 steel

The formability of DP980 sheet steel is comparatively lower than that of the DP600 sheet material. The reason for this is the greater martensite volume fraction in the DP980 sheet metal.

The shear strains in the gauge area of the specimen were recorded by the ARAMIS system during the loading and reverse loading and are shown in Fig. 5.18(a), and (b). A section was made along the centre of the gauge region and the shear strains along this section are plotted in Fig. 5.19. It can be seen that the strain distribution after loading and reverse loading are significantly different. The shear strain in the centre of the gauge after reverse loading (0.07) was higher than that after the initial loading (0.04), as shown in Fig. 5.19. The increase in shear strain indicates that significant additional work hardening took place during reverse loading.
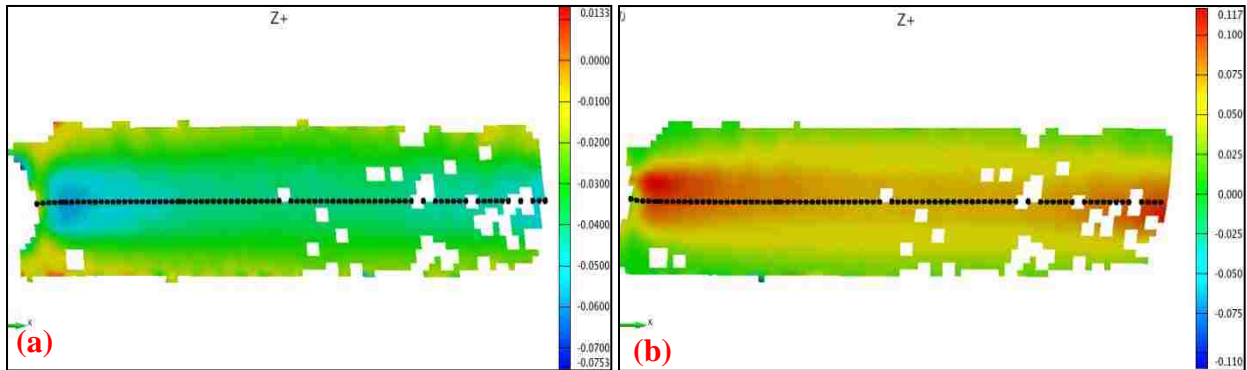
Figure 5.18 ARAMIS images of the shear strain in the gauge of DP980 shear specimen after (a) forward loading and (b) reverse loading
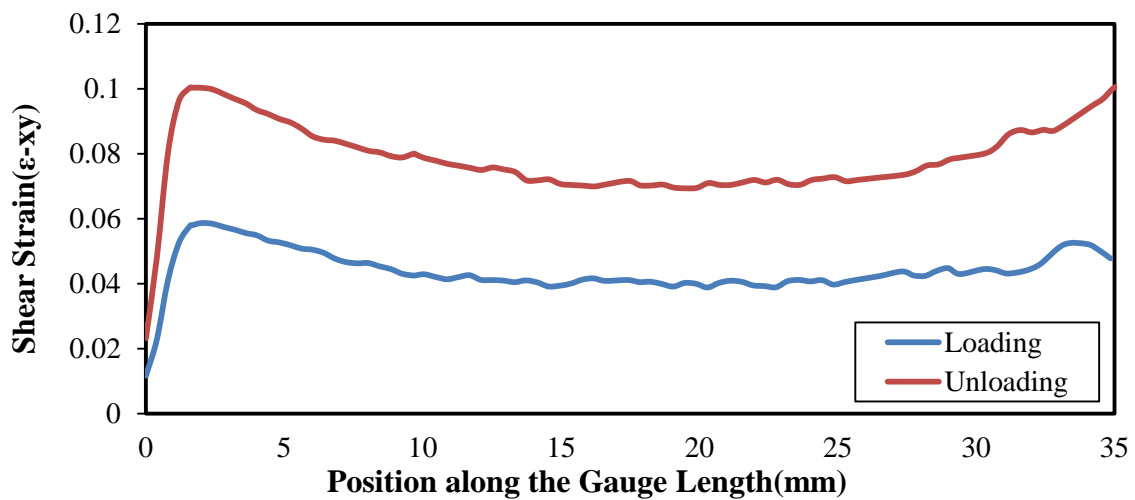
Figure 5.19 Shear strain distributions measured with the ARAMIS system along the centre of the gauge of the DP980 shear specimen after forward and reverse loading

106

5.2.3 TRIP780 CYCLIC SHEAR TEST

The predicted stress and strain distributions in the TRIP780 shear test specimens are presented. Fig. 5.20 shows the von Mises stresses and the effective plastic strains calculated by finite element analysis after a displacement of 2 mm was imposed on the TRIP780 shear specimen. Fig. 5.20 shows that the stress and the strain distributions are quite uniform, except near to the two ends of the gauge zone. According to the fringe levels, the effective stress varies from 638 MPa to 729 MPa in the majority of the gauge region, and the effective plastic strain lies between 0.0708 and 0.0885 in the gauge area. Stress and strain concentrations can nevertheless be seen at the edge of the slots, near the corner radii.
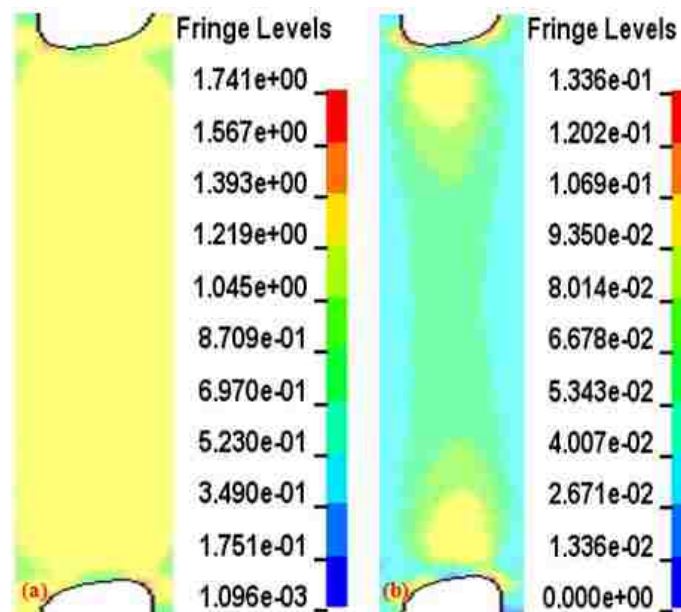

Figure 5.20 (a) von Mises effective stress (in GPa) and (b) effective plastic strain predicted in the gauge region of the TRIP780 shear specimen after a 2 mm displacement

The uniformity of the stresses and strains in the gauge region was also analyzed by plotting the shear stress and shear strain along a section at the centre of the gauge region (section A-A in Fig. 5.7). The shear stress and shear strain distributions along this central section of the

gauge region are shown in Fig. 5.21. It can be seen that there is a region of uniform shear stress and shear strain in the central part of the gauge, even though peaks inevitably exist at each end of this region. The values of the shear stress and shear strain in the centre of the gauge are 380 MPa and 0.054, respectively, as indicated in Fig. 5.21.

Figure 5.21 Predicted shear stresses and shear strains distributions along the gauge length of the TRIP780 shear specimen

In the experimental cyclic shear tests conducted on TRIP780 shear specimens, the maximum displacement applied to the specimen was 2 mm, both in forward and reverse loading. The load-displacement diagram and the shear stress shear strain diagram are shown in Fig. 5.22 and Fig. 5.23, respectively. Fig. 5.22 shows that while there is significant transient hardening upon reverse loading, there is virtually no work hardening stagnation in this TRIP780.
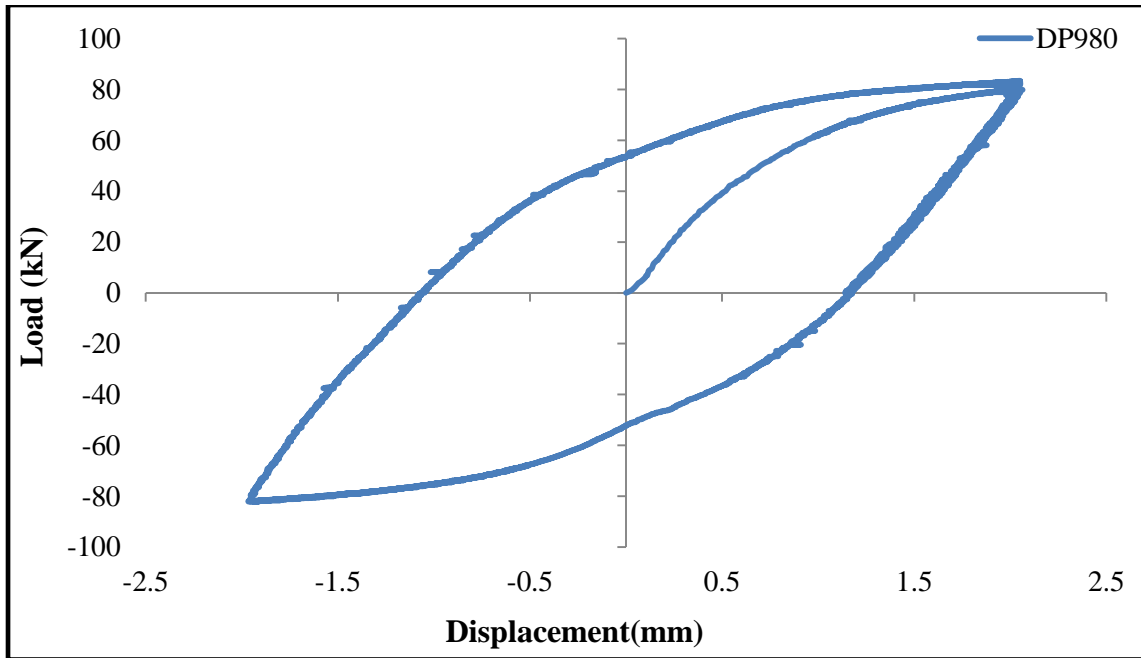
Figure 5.22 Experimental load-displacement curves obtained by cyclic shear for TRIP780 steel
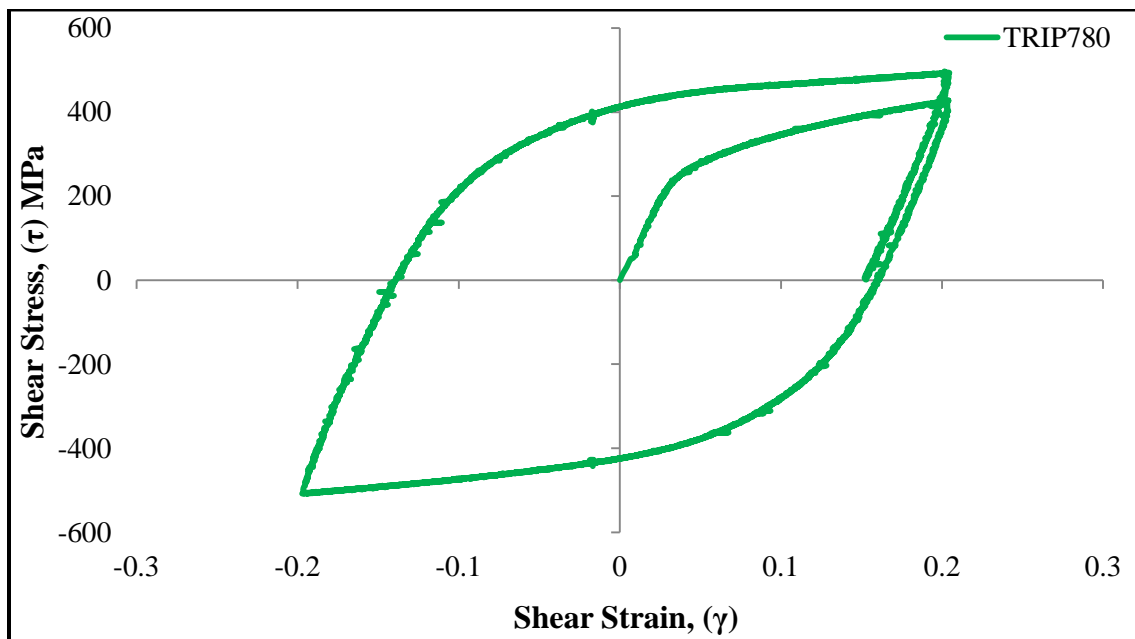
Figure 5.23 Experimental shear stresses - shear strains curves for TRIP780 steel

The shear strain distributions measured by the ARAMIS system after forward and reverse

loading are shown in Fig. 5.24(a), and (b). A section was created down the centre of the gauge to

verify the uniformity of strain distributions in the gauge region. It can be seen that the strain distributions after loading and reverse loading are almost identical; indeed, the shear strain after forward loading was about 0.062, whereas it was about 0.068 after reverse loading, as shown in Fig. 5.25.
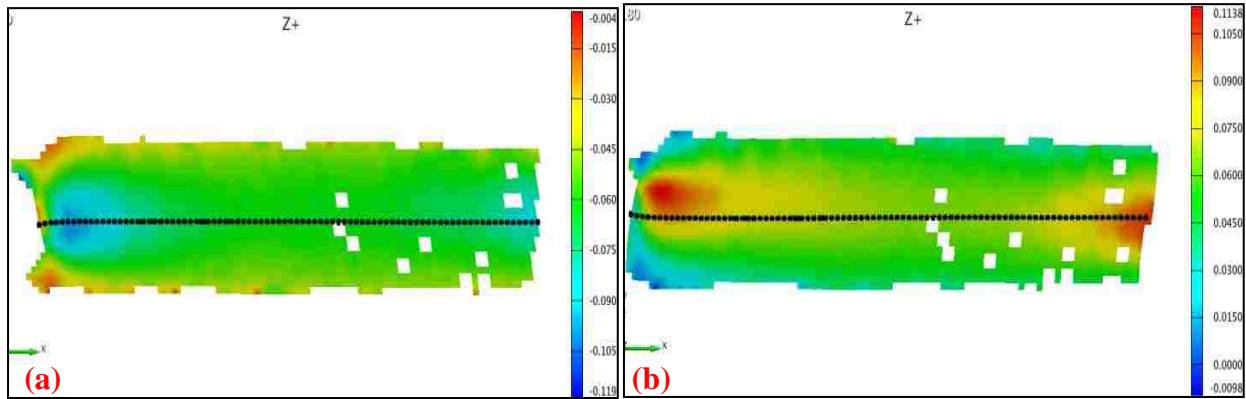
Figure 5.24 ARAMIS images of shear strain distribution of TRIP780 sheet steel (a) forward cyclic loading (b) reverse cyclic loading
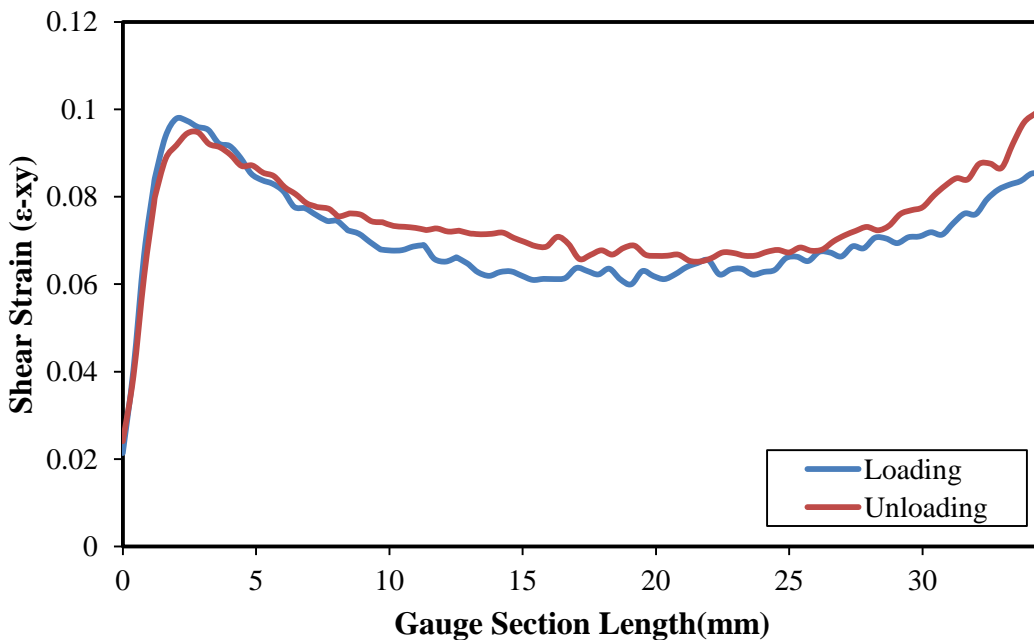
Figure 5.25 Shear strain distributions at the centre of the gauge section of TRIP780 steel sheet during the cyclic loading and unloading condition obtained from ARAMIS system

110

5.2.4 HSLA CYCLIC SHEAR TEST

This section presents the predicted stress and strain distributions in the HSLA shear test specimens. Fig. 5.26 shows the von Mises effective stresses and the effective plastic strains predicted by LS-DYNA when a 1.5 mm displacement was applied to the HSLA shear test specimen. Fig. 5.26 shows that in the majority of the gauge region the stress and the strain distributions are uniform, except near to the two ends. According to the fringe levels, the stress in the centre of the gauge varies from 451 MPa to 507 MPa; the effective plastic strains in the same region vary from 0.0857 to 0.1144. Given the geometry of the shear specimen, it can be expected that stress and strain concentrations will exist near the ends of the slots; however, there remains a significant region of the gauge in which the stresses and strains are reasonably uniform.
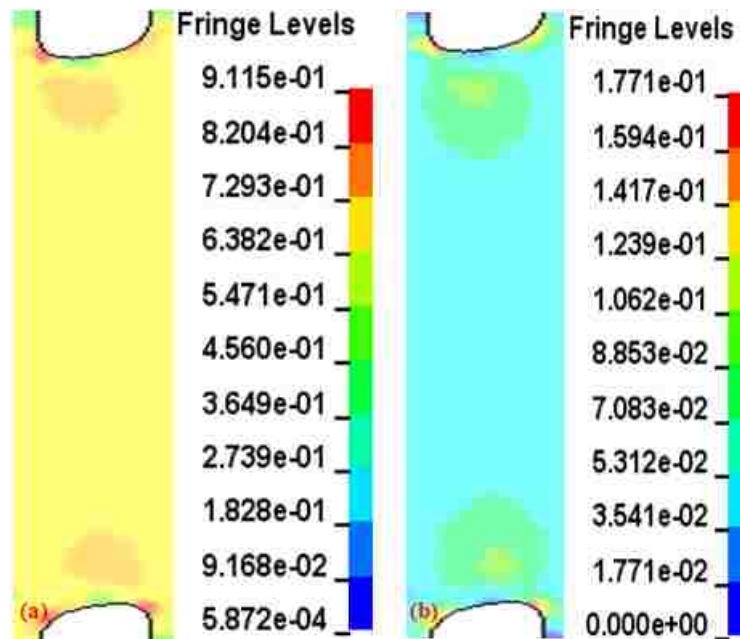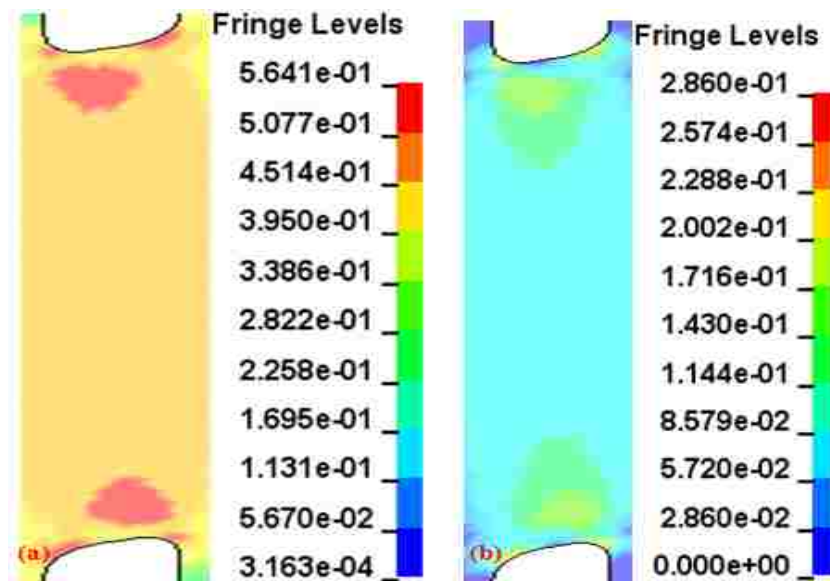

Figure 5.26 (a) von Mises effective stress (in GPa) and (b) effective plastic strain predicted in the gauge region of the HSLA shear specimen after a 2 mm displacement

The uniformity of the stresses and strains in the gauge region was also analyzed by plotting the predicted shear stress and shear strain along a section at the centre of the gauge area

(section A-A in Fig. 5.7). The shear stress and shear strain distributions along this central section of the gauge region are shown in Fig. 5.27. It can be seen that the shear stress distribution, and to a lesser extent the shear strain distribution, is relatively uniform. The values of the shear stress and shear strain in the centre of the gauge are approximately 283 MPa and 0.086, respectively, as shown in Fig. 5.27.
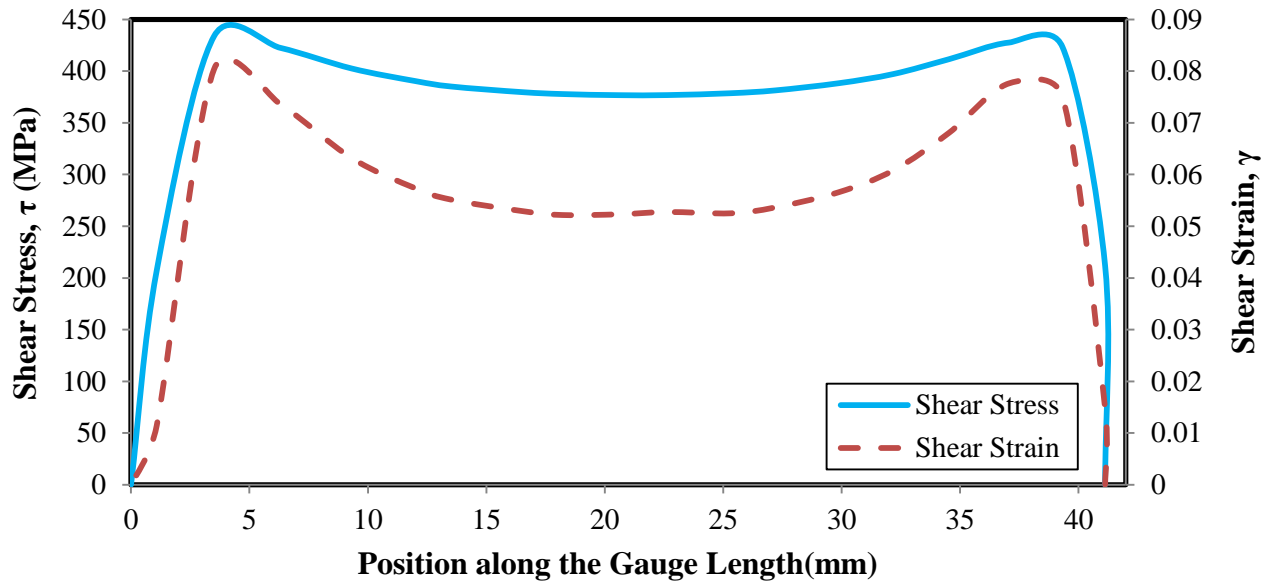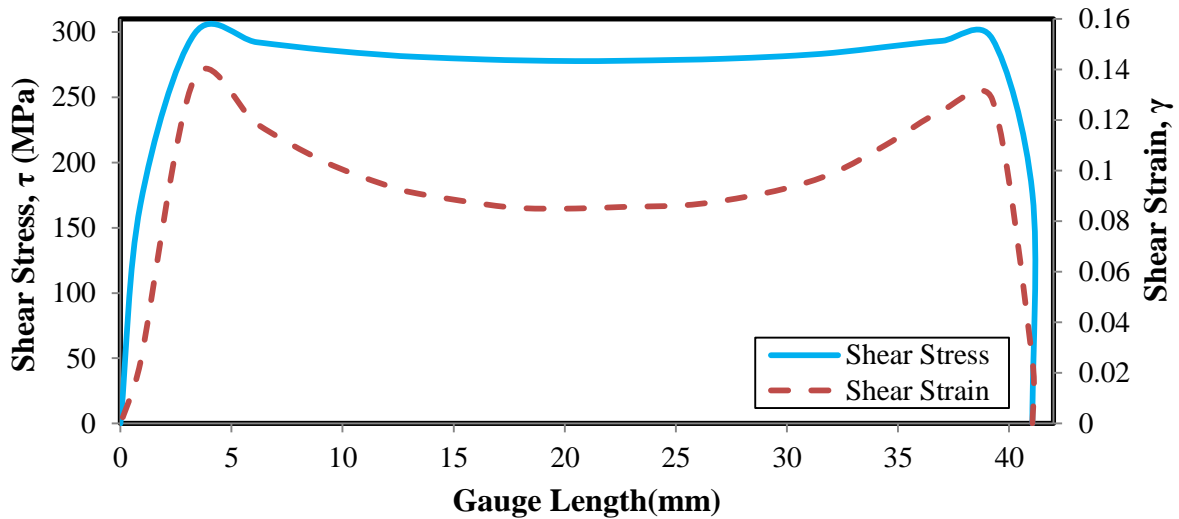

Figure 5.27 Predicted shear stresses and shear strains distributions along the gauge length of the HSLA shear specimen

In the experimental cyclic shear tests conducted on HSLA sheet specimens, maximum displacement applied to the central portion of the shear specimen was 1.5 mm distance, both in forward and reverse loading (the 0.8 mm thickness of the HSLA sheet made it difficult to apply a displacement amplitude greater than ±1.5 mm, because of the risk of tearing in the ends of the slots). The load-displacement diagram and the shear stress shear strain diagram are shown in Fig. 5.28 and Fig. 5.29, respectively.
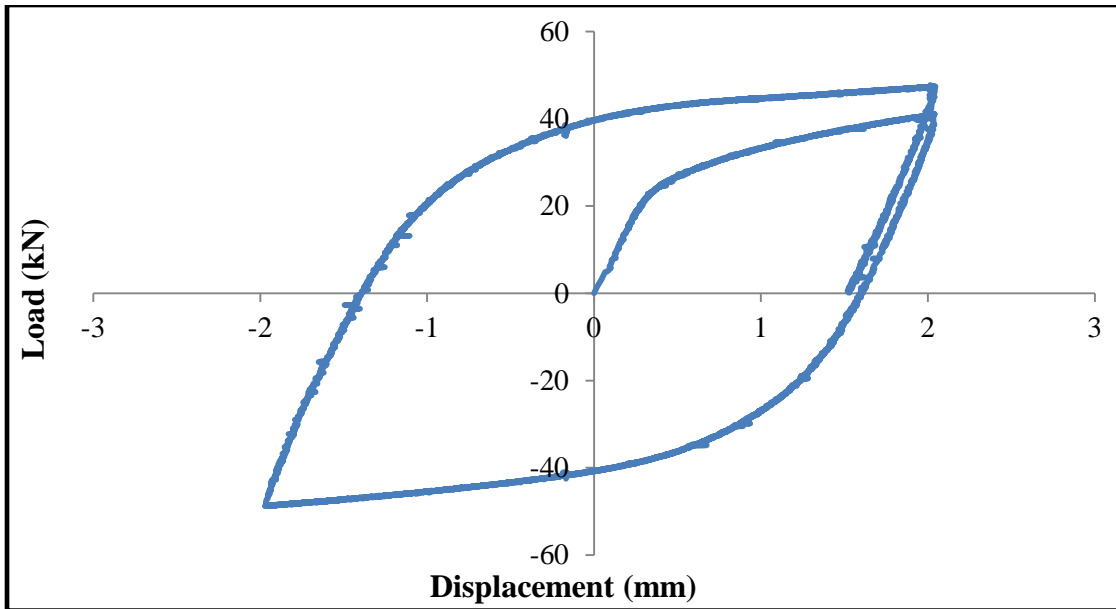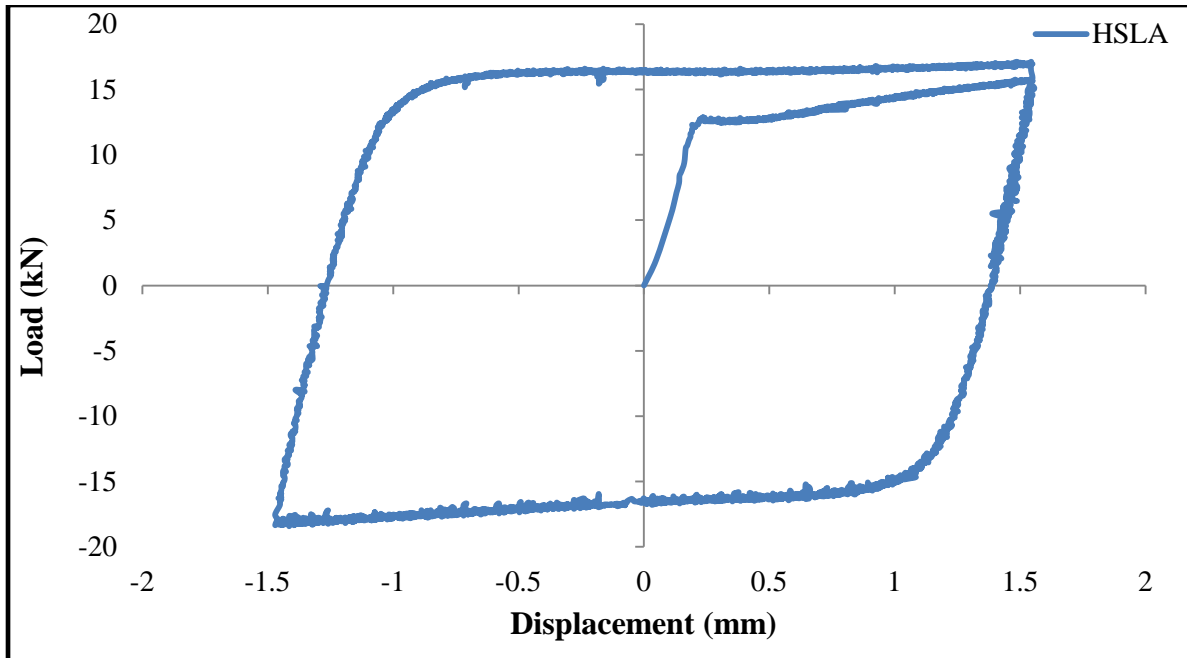
Figure 5.28 Experimental load-displacement curves obtained by cyclic shear for HSLA steel
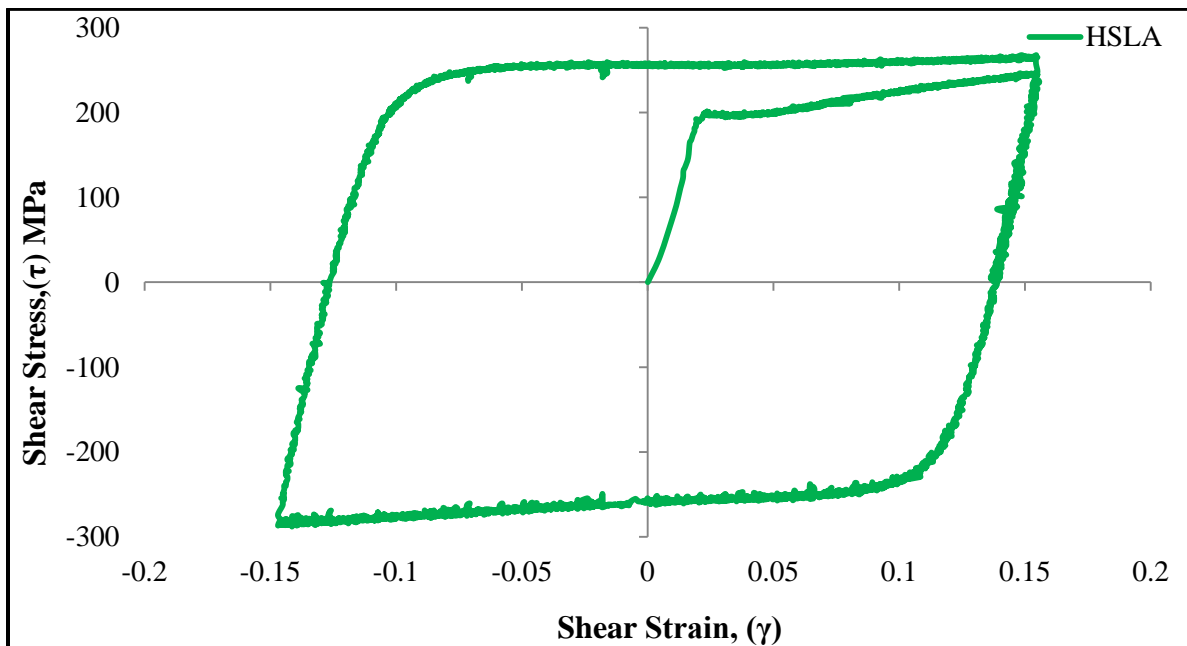
Figure 5.29 Experimental shear stresses - shear strains curves for HSLA steel

The shear strain distributions measured by the ARAMIS system after loading and reverse

loading cycle are shown in the Fig. 5.30 (a), and (b). Once again, a section was made down the

middle of the gauge area to verify the uniformity of strain distributions in the gauge region. It can be observed that the strain distributions are reasonably uniform in the centre of the gauge. The shear strain during forward loading was found 0.072, whereas in reverse loading the shear strain decreased to 0.068, as shown in Fig. 5.31.
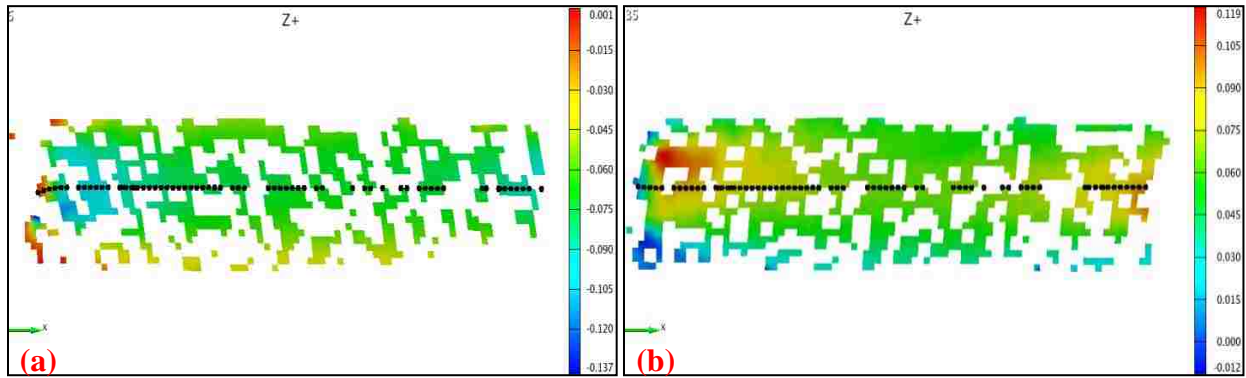
Figure 5.30 ARAMIS images of shear strain in the gauge of HSLA specimen after (a) forward loading and (b) reverse loading
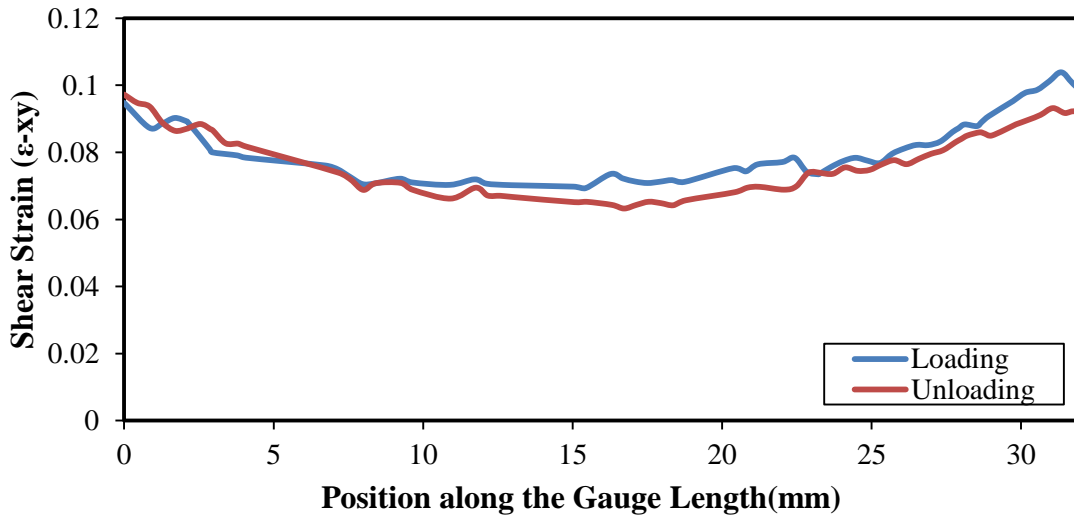
Figure 5.31 Shear strain distributions measured with the ARAMIS system along the centre of the gauge of the HSLA shear specimen after forward and reverse loading

The numerical simulation of the shear test showed that the stress and strain distributions in the shear specimen were reasonably uniform for all four grades of sheet steel. This signifies

that the shear specimen design was adequate for the purpose of determining the experimental work hardening behaviour of sheet metal alloys.

The experimental cyclic shear tests were carried out successfully with the proposed designs for the testing fixture and the test specimen. The work hardening behaviour was obtained for a complete loading - reverse loading - reloading cycle for each sheet material. The strain amplitude that was achieved was ± 0.2 for the AHSS, and ± 0.15 for the thinner HSLA sheet. This is significantly greater than the strain amplitude that can be achieved in typical tension-compression tests for sheet specimens.

6. CONCLUSIONS

Cyclic shear testing of sheet materials has been well investigated during the last few years; nevertheless the present work represents a further contribution to this field. First of all, a new sheet specimen was developed to carry out cyclic shear tests. Secondly, a very simple cyclic shear test fixture was developed, that is easy to install and use in a conventional testing machine. This testing fixture was used to successfully obtain the cyclic shear stress-strain behaviour of four anisotropic steel sheets (DP600, DP980, TRIP780 and HSLA). This chapter summarizes the conclusions that can be made from the current research, and proposes some ideas for future research.

After completing the development of this cyclic shear test, the following observations and conclusions can be made:

- The proposed fixture is able to apply balanced symmetrical shearing loads to a sheet specimen without generating adverse bending moments.

- The lateral deflections in the designed fixture were negligible under maximum loads; therefore, this fixture is sufficiently rigid to apply shearing loads on sheet materials with a tensile strength around 1000 MPa without inducing excessive bending moments.

- The proposed specimen design (Fig. 3.10) provides two gauge areas that are equidistant to the central plane of symmetry, and whose aspect ratio is such that the stress and strain distributions in the gauge area are relatively uniform. However, the numerical analysis showed that a gauge area with a length-to-width ratio greater than 8 should lead to even more uniform stress and strain distributions.

116

- The 2-mm corner radii at the end of the slots help to minimize the stress concentrations at the extremities of the gauge areas and delay the onset of cracking and failure. This allows the shear test to generate stress-strain data up to relatively large strain amplitudes (±0.2).

- Finite element simulations of the shear test were required to compute the stress and strain distributions in the designed specimens (using LS-DYNA), and were necessary to complete the design optimization process.

- The fabricated test fixture was used to effectively obtain the shear stress vs. shear strain curves of four grades of sheet steel up to strain amplitudes of ±0.2.

- The ARAMIS optical strain measurement system was successfully used to accurately determine the strains in the gauge area of the shear test specimen.

- It was observed that DP600, DP980 and TRIP780 steels showed more or less Bauschinger effect.

- TRIP780 showed evidence of a significant transient behaviour upon reverse loading.

- HSLA seemed to exhibit isotropic hardening behaviour and no Bauschinger effect.

- In the shear tests on DP980 sheet specimens, experimental data showed that there is likely some slippage of the specimen in the clamps even though knurled blocks were mounted into the fixture to increase friction. Additional effort will be required to eliminate slippage in specimens made from higher strength materials.

- In spite of differences in deformation mode between simple shear, tension-compression and bending, the shear test appears to be a good way of characterizing the cyclic behaviour of sheet materials up to large strains.

The development of this simple test to experimentally determine the cyclic behaviour of sheet materials will allow further progress to be made in the numerical simulation of forming and springback behaviour. Future work in this area should consider developing an optimization technique to calculate the material parameters in various advanced material models from the experimental cyclic shear test data. Finally, it would be of great practical interest to evaluate whether work hardening data obtained from the cyclic shear test or the tension-compression test or the bending-unbending test lead to the most accurate predictions of forming and springback behaviour.

APPENDIX A

CYCLIC SHEAR TEST FIXTURE COMPONENTS AND ASSEMBLY DRAWINGS WITH BILL OF MATERIALS

BILL OF MATERIALS

PART NUMBER	PART NAME	MATERIALS	QUANTITY
1	FIXED UPPER PART	AISI 4140	1
2	MOVABLE LOWER PART	AISI 4140	1
3	HOLDING BLOCK	AISI 4140	3
4	SHEET METAL SPECIMEN	DP600	5
4	SHEET METAL SPECIMEN	DP980	5
4	SHEET METAL SPECIMEN	TRIP780	5
4	SHEET METAL SPECIMEN	HSLA	5
5	HEX SOCKET HEAD BOLT	ASTM 574	9

Detail A

Section view B-B

0.5

0.5

2.3

2.3

5

20

CYCLIC SHEAR TEST FIXTURE

UNIVERSITY OF WINDSOR

MECHANICAL ENGINEERING DEPARTMENT

DIMENSIONS ARE IN MILLIMETERS
THIRD ANGLE PROJECTION

MATERIAL:
AISI/SAE 4140

DRAWING TITLE:
FIXTURE ASSEMBLY

DRAWN BY: SAMRUL ALAM SARKER

CHECKED BY: DANIELA PUSCA, P. Eng.

APPROVED BY: DANIEL E. GREEN, P. Eng.

CAD APPLICATION: CATIA V5

PART NO.

QUANTITY: 1

SCALE 1:3   SHEET 1 of 1

PROPRIETARY AND CONFIDENTIAL

NOTES:
ALL SHARP CORNERS 0.5 x 0.5 UNLESS OTHERWISE SPECIFIED

DIMENISONS ARE IN MILIMITERS		MATERIAL: AISI/SAE 4140		CYCLIC SHEAR TEST FIXTURE
THIRD ANGLE PROJECTION		DRAWING TITLE: FIXED UPPER PART		
UNLESS OTHERWISE SPECIFIED LINEAR TOLERANCES:	UNLESS OTHERWISE SPECIFIED ANGULAR TOLERANCES:	DRAWN BY: SAMSUL ALAM SARKER	DATE: 28/10/2010	UNIVERSITY OF WINDSOR
X ±0.5 X.Xx ±0.25 X.XX ±0.01 X.XXX ±0.001	X ± 1° X.X ± 0°50' X.XX ± 0°30'30"	CHECKED BY: DANIELA FUSCA, P. Eng.	DATE: 04/11/2010	MECHANICAL ENGINEERING DEPARTMENT
PROPRIETARY AND CONFIDENTIAL		APPROVED BY: DANIEL E. GREEN, P. Eng.	DATE: 18/10/2010	PART NO: 1 QUANTITY: 1
THE INFORMATION CONTAINED IN THIS DRAWING IS THE SOLE PROPERTY OF THE UNIVERSITY OF WINDSOR MECHANICAL ENGINEERING DEPARTMENT. ANY REPRODUCTION IN PART OR AS A WHOLE WITHOUT THE WRITTEN PERMISSION OF THE UNIVERSITY OF WINDSOR IS PROHIBITED.		CAD APPLICATION: CATIA V5		SCALE 1:5 SHEET 1 of 2

Ø100

6 x Ø12.9
Ø12.4
⌴Ø18
⎍8

⌖ Ø0.2Ⓜ A

Ø38
⎍3

360 ±0.5
30 ±0.3
120 ±0.3
30 ±0.2
80 ±0.3
30 ±0.2   ⊥ 0.2Ⓜ A
60 ±0.3
⬦ 0.2   B
R 0.5

A   ⬦ 0.2
4 x 0.5 x 45°
2 x R5
6 x Ø8.5 ± 0.1
⎍22
M10 x 1.50
⎍20
⌖ Ø0.2Ⓜ B
15
30 +0.3 +0.1
⊥ 0.1Ⓜ A B

Ø 140 ±0.5
30 ±0.1
160.5° ±0.25°
25
25
25
15
30
100 ±0.3
⊥ 0.1Ⓜ A B
100 ±0.3

121

CYCLIC SHEAR TEST FIXTURE

UNIVERSITY OF WINDSOR

MECHANICAL ENGINEERING DEPARTMENT

| DIMENISONS ARE IN MILIMITERS | | MATERIAL: AISI/SAE 4140 |
| THIRD ANGLE PROJECTION | | DRAWING TITLE: **MOVABLE LOWER PART** |

UNLESS OTHERWISE SPECIFIED LINEAR TOLERANCES:	UNLESS OTHERWISE SPECIFIED ANGULAR TOLERANCES:
X ± 0.5	X ± 1°
X.XX ± 0.25	X.X ± 0°30'
X.XXX ± 0.01	X.XX ± 0°30'00"
X.XXXX ± 0.001	

DRAWN BY: SAMSUL ALAM SARKER — DATE: 29/10/2010

CHECKED BY: DANIELA PUSCA, P. Eng. — DATE: 04/11/2010

APPROVED BY: DANIEL E. GREEN, P. Eng. — DATE: 18/10/2010

CAD APPLICATION: **CATIA V5**

PART NO: 2

QUANTITY: 1

SCALE 1:5

SHEET 1 of 3

PROPRIETARY AND CONFIDENTIAL

THE INFORMATION CONTAINED IN THIS DRAWING IS THE SOLE PROPERTY OF THE UNIVERSITY OF WINDSOR MECHANICAL ENGINEERING DEPARTMENT. ANY REPRODUCTION IN PART OR AS A WHOLE WITHOUT THE WRITTEN PERMISSION OF THE UNIVERSITY OF WINDSOR IS PROHIBITED.

⊥ | 0.1 (M) | A | B

▱ | 0.2 | B

60 ±0.3

30 ±0.3

330 ±0.5

220 ±0.5

30 ±0.3

R 0.5

⊥ | 0.1 (M) | A | C

30 ⁻⁰·³₋₀.₅

3 x ⌀8.5 ± 0.1 ▽22
M10 x 1.50 ▽20
⊕ | 0.2 (M) | B

15

15

25

15

80 ±0.3

4 x 0.5 x 45°

▱ | 0.2 | A

⌀140 ±0.5

⌀100

6 x ⌀12.9
⌀12.4
⌀18 ▽8

⊕ | ⌀0.2 (M) | A

⌀38 ▽3

NOTES:
ALL SHARP CORNERS 0.5 x 0.5 UNLESS OTHERWISE SPECIFIED

122

CYCLIC SHEAR TEST FIXTURE

UNIVERSITY OF WINDSOR

MECHANICAL ENGINEERING DEPARTMENT

DIMENISONS ARE IN MILIMITERS	MATERIAL:- AISI/SAE 4140		
THIRD ANGLE PROJECTION	DRAWING TITLE: HOLDING BLOCK		

UNLESS OTHERWISE SPECIFIED LINEAR TOLERANCES:
UNLESS OTHERWISE SPECIFIED ANGULAR TOLERANCES:
X ± 0.5
X.X ± 0.25
X.XX ± 0.01
X.XXX ± 0.001
X ± 1°
X.X ± 0°30'
X.XX ± 0°30'30"

PROPRIETARY AND CONFIDENTIAL

THE INFORMATION CONTAINED IN THIS DRAWING IS THE SOLE PROPERTY OF THE UNIVERSITY OF WINDSOR MECHANICAL ENGINEERING DEPARTMENT. ANY REPRODUCTION IN PART OR AS A WHOLE WITHOUT THE WRITTEN PERMISSION OF THE UNIVERSITY OF WINDSOR IS PROHIBITED.

DRAWN BY: SAMSUL ALAM SARKER	DATE: 29/10/2010	
CHECKED BY: DANIELA PUSCA, P. Eng.	DATE: 04/11/2010	
APPROVED BY: DANIEL E. GREEN, P. Eng.	DATE: 18/10/2010	
CAD APPLICATION: CATIA V5	PART NO: 3	QUANTITY: 3
	SCALE 1:1	SHEET 1 of 4

3 X | ⌖ | 0.2 (M) | A | B | C |

3 X Ø10.7
Ø10.2

3
19
25 +0.4 +0.2
15
25
25
80 ±0.3

C
B
A

6 x 0.5 x45°
12.7

| ▱ | 0.2 | A |

SECTION A-A

NOTES:
ALL SHARP CORNERS 0.5 x 0.5 UNLESS OTHERWISE SPECIFIED
USE M10 x 1.50 FASTENERS WITH MMC 10.0

1.5 ±0.2

123
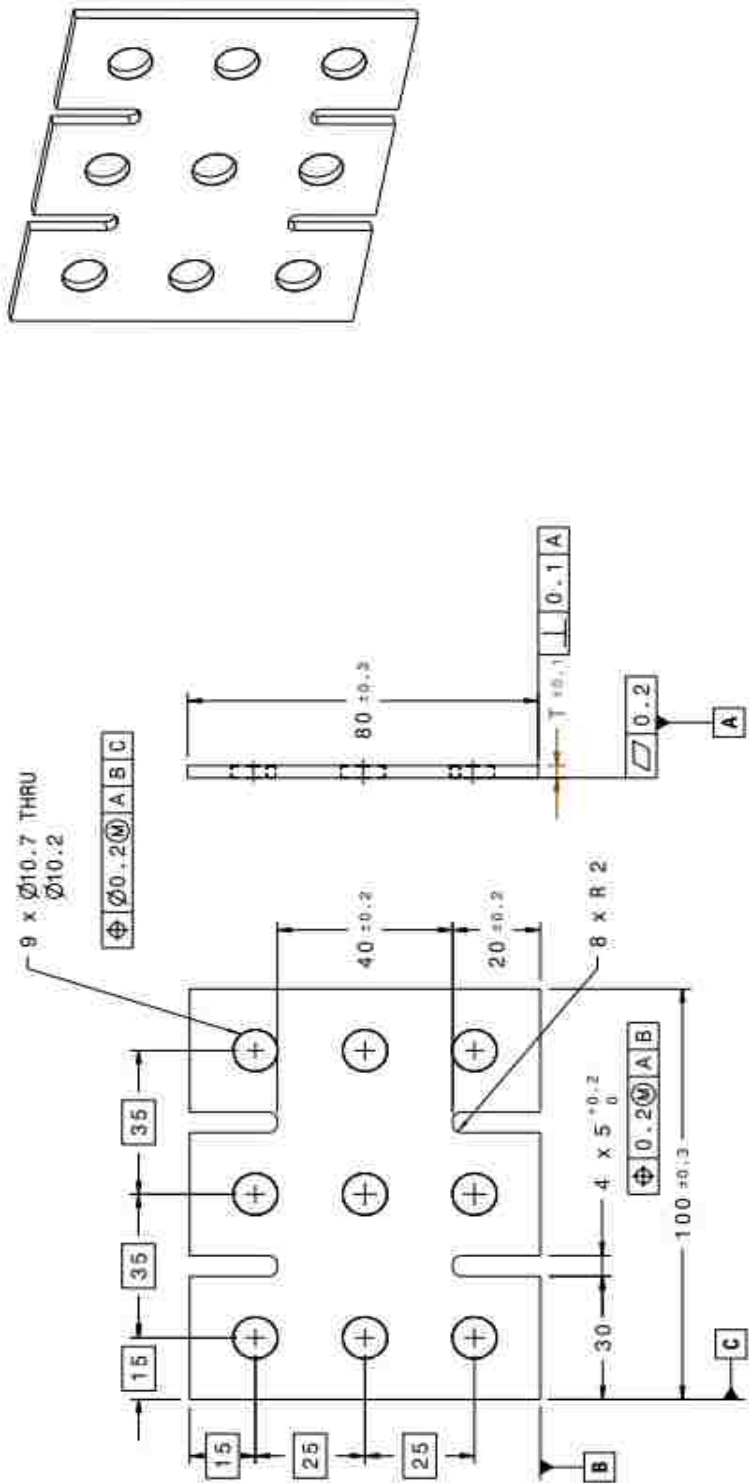
NOTES:
ALL SHARP CORNERS 0.5 x 0.5 UNLESS OTHERWISE SPECIFIED
USE M10 FASTENERS WITH MMC 10.0

Materials	Thickness(T)
DP600	1.00
DP980	1.50
TRIP780	1.20
HSLA	0.80

CYCLIC SHEAR TEST FIXTURE

UNIVERSITY OF WINDSOR

MECHANICAL ENGINEERING DEPARTMENT

MATERIAL:
DP 600/DP980/TRIP780/HSLA

DRAWING TITLE:
SHEET METAL SPECIMEN

DRAWN BY: SAMMIE ALAM SARKER
DATE: 29/10/2018

CHECKED BY: DANIELA PUSCA, P. Eng
DATE: 06/11/2018

APPROVED BY: DANIEL E. GREEN, P. Eng
DATE: 16/10/2018

CAD APPLICATION: CATIA V5

PART NO. 4

QUANTITY: 5

SCALE 1:1

SHEET 1 of 5

DIMENSIONS ARE IN MILLIMETERS

THIRD ANGLE PROJECTION

PROPRIETARY AND CONFIDENTIAL

M10 x 1.50

Ø10

HEX 8

20

35

10

Ø 16

125

REFERENCES

1) Zhao, K., and Lee, J., "Generation of Cyclic Stress Strain Curves for Sheet Metals", *Proceedings in the ASME Journal of Engineering Materials and Technology*, 2001, vol.123, pp.391-397

2) Taherizadeh, A., "Numerical Simulation of Sheet Metal Forming Using Non-Associated Flow Rule and Mixed Isotropic Nonlinear Kinematic Hardening Model", *Doctor of Philosophy Dissertation*, 2009, The University of Windsor, Windsor, Ontario, Canada

3) Yi, K., Kim, W., Tyne, J., and Moon, H., "Analytical Prediction of Springback Based on Residual Differential Strain during Sheet Metal Bending", *Proceedings in the Journal of Mechanical Engineering Science,* 2008, vol. 222, pp. 117-129

4) Buranathiti, T., "Design Optimization under Uncertainty in Sheet Metal Forming Process Constrained with Failure Analysis", *Doctor of Philosophy Dissertation*, 2005, Northwester University, Evanston, Illinois, USA

5) Barlat, F., Garcio, J., Lee, M., Rauch, D., and Vincze, G., "An Alternative to Kinematic Hardening in Classical Plasticity", *Proceedings in the International Journal of Plasticity*,2011, doi:10.106/j.ijplas.2011.03.003

6) Ogawa, T., Hirahara, A., and Yoshida, F., "Reduction of Springback of Sheet Metals by Bottoming", *Proceedings of the Conference of American Institute of Physics*, 2010, vol. 1252, pp. 919-926

7) Fu. Z., and Mo. J., "Springback Prediction of High-Strength Sheet Metal under Air Bending Forming and Tool Design Based on GA-BPNN", *Proceedings in the International Journal of Advanced Manufacturing Technology*, 2011, vol.53, pp. 473-483

8) Sanchez, L., "Modeling of Springback, Strain Rate and Bauschinger Effects for Two Dimensional Steady State Cyclic Flow of Sheet Metal Subjected to Bending under Tension", *Proceedings in the International Journal of Mechanical Science*, 2010, vol.52, pp.429-439

9) Schilp, H., Suh, J., and Hoffmann, H., "Reduction of Springback using Simultaneous Stretch Bending process", *Proceedings in the International Journal of Material Forming*, 2011, pp.1-6, doi. 10.1007/s 12289-011-1031-1

10) Lim, H., Lee, M., Sung, J., Wagoner, R., " Time Dependent Springback", *Proceedings in the International Journal of Material Forming*, 2008, vol.1, pp.157-160

11) Wagoner, R., Carden, W., and Matlock, D., "Springback after Drawing and Bending of Metal Sheets", *Proceedings in the Intelligent Processing and Manufacturing of Materials (IPMM)*, 1997, vol.1, pp. 1-10

12) Wagoner, R., Geng, L., and Li, K., "Simulation of Springback with the Draw / Bend Test", *Proceedings in the Conference on Intelligent Processing and Manufacturing of Materials (IPMM)*, 1999, Honolulu, HI, USA, vol.1, pp. 91-104

13) Wagoner, R., and Li, M., "Simulation of Springback: Through Thickness Integration", *Proceedings in the International Journal of Plasticity*, 2007, vol. 23, pp.345-360

14) Wagoner, R., Geng, L., and Balakrishnan, V., "Springback Simulation with Non-Isotropic Hardening", *Proceedings in the 3rd ESAFORM Conference on Material Forming*, 2000, Stuttgart, Germany, vol. 7, pp.3-6

15) Wagoner, R., Geng, L., and Balakrishnan, V., "Role of Hardening Law in Springback", *Proceedings in the Plastic and Viscoplastic Response of Materials and Metal Forming*, 2000, Neat Press, Baltimore, MD, USA, pp.609-611

16) Wagoner, R., and Li, M., "Advances in Springback", *Proceedings in the NUMISHEET*, 2005, Detroit, MI, USA, vol. 778, pp.209-214

17) Carden, W., Geng, L., Matlock, D., Wagoner, R., "Measurement of Springback", *Proceedings in the International Journal of Mechanical Sciences*, 2002, vol. 44, pp. 79-101

18) Tresca, H., "Journal of Academy of Science", Paris, 1864, vol. 59, pp.754

19) von Mises, R., "Mechanics of the Body in the Plastically deformable States", *Proceedings in the Journal of Mathematics and Physics*, 1913, vol.1, pp.582-592

20) Liewald, M., Held, C., and Schleich, R., "Characterization of Sheet Metal Formability-A Review and New Approaches", *Proceedings in the Journal of Steel Research International*, 2009, vol. 80 (4), pp. 275-280

21) Palaniswasmy, H., "Deformation of Process Parameters for Stamping and Sheet Hydroforming of Sheet Metal Parts using Finite Element Method" *Doctor of Philosophy Dissertation*, 2007, The Ohio State University, Columbus, Ohio, USA

22) Hill, R., "A Theory of the Yielding and Plastic Flow of Anisotropic Metals", *Proceedings of the Royal Society of London in the Journal of Mathematical and Physical Science*, 1948, vol.193, pp.281-297

23) Taherizadeh, A., Green, D., Ghaei, A., and Yoon, J., "A non Associated Constitutive Model with Mixed Iso-Kinematic Hardening for Finite Element Simulation of Sheet Metal Forming", *Proceedings in the International Journal of Plasticity*, 2010, vol. 26, pp.288-309

24) Barlat, F., and Lian, K., "Plastic Behaviour and Stretchability of Sheet Metals. Part1: A Yield Function for Orthotropic Sheets under Plane Stress Conditions", *Proceedings in the International Journal of Plasticity*, 1989, vol. 5, pp. 51-66

25) Barlat, F., "A 6-Component Yield Function for Anisotropic Materials", *Proceedings in the International Journal of Plasticity*, 1991, vol. 7, pp. 693-712

26) Chun, B., "Study on Hardening Models and Numerical Implementation for Springback Prediction", *Doctor of Philosophy Dissertation*, 2001, Ohio State University, Ohio, USA

27) Zang, S., Thuillier, S., Port, A., and Manach, P., "Prediction of Anisotropy and Hardening for Metallic Sheets in Tension, Simple Shear and Biaxial Tension", *Proceedings in the International Journal of Mechanical Sciences*, 2011, vol. 53, pp.338-347

28) Dunne, F., and Petrinic, N., "Introduction to Computational Plasticity", *Oxford University Press*, 2006, Oxford, UK, pp.1-259

29) Khan, S., and Huang, S., "Continuum Theory of Plasticity" *John Wiley & Sons Inc.*, 1995, New York

30) Geng, L., "Application of Plastic Anisotropy and Non Isotropic Hardening to Springback Prediction", *Doctor of Philosophy Dissertation*, 2000, The Ohio State University, Ohio, USA

31) Ziegler, H., "A Modification of Prager's Hardening Rule", *Proceedings in the Quarterly of Applied Mechanics,* 1959, vol. 17, pp. 55-65

32) Prager, W., "A New Method of Analyzing Stresses and Strains in Work-Hardening Plastic Solids", *Proceedings in the Journal of Applied Mechanics*, 1957, vol.23, pp.493-496

33) Cao, J., Lee, W., Cheng, H., Seniw, M., Wang, H., and Chung, K., "Experimental and Numerical Investigation of Combined Isotropic-Kinematic Hardening Behaviour of Sheet Metals", *Proceedings in the International Journal of Plasticity*, 2009, vol.25, pp. 942-972

34) Armstrong, P., and Frederick, C., "A Mathematical Representation of the Multiracial Bauschinger Effect", *General Electric General Board*, 1966, Technical Report RD/B/N 731, Berkeley Nuclear Laboratories, Berkeley, UK

35) Chaboche, L., "Time Independent Constitutive Theories for Cyclic Plasticity", *Proceedings in the International Journal of Plasticity*, 1986, vol.2, pp. 149-188

36) Li, X., "Kinematic Shakedown Analysis under A General Yield Condition with Non-Associated Plastic Flow", *Proceedings in the International Journal of Mechanical Science*, 2010, vol.52, pp.1-10

37) Taherizadeh, A., Green, D., Yoon, J., "Evaluation of Advanced Anisotropic Models with Mixed Hardening for General Associated and Non-Associated Flow Metal Plasticity", *Proceedings in the International Journal of Plasticity*, 2011, vil. 27, pp. 1781-1802

38) Yoshida, F., Hino, R., and Okada, T., "Deformation and Fracture of Stainless Steel/Aluminum Sheet Laminates in Stretch Bending, *Proceedings of the 5th International Symposium on Plasticity and its Current Applications*,1990, Amsterdam, pp.869-872

39) Chun, K., Jinn, T., and Lee, K., "Modeling the Bauschinger Effect for Sheet Metals, Part I: Theory", *Proceedings in the International Journal of Plasticity*, 2002, vol. 18, pp.571-595

40) Chun, K., Jinn, T., and Lee, K., "Modeling the Bauschinger Effect for Sheet Metals, Part II: Applications", *Proceedings in the International Journal of Plasticity*, 2002, vol. 18, pp.597-616

41) Vladimirov, N., Pretryga, P., and Reese, S., "Anisotropic Finite Elasto-Plasticity with Non Linier Kinematic and Isotropic Hardening and Application to Sheet Metal Forming", *Proceedings in the International Journal of Plasticity*, 2010, vol.26, pp.659-687

42) Brunet, M., Morestin, F., and Godereaux, S., "Nonlinear Kinematic Hardening Identification for Anisotropic Sheet Metals with Bending-Unbending Tests', *Proceedings in the ASME Journal of Engineering Materials and Technology*, 2001, vol.123, pp.378-383

43) Yoshida, F., Uemori, T, "A Model of Large-Strain Cyclic Plasticity Describing the Bauschinger Effect and Work hardening Stagnation", *Proceedings in the International Journal of Plasticity*, 2002, vol.18, pp. 661-686

44) Geng, L., Shen,Y., and Wagoner, H., "Anisotropic Hardening Equations Derived from Reverse Bend Testing", *Proceedings in the International Journal of Plasticity*,2002, vol. 18, pp.743-767

45) Chaboche, J., and Rousselier, G., "On The Plastic and Visco-Plastic Constitutive Equations, Part 1: Rules Developed with Internal Variable Concept", *Proceedings in the Journal of Pressure Vessel Technology*, 1983, vol.105, pp.153-158

46) Khan, A., and Jackson, K., "On the Evaluation of Isotropic and Kinematic Hardening with Finite Plastic Deformation Part I: Compression/Tension Loading of OFHC Copper Cylinders", *Proceedings in the International Journal of Plasticity*, 1999, vol.15, pp.1265-1275

47) Chung, K., Lee, G., Kim, D., Kim, C., Wenner, L., and Barlat, F., "Springback Evaluation of Automotive Sheet Based on Isotropic-Kinematic Hardening Laws and Non Quadratic Anisotropic Yield Functions, Part I, Theory and Formulation", *Proceedings in the International Journal of Plasticity*, 2005, vol.21, pp.861-882

48) Lee, G., Kim, D., Kim, C., Wenner, L., and Chung, K., "Springback Evaluation of Automotive Sheet Based on Isotropic-Kinematic Hardening Laws and Non Quadratic Anisotropic Yield Functions, Part III, Applications", *Proceedings in the International Journal of Plasticity*, 2005, vol.21, pp.915-953

49) Kim, J., Lee, W., Kim, D., Kong, J., Kim, C., Wenner, M., Chung, K., "Effect of Hardening Laws and Yield Function Types on Springback Simulations Duel-Phase Steel Automotive Sheets", *Proceedings in the Journal of Metals and Materials*,2006, vol.12, pp.293-305

50) Chow, Y., and Yang, J., "A generalized Mixed Isotropic-Kinematic Hardening Plastic Model Coupled with Isotropic Damage for Sheet Metal Forming", *Proceedings in the Journal of Damage Mechanism*, 2004, vol.13, pp.81-101

51) Taejoon, P., Kwansoo, C., Hansun, R., Myoung, L., and Wagoner, R., " Numerical Simulation of Time Dependent Springback Behaviour for Aluminum Alloy 6022-T4 Sheet", *Proceedings in the American Institute of Physics*, 2010, vol.1252, pp.153-160

52) Collin, J., Paranteau, T., Mauvoisin, G., and Pilvin, P., "Material Parameters Identification using Experimental Continuous Spherical Indentation for Cyclic Hardening", *Proceedings in the Journal of Computational Materials*, 2009, vol.46, pp. 333-338

53) Choi, Y., "Modeling Evaluation of Anisotropy and Hardening for Sheet Metals", *Doctor of Philosophy Dissertation*, 2003, Ohio State University, Ohio, USA

54) Dafalias, F., and Popov, P., "A Model of Nonlinearity Hardening Materials for Complex Loading", *Proceedings in the Journal Acta Metallurgica*, 1975, vol.21, pp. 173-192

55) Krieg, D., "A Practical Two Surface Theory", *Proceedings in the Journal of Applied Mechanics*, 1975, vol. 42, pp. 641-646

56) Ghaei., A, "Optimization Modeling Springback in Stamped Automotive Structures", *Doctor of Philosophy Dissertation*, 2009, University of Windsor, Windsor, ON, Canada

57) McDowell, D., "A Two Surface Model for Transient Non-Proportional Cyclic Plasticity, Part 1: Development of Appropriate Equations", *Proceedings in the Journal of Applied Mechanics*, 1985, vol.52, pp. 298-303

58) Lee, G., Kim, D., Kim, C., Wenner, L., Wagoner, H., and Chung, K., "A practical Two Surface Plasticity Model and Its Application to Prediction of Springback Prediction", *Proceedings in the International Journal of Plasticity*, 2007, vol.23, pp.1189-1212

59) Cardoso, R., and Yoon, W., "Stress Integration Method for a Nonlinear Kinematic/Isotropic Hardening Model and It's Characterization based on Polycrystal Plasticity", *Proceedings in the International Journal of Plasticity*, 2009, vol.25, pp.1684-1710

60) Hashiguchi, K., "Constitutive Equations of Elastoplastic Materials with Elastic-Plastic Transition", *Proceedings in the ASME Journal of Applied Mechanics*, 1980, vol.47, pp. 266-272

61) Hassan, T., and Kyriakides, S., "Ratcheting in Cyclic Plasticity-Part I: Uniaxial Behaviour", *Proceedings in the International Journal of Plasticity*, 1992, vol.8, pp. 91-116

62) Hassan, T., Corona, E., and Kyriakides, S., "Ratcheting in Cyclic Plasticity-Part II: Multi-Axial Behaviour", *Proceedings in the International Journal of Plasticity*, 1992, vol.8, pp. 117-146

63) Mroz, Z., "On the Description of Anisotropic Work Hardening", *Proceedings in the Journal of Mechanics and Physics of Solids*, 1967, vol.15, pp. 163-175

64) Hubnatter, W., and Merklein, M., "Characterization of Material Behaviour under Pure Shear Condition", *Proceedings in the International journal of Material Forming*, 2008, vol. 1, pp. 233-236

65) Thuillier, S., and Manach, P.Y., "Comparison of Work Hardening of Metallic Sheets using Tensile and Shear Strain Paths", *Proceedings in the International Journal of Plasticity*, 2009, vol.25, pp.733-751

66) Oliveira, C., Alves, L., Chaparro, M., and Menzes, F., "Study on the Influence of Work Hardening Modeling in Springback Prediction", *Proceedings in the International Journal of Plasticity*, 2007, vol.23, pp.516-543

67) Cao, J., "Prediction of Plastic Wringking using the Energy Method", *Proceeding in the ASME Journal of Applied Mechanics*, 1999, vol.66, pp.646-652

68) Verma, R., Noma, N., Chung, K., and Kuwabara, T., "Draw Bending Analysis of a Cold Rolled DP980 Steel Sheet", *Proceedings in the 14th International Conference on Material Forming ESAFORM and American Institute of Physics*, 2011, vol. 1353, pp.1405-1410

69) Lemaitre, J., and Chaboche, J., "Mechanics of Solid Materials", *Cambridge University Press*, 1985, Cambridge, UK

70) Banu, M., Takamura, M., Hama, T., Naidim, O., Teodosiu, C., and Makinouchi, A., "Simulation of Springback and Wrinkling in Stamping of Duel Phase Steel Rail Shaped Part", *Proceedings in the Journal of Material Processing Technology*, 2006, vol.173, pp.178-184

71) Vladimirov, N., Pretryga, P., and Reese, S., "Anisotropic Finite Elasto-Plasticity with Non Linier Kinematic and Isotropic Hardening and Application to Sheet Metal Forming", *Proceedings in the International Journal of Plasticity*, 2010, vol.26, pp.659-687

72) Yoshida, F., "Material Models for Accurate Simulation of Sheet Metal Forming and Springback", *Proceedings of the 10th International Conference on Numerical Methods in Industrial Processes*, American Institute of Physics, pp.71-78

73) Zhang, T., and Hu, J., "Stress and Residual Stress Distributions in Plane Strain Bending", *Proceedings in the International Journal of Mechanical Science*, 1998, vo.40, pp.533-543

74) Campana, F., Cortese, L., and Placidi, F., "FEM Evaluation of Springback after Sheet Metal Forming: Application to High Strength Steels of a Combined Isotropic Kinematic Hardening Model" , *Department of Mechanical and Aeronautical*, University of Roma, Italy

75) Arwidson, C., "Numerical Simulation of Sheet Metal Forming for High strength Steels," *Licensee Thesis*, 2005, Department of Applied Physics and Mechanical Engineering, Lulea University of Technology, Lulea, Sweden

76) Chun, K., Jinn, T., and Lee, K., "Modeling of the Bauschinger effect for Sheet Metals, Part-I; Theory", *Proceedings in the International Journal of Plasticity*, 2002, vol. 18, pp.571-595

77) Chun, K., Jinn, T., and Lee, K., "Modeling of the Bauschinger effect for Sheet Metals, Part-II; Applications", *Proceedings in the International Journal of Plasticity*, 2002, vol. 18, pp.597-616

78) Taherizadeh, A., Ghaei, A., Green, D., and Altenhof, J., "Finite Element Simulation of Springback for a Channel Draw Process with Drawbead using Finite Different Hardening Models", *Proceedings in the International Journal of Mechanical Science*, 2009, vol.51, pp.314-325

79) Inamdar, V., Date, P., and Deai, B., "Studies on the Prediction of Springback in Air Vee Bending of Metallic Sheets using an Artificial Neural Network", *Proceedings in the Journal of Materials Processing Technology*,2000, vol.108, pp.45-54

80) Lepadatu, D., Hambli, H., Kobi, A., and Barreau, A., "Optimization of Springback in Bending Processes using FEM Simulation and Response Surface Method", *Proceedings in the International Journal of Advanced Manufacturing Technology*, 2005, vol.27, pp.40-47

81) Gassara, F., Hambli, R., Bouraoui, T., Halouani,F., and Soulat, D., "Optimization of Springback in L-Bending Process using a Coupled Abaqus/Python Algorithm", *Proceedings in the International Journal of Advanced Manufacturing Technology*, 2009, vol.44, pp.61-67

82) Ruan, F., Feng, Y., and Liu, W., "Springback Prediction for Complex Sheet Metal Forming Parts Based on Genetic Neural Network," *Proceedings in the Journal of IEEE*, 2008

83) Liew, M., Tan, H., Ray, T., and Tan, J., "Optimal Process Design of Sheet Metal Forming for Minimum Springback via an Integrated Neural Network Evolutionary Algorithm," *Journal of Industrial Application and Design*, 2004, vol. 26, pp. 284-294

84) Merklein, M., and Biasutti, M., "A Contribution to the Optimization of Simple Shear Test", *Proceedings in the Key Engineering Materials*, 2009, vol.410-411, pp. 467-472

85) Yoshida, F., Uemori, T., and Fujiwara, K., "Elastic-Plastic Behaviour of Steel Sheets under In-Plane Cyclic Tension-Compression at Large Strain", *Proceedings in the International Journal of Plasticity*, 2002, vol.18, pp.633-659

86) Uemori, T., and Yoshida, F., "Investigation of Cyclic Elasto-Plastic Behaviour of Copper Sheet", *Proceedings in the Journal of key Engineering Materials*, 2003, vol. 233-236, pp. 287-292

87) Kuwabara, T., Morita, Y., Miyashita, Y., Takahashi, S., "Elastic–Plastic Behaviour of Sheet Metal Subjected to In-Plane Reverse Loading", *Proceedings in the International Journal of Plasticity*, 1995, vol. 12, pp.841-844

88) Masendorf, R., and Zenner, H., "Experimental Investigation of the Cyclic Behaviour of Transformed Sheet Metal", *Proceedings on the Journal of Low Cycle Fatigue and Elasto-Plastic Behaviour of Materials*, 1988, pp 691-696

89) Cheng, H., Lee, W., Cao, J., Seniw, M., Wang, H., and Chung, K., "Experimental and Numerical Investigation of Kinematic Hardening Behaviour in Sheet Metals", *Proceedings in the 10th ESAFORM Conference on Material, April, 2007*, Zaragoza, Spain, pp.337-342

90) Wang, J., Carden, F., Wagoner, R., Matlock, D., and Barlat, F., "Creep and Anelasticity in the Springback of Aluminum", *Proceedings in the International Journal of Plasticity*, 2004, vol. 20, pp. 2219-2232

91) Boger, K., Wagnor, R, Barlat, F., Lee, M, and Chung, K., "Continuous Large Strain, Tension/Compression Testing of Sheet Materials", *Proceedings in the International Journal of Plasticity*, 2005, vol.21, pp.2319-2343

92) Zhao, K., and Lee, J., "Finite Element Analysis of the Three-Point Bending of Sheet Metals" *Proceedings in the Journal of Materials Processing Technology*, 2002, vol.122, pp. 6-11

93) Jiang, S., "Springback Investigations", *Master of Science Thesis*, 1997, the Ohio State University, Ohio, USA

94) Shen, Y., "Simple/Reverse Bend Tests for Measurement of Bauschinger Effect in Sheet Materials", *Master of Science Thesis*, 1999, the Ohio State University, Ohio, USA

95) Eggertsen, P., and Mattiason, K., "Uniaxial Tension/Compression Tests and Cyclic Bending Tests for Hardening Parameter Identification", *Proceedings of the 10th Conference of International Deep Drawing Research Group*, 2010, Graz, Austria, pp.575-574

96) Urrilagoitia-Sosa, G., Durodola, F., Fellows, A., "Determination of Tensile and Compressive Stress-Strain Curves from Bend Tests", *Proceedings in the Journal of Applied Mechanical Materials*, 2004, vol. 1-2, pp.133-138

97) Yoshida, F., Urabe, M., Toropov, V., "Identification of Material Parameters in Constitutive Model for Sheet Metals from Cyclic Bending Tests", *Proceedings in the International Journal Mechanical Science*, 1998, vol.40, pp.237-249

98) Meyer, L., Malek, S., and Herzig, N., "Experimental Methods for Characterization of Sheet Metals at High Strain Rates", *Proceedings in the Key Engineering Materials*, 2011, vol.473,pp.474-481

99) Schikorra, M., Brosius, A., and Kleiner, M., "Determination of Anisotropic Hardening of Sheet Metals by Shear Test", *Proceedings in the AIP Conference of NUMISHEET*, 2005, vol.778, pp.389-394

100) Genevois, P., "Study Experimental and Modeling of Plastic Behaviour Anisotropic Steel Sheet in Large Deformation", *Ph.D Thesis*, 1992, National Institute Polytechnique de Grenoble, France

101) Rauch, E., "Plastic Anisotropy of Sheet Metals Determined by Simple Shear Tests", *Proceedings in the Journal of Material Science and Engineering,* 1998, vol. A 241, pp. 179-183

102) Barlat, F., Ferreira, Duarte J., Gracio, J., Lopes A., Rauch, E., "Plastic Flow for Monotonic Loading Conditions of an Aluminum Alloy Sheet Sample", *Proceedings in the International Journal of Plasticity,* 2003, vol. 19, pp.1215-1244

103) Zhao, K., "Cyclic Stress–Strain Curve and Springback Simulation", *Doctor of Philosophy Dissertation*, 1999, Ohio State University, Ohio, USA

104) Miyauchi, K., "Stress Strain Relationship in Simple Shear of In-Plain Deformation for Various Steel Sheets", *Proceedings in the journal of IDDRG*, 1984, vol. 1, pp.360-371

105) Miyauchi, K., "Bauschinger Effect In Planar Shear Deformation of Sheet Metals", *Proceedings in the Journal of Advanced Technology of Plasticity*, 1984, vol. 1, pp.623–682

106) Miyauchi, K., "A Proposal of a Planar Simple Shear Test in Sheet metals", *Proceedings of the Scientific Papers of the Institute of Physical and Chemical Research*, 1984, vol.78(3), pp. 27–40

107) G'Sell, C., Boni, S., and Shrisvastava, S., "Application of Simple Shear for Determination of the Plastic Behaviour of Solid Polymers at Large Strains", *Proceedings in the International Journal of Material Science*, 1983, vol. 18, pp. 903-918

108) Bae, D., and Ghosh, A., "A Planer Simple Shear Test and Flow Behaviour in a Super-Elastic Al-M Alloy', *Proceedings in the International Journal of Metallurgy and Material Transaction*, 2003, vol. 34A, pp. 2465-2471

109) An, Y., Vegter, H., and Heijne, J., "Development of Simple Shear Test for The Measurement of Work Hardening", *Proceedings in the journal of Materials Processing Technology*, 2009, vol. 209, pp.4248-4254

110) Bouvier, S., Haddadi, H., Levee, P., and Teodosiu, C., "Simple Shear Tests: Experimental Techniques and Characterization of the Plastic Anisotropy of Rolled Sheets at Large Strains", *Proceedings in the journal of Material Processing Technology*, 2006, vol. 172, pp. 96-103

111) Wack, B., and Tourabi, A., "Cyclic Simple Shear of Metallic Sheets: Application to Aluminum Lithium Alloy", *Proceedings in the Journal of Materials Science*, 1993, vol.28, pp.4735-4743

112) Rauch, E., and G'Sell, C., "Flow Localisation Induced by a Change in Shear Strain Path in Mild Steel", *Proceedings in the Journal of Materials Science and Engineering*,1989, vol. A111, pp. 71-80

113) Yoon, J., Barlat, F., Gracio, J., and Rauch, E., "Anisotropic Strain Hardening Behaviour in Simple Share for Cube Textured Aluminum Alloy Sheets", *Proceedings in the International journal of Plasticity*, 2005, vol. 21, pp. 2426-2447

114) Tekkaya, A., and Pohlandt, K., "Determining Stress-Strain Curves of Sheet Metal in the Plane Torsion Test", *Proceedings of the Annual CIRP magazine*, vol.31, pp.171-174

115) Liewald, M., Held, C., and Schleich, R., "Characterization of Sheet Metal Formability-A Review and New Approaches", *Proceedings in the International Journal of Steel Research*, 2009, vol. 80 (4), pp. 275-280

116) World Auto Steel, *Advanced High Strength Steel (AHSS) Applications Guidelines*, 2009

117) Advance High Strength Steel Application Guidelines, *World Auto Steel*, Version 4, March 15, 2009

118) ASTM Standard B 831-893: Standard Test Method for Shear Testing of Thin Aluminum Alloy Products, "*ASTM Standards*, West Conshohocken, PA 19428-2959, USA

119) Brosius, A., Yin, Q., Guner, A., and Tekkaya, A., "A New Shear Test for Sheet Metal Characterization" , *Proceedings in the International Journal of Steel Research*, 2011, vol. 82, pp. 323-328

120) Chang, C., "Correlation Between the Microstructure of Duel Phase Steel and Industrial Tube Bending Performance" *Masters of Applied Science*, 2010, University of Windsor, Windsor, ON, Canada

121) Schaeffler, D., "Introduction to Advanced High Strength Steels", *Engineering Quality Solution Inc*, Southfield, Michigan, USA

122) Koc, M., and Cora, O., "Introduction and State of the Art of Hydroforming", *Hydroforming for advanced manufacturing*, 2008, pp.1-28, CRC Press, New York, USA

123) Farabi, N., Chen, D.L., and Zhou, Y., "Microstructure and Mechanical Properties of Laser Welded Dissimilar DP600/DP980 Duel Phase Steel Joints", *Proceedings in the Journal of Alloys and Compounds*, 2011, vol. 509, pp. 982-989

124) Davies, R., and Magee, C., "Physical Metallurgy of Automotive High Strength Steels", *In Structure and Properties of Dual-Phase Steels*, by Kot, R.A., and Morris, J., pp. 1-19, TMS-AIME, 1979

125) ASTM E8M Standard Test Methods for Tension Testing of Metallic Materials, 2002, pp. 60-81

126) GOM GmbH, *ARAMIS User Manual*, 2005, Braunschweig, Germany

127) Rao, K., and Mohan, E., "A Unified Test for Evaluating Material Parameters for Use in the Modeling of the Sheet Metal Forming", *Proceedings in the Journal of Materials Processing Technology*, 2001, vol.113, pp.725-731

128) Turton, N., "Experimental Determination of the Yield Locus of Anisotropic Sheets Using Digital Image Correlation", *Masters of Applied Science Thesis*, 2009, University of Windsor, Windsor, Ontario, Canada

129) Ragai, I., "Experimental and Finite Element Investigation of Springback of Aerospace / Automotive Sheet Metal Products", *Doctor of Philosophy Dissertation*, 2006, The University of McGill, Montreal, Quebec, Canada

VITA AUCTORIS

Md. Samsul Alam Sarker was born in 1972 at Narsingdi in Bangladesh. He graduated from Dhaka University of Engineering and Technology (DUET), Gazipur, Bangladesh, where he obtained B.A.Sc. in Mechanical Engineering in 1997. He started his career in 1997 at Partex Group, a renewed industrial organization in Bangladesh as a Production Engineer. In 1999 he joined Bangladesh Industrial Technical Assistance Centre (BITAC) under the Ministry of Industries of Bangladesh as an Assistant Mechanical Engineer. He worked for this organization until he came to Canada in 2005 as a landed immigrant and obtained a Computer Numerical Control (CNC) diploma from Humber College in 2007. He also successfully completed his Masters of Mechanical Engineering from the University of Windsor in 2009. He is currently a candidate for the Masters of Applied Science in Mechanical Engineering at the same university and is expecting to graduate in Summer 2011.